2019

Efficient Blind Source Separation Algorithms with Applications in Speech and Biomedical Signal Processing

Luay Yassin Taha
University of Windsor

Efficient Blind Source Separation Algorithms with Applications in Speech and Biomedical Signal Processing

By

Luay Yassin Taha

A Dissertation
Submitted to the Faculty of Graduate Studies
through the Department of Electrical and Computer Engineering
in Partial Fulfillment of the Requirements for
the Degree of Doctor of Philosophy
at the University of Windsor

Windsor, Ontario, Canada

2019

Efficient Blind Source Separation Algorithms with Applications in Speech and Biomedical Signal Processing

By

Luay Yassin Taha

APPROVED BY:

P. Agathoklis, External Examiner
University of Victoria

I. Ahmad
School of Computer Science

K. Tepe
Department of Electrical & Computer Engineering

M. Khalid
Department of Electrical & Computer Engineering

E. Abdel-Raheem, Advisor
Department of Electrical & Computer Engineering

March 27^{th}, 2019

Declaration of Co-Authorship/Previous Publication

I. Co-Authorship

I hereby declare that this thesis incorporates material that is result of joint research. Chapters 2-5 of this thesis were completed under the supervision of Dr. Esam Abdel-Raheem. In all cases, the key ideas, primary contributions, experimental designs, data analysis, interpretation, statistical analysis, graphing results, and writing, were performed by the author. The contribution of my supervisor (the co-author) was primarily through the provision of checking and comments on the literature review, mathematical derivations, systems architectures, algorithms, providing feedback on refinement of ideas, editing of the manuscript, and advice on selecting peer reviewed journals for publication.

I am aware of the University of Windsor Senate Policy on Authorship and I certify that I have properly acknowledged the contribution of other researchers to my thesis, and have obtained written permission from the supervisor to include the above material in my thesis.

I certify that, with the above qualification, this thesis, and the research to which it refers, is the product of my own work.

II. Previous Publication

This thesis includes five original papers that have been previously published/submitted for publication in peer reviewed journals and conferences, as follows:

Thesis Chapter	Publication title/full citation	Publication Status
Chapter 2	Taha, L.Y. and Abdel-Raheem, 2018. Efficient blind source extraction of noisy mixture utilising a class of parallel linear predictor filters. IET Signal Processing, 12(8), pp.1009-1016, 2018.	Published
Chapter 3	Taha, L.Y. and Abdel-Raheem, 2018. Extraction of Fetal Electrocardiogram signals using Blind Source Extraction Based Parallel Linear Predictor Filter. (ISSPIT 2018).	Published
Chapter 4	Taha, L.Y. and Abdel-Raheem, 2018. A Computationally Efficient Blind Source Extraction Using Idempotent Transformation Matrix. Circuits, Systems, and Signal Processing, pp.1-21, 2018, Springer publisher.	Published
Chapter 5	Taha, L.Y. and Abdel-Raheem, 2019. Detection and Extraction of Fetal Electrocardiogram Signals Using Null Space Transformation Matrices.	Submitted

I certify that I have obtained a written permission from the copyright owners to include the above published materials in my thesis. I certify that the above material describes work completed during my registration as a graduate student at the University of Windsor.

III. General

I declare that, to the best of my knowledge, my thesis does not infringe upon anyone's copyright nor violate any proprietary rights and that any ideas, techniques, quotations, or any other material from the work of other people included in my thesis, published or otherwise, are fully acknowledged in accordance with the standard referencing practices. Furthermore, to the extent that I have included copyrighted material that surpasses the bounds of fair dealing within the meaning of the Canada Copyright Act, I certify that I have obtained a written permission from the copyright owners to include such materials in my thesis.

I declare that this is a true copy of my thesis, including any final revisions, as approved by my thesis committee and the Graduate Studies office, and that this thesis has not been submitted for a higher degree to any other University or Institution.

Abstract

Blind source separation/extraction (BSS/BSE) is a powerful signal processing method and has been applied extensively in many fields such as biomedical sciences and speech signal processing, to extract a set of unknown input sources from a set of observations. Different algorithms of BSS were proposed in the literature, that need more investigations, related to the extraction approach, computational complexity, convergence speed, type of domain (time or frequency), mixture properties, and extraction performances. This work presents a three new BSS/BSE algorithms based on computing new transformation matrices used to extract the unknown signals. Type of signals considered in this dissertation are speech, Gaussian, and ECG signals. The first algorithm, named as the BSE-parallel linear predictor filter (BSE-PLP), computes a transformation matrix from the the covariance matrix of the whitened data. Then, use the matrix as an input to linear predictor filters whose coefficients being the unknown sources. The algorithm has very fast convergence in two iterations. Simulation results, using speech, Gaussian, and ECG signals, show that the model is capable of extracting the unknown source signals and removing noise when the input signal to noise ratio is varied from -20 dB to 80 dB.

The second algorithm, named as the BSE-idempotent transformation matrix (BSE-ITM), computes its transformation matrix in iterative form, with less computational complexity. The proposed method is tested using speech, Gaussian, and ECG signals. Simulation results show that the proposed algorithm significantly separate the source signals with better performance measures as compared with other approaches used in the dissertation.

The third algorithm, named null space idempotent transformation matrix (NSITM) has been designed using the principle of null space of the ITM, to separate the unknown sources. Simulation results show that the method is successfully separating speech, Gaussian, and ECG signals from their mixture. The algorithm has been used also to estimate average FECG heart rate. Results indicated considerable improvement in estimating the peaks over other algorithms used in this work.

I dedicate my thesis to my lovely wife Salima.

Acknowledgments

First and foremost, I would like to thank my mother for always keeping me in her prayers. My father, god bless his soul, for teaching me everything I needed to know about life.
To my lovely wife, Salima, thank you for caring about me and for the continuous support that you provide me with. Thank you for giving me the inspiration, power, and dedication I needed to complete this work.
I cannot thank enough my honorable advisor Dr. Esam Abdel-Raheem for believing in my research and providing me with the tools and wisdom to excel in my research. You have continuously encouraged my progress with your insightful advises.
I would like to extend my gratitude to members of my committee, Dr. Pan Agathoklis, Dr. Imran Ahmed, Dr. Mohammed Khalid, and Dr. Kamal Tepe, for putting in the time and effort to evaluate my work.
I would like to thank my college Dr. Farook who have given me their valuable advises on various aspects during my research.
To my wonderful sister Iman, thank you for encouraging me to finish a PhD at the University of Windsor. You have supported me through the degree and cared about me and my professional career.
To my lovely daughter Mariam, thank you for caring about me and your continuous support and love, made my life as graduate student much easier. Thank you Mariam.
To my sons, Laith, Abdulrahman, my daughter Asmaa, and my daughter-in-law Fatima and Eman, you have all been so supportive throughout my research to finish my doctorates.

Table of Contents

List of Tables

List of Figures

Chapter 1

Introduction

1.1 Motivation of this work

Blind source separation (BSS) is a powerful signal processing method that was proposed in the late 1980s. As the product of artificial neural networks, statistical signal processing, and information theory, BSS has become an important topic in research and development in the biomedical sciences, speech signal communication, image processing, earth science, and text data mining [1]. The Source Separation (SS), also called Signal Separation, is defined as the process of recovering a set of unknown source "signals" (time series, images...) from a set of observations (i.e. measured signals), which are mixtures of these source signals. The BSS configuration corresponds to the case when the parameter values of the considered mixing model are unknown [1]. In BSS, we can either simultaneously recover all the source signals from their mixtures, or extract only one or a subset of the sources at a time. The latter case is also referred to as blind source extraction (BSE) [3]. Fig. 1.1 illustrates a block diagram of BSS system. The signals $s_1(n), s_2(n), \ldots, s_L(n)$ are L unknown source signals, where n is the sampling index. The mixing system produces M mixing signals $x_1(n), x_2(n), \ldots, x_M(n)$.

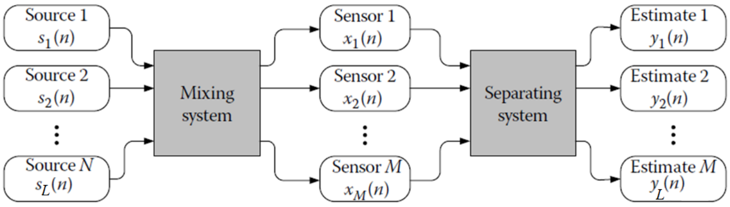

FIGURE 1.1: Block diagram of BSS system [1]

These signals are captured by M sensors. The mixing system can be regarded as an $M \times L$ matrix $\boldsymbol{A}$, with entries $[\boldsymbol{A}]_{ij} = a_{ij}, i = 1, 2, \ldots, M, j = 1, 2, \ldots, L$, such that [2, 3]

$$\boldsymbol{x}(n) = \boldsymbol{A}\boldsymbol{s}(n), \tag{1.1}$$

where

$$\boldsymbol{x}(n) = \begin{bmatrix} x_1(n) \\ x_2(n) \\ \vdots \\ x_M(n) \end{bmatrix}, \qquad \boldsymbol{A} = \begin{bmatrix} a_{11} & a_{12} & \cdots & a_{1N} \\ a_{21} & a_{22} & \cdots & a_{2N} \\ \vdots & \vdots & \vdots & \vdots \\ a_{M1} & a_{M2} & \cdots & a_{MN} \end{bmatrix},$$

$$\boldsymbol{s}(n) = \begin{bmatrix} s_1(n) \\ s_2(n) \\ \vdots \\ s_L(n) \end{bmatrix}. \tag{1.2}$$

1.2 BSS problem

The aim of BSS problem is to solve (1.1) in which $\boldsymbol{s}(n)$ and $\boldsymbol{A}$ are unknowns [4]. The solution involves finding an $L \times M$ demixing matrix $\boldsymbol{H}$ such that

$$\boldsymbol{y}(n) = \boldsymbol{H}\boldsymbol{x}(n), \tag{1.3}$$

where $\boldsymbol{y}(n)$ is the extracted source signals, given by

$$\boldsymbol{y}(n) = \begin{bmatrix} y_1(n) \\ y_2(n) \\ \vdots \\ y_L(n) \end{bmatrix},$$

and $\boldsymbol{H}$ is the generalized inverse of $\boldsymbol{A}$. As $\boldsymbol{A}$ is an $M \times L$ matrix, three possible situations arises:

First: $M = L$, the complete problem, or the critically-determined case [7]. This is the BSS problem in which $\boldsymbol{H} = \boldsymbol{A}^{-1}$. Both $\boldsymbol{H}$ and $\boldsymbol{A}$ are square matrices. Many algorithms in BSS have been developed for the linear instantaneous mixtures assume $M = L$, which is referred to as "complete".

Second: $M > L$, the over-determined problem in which number of mixtures are greater than the unknown sources, and $\boldsymbol{H} = A^{+}$ is the Moore-Penros inverse of $\boldsymbol{A}$, such that $\boldsymbol{H} = \boldsymbol{A}^T(\boldsymbol{A}\boldsymbol{A}^T)^{-1}$ [6, 7].

Third: $M < L$, the under-determined problem in which number of mixtures are less than the unknown sources. This problem is complex and required special algorithms to extract the sources [8, 9].

In this dissertation, we consider only the first two cases, i.e, the critically determined case ($M = L$), and the over-determined case $M > L$.

1.3 BSS algorithms

Several BSS approaches were proposed in the literature to solve (1.3) and estimate $\boldsymbol{H}$ and $\boldsymbol{s}(n)$. Most of these algorithms assumed prior knowledge about the unknown sources.
The independent component analysis (ICA) approach assumes statistically independent sources [2, 3]. The core concept of ICA is to use higher order statistics to minimize the statistical dependence between the sources. This can be achieved using different algorithms such as FastICA [10], Joint approximate diagonalization of eigen-matrices (JADE) [11], Infomax [12], and c-ICA [14]. Note that statistical independence is a strong condition that makes the BSS solution unique up to scaling and permutation ambiguity [14].
The second-order blind identification (SOBI) approach assumes that sources are stationary, but mutually uncorrelated in time. Under this assumption, the BSS problem can be resolved using the second-order statistics rather than the higher order statistics used for ICA [13].
The BSE based linear predictor (BSE-LP) approach assumes that the sources are not correlated with each other and every source has a different temporal structure. The core concept of BSE-LP is to minimise the normalized mean squared prediction error (MSPE) and address the optimized extracted sources [3].
The null space component (NCA) approach uses a deterministic method based on

the assumption that the sources are linearly independent rather than statistically independent. The NCA approach associates each signal with a signature operator so that the rotation ambiguity can be removed. Both ICA and NCA represent the smallest amount of information that can be adopted for solving the BSS problem [14].

The BSS based non-negative matrix factorization (BSS-NMF) approach assumes non-negativity of the observations, mixing coefficients and sources. The principle of BSS-NMF consists in finding non-negative matrix product factors of the input mixture then apply different updating rules to address the optimum source and demixing matrix solution [15].

BSS based Sparse component analysis (BSS-SCA) approach assumes that the sources are sparse or can be "sparsified", and contains as many zeros as possible. The sources need not be statistically independent. The mixing matrix entries can be retrieved from the scatter plot of the sparsified mixtures [16].

1.4 BSS applications

The BSS found many applications such as acoustics, biomedical signal processing, and image processing.

1.4.1 BSS based Acoustics

A wide range of BSS applications in acoustics were recorded in the literature, including cross-talk removal, speech separation, auditory perception, scene analysis,coding, recognition, synthesis and segmentation, psycho-acoustics, reverberation, echo and noise suppression and cancellation, signal enhancement, automatic speech recognition (ASR) in reverberant and noisy acoustical settings. Potential uses in mobile telephony, hands-free devices, human-machine interfaces (HMIs),

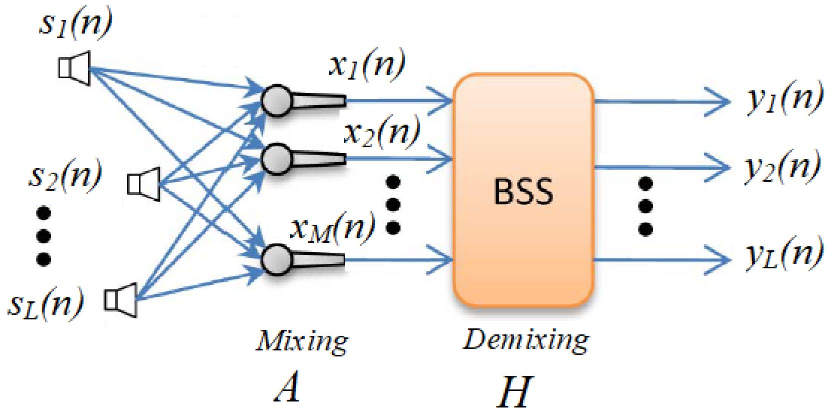

FIGURE 1.2: Speech signal separation using BSS [20].

hearing aids, cochlear implants, airport surveillance, automobiles and aircraft cockpit environments [17, 18, 20–23]. Speech Signal Separation is one of the important applications in acoustic. The method solves the well known cocktail-party problem. Fig. 1.2 illustrates an example of a speech separation system using BSS [20]. The observed signal is the convolution of impulse responses produced by the comprehensive interaction of the source speech signal, the sensor, and the surrounding environment. Since in real-life situations the positions of the microphones with respect to the sources can be rather arbitrary, the mixing process is not known, and thus has to be estimated blindly. In this situation, BSS algorithms are important.

1.4.2 BSS based biomedical signal processing

This is a very promising area of application for BSS techniques, not only because it is an area of rapid growth and great importance, but also because certain kinds of brain imaging data seem to be quite well described by the BSS model [1]. In biomedical signal processing, the BSS algorithms were applied to solve many problems, including non-invasive separation of fetal from maternal electrocardiograms (ECGs), enhancement, and decomposition [25–28]. The fetal ECG (FECG) extraction and enhancement method requires the elimination of the maternal ECG

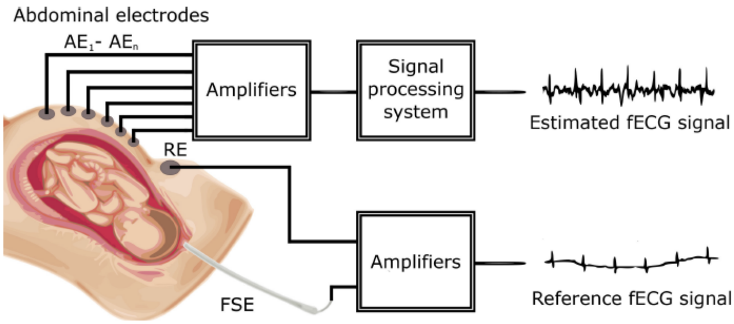

FIGURE 1.3: Block diagram of FECG extraction system [29]. RE is the reference electrode, and FSE is the Fetal Scalp Electrode.

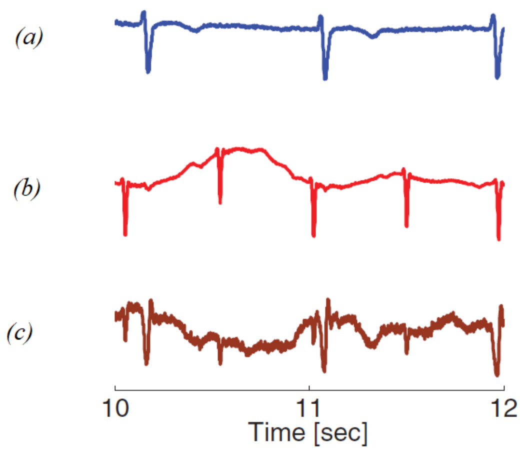

FIGURE 1.4: Typical ECG signals. (a) maternal ECG (MECG). (b) fetal ECG (FECG). (c) abdominal ECG (mixture of FECG and MECG) [30].

(MECG) from the ECG mixture which is the abdominal signals. The frequencies of both signals (FECG and MECG) are few Hertz's and are possibly overlapping. Thus, separating them using the conventional linear filter fails. To address this problem, a non-invasive BSS based FECG extraction algorithms have been proposed. Fig. 1.3 illustrates an example of a FECG extraction system. The abdominal signals were passed to the BSS algorithm to separate the FECG from the MECG signals. Fig. 1.4 illustrates examples of MECG, FECG, and the abdominal signals. The aim of the non-invasive BSS is to recover the FECG signal from the knowledge of the abdominal signals.

FIGURE 1.5: separation of overwriting and underwriting from an RGB real-fake palimpsest. (a) the red channel; (b) the green channel; (c) the blue channel; (d) first separated text; (e) second separated text [36]

1.4.3 BSS based image processing

BSS based image processing is widely used in image feature extraction, face recognition, moving object detection, digital image watermarks, image denoising, image separation, and image restoration [1, 32, 36]. Fig. 1.5 illustrates separation of overwriting and underwriting from an RGB real-fake palimpsest [36], generated by hand and then scanned. The purpose of this analysis is the recovery of the underwriting, which simulates an older text erased and then overwritten. Figure. 1.5(a-c) illustrates the red, green, and blue channels, respectively. Figure. 1.5(d-e) illustrates the first and second ICA outputs which represent the extracted underwriting.

1.5 Research contribution

The main research contributions described in this dissertation are as follows.

1.5.1 Efficient blind source extraction of noisy mixture utilizing a class of parallel linear predictor filters

An efficient blind source extraction algorithm of a noisy mixture using a class of parallel linear predictor filters has been designed. Analysis of a noisy mixture equation is carried out to address new autoregressive source signal model based on the covariance matrix of the whitened data. A method of interchanging the rules of filter inputs is proposed such that this matrix becomes the filter input while the estimated source signals are considered as the parallel filter coefficients. As the matrix has unity norm and unity eigenvalues, the filter becomes independent on the mixture signal norm and eigenvalues variations, thus solving drastically the ambiguity due to the dependency of the filter on the mixture power levels if the mixture is considered as the filter input. Furthermore, the unity eigenvalues of the matrix result in a very fast convergence in two iterations. Simulation results, using speech and Gaussian signals, show that the model is capable of extracting the unknown source signals and removing noise when the input signal to noise ratio is varied from –20 dB to 80 dB. The work has been published in IET signal processing [37].

1.5.2 Extraction of fetal electrocardiogram signals using Blind Source Extraction Based Parallel Linear Predictor filter (BSE-PLP)

The blind source extraction (BSE) based parallel linear predictor filter (PLP) algorithm has been applied to extract Fetal Electrocardiogram (ECG) signals. First, the ECG signals are modelled using the linear mixture model. Then, the BSE-PLP algorithm is applied to extract both the maternal and fetal ECG signals. Simulation results show that the model is successfully extracting all the unknown FECG and MECG signals, for both synthesized and real ECG data. The algorithm is also tested using the sensitivity and accuracy R-peak extraction metrics. The recorded values for the two metrics are 95.45% and 91.3%, respectively, and show considerable improvements as compared to PCA, FastICA, and SOBI algorithms. The work has been accepted for publication in the proceedings of the 2018 IEEE international symposium on signal processing and information technology (ISSPIT).

1.5.3 A computationally efficient blind source extraction using Idempotent Transformation Matrix (ITM)

A computationally efficient blind source extraction algorithm based on idempotent transformation matrix (ITM) has been designed. The algorithm computes the ITM with less computational complexity as compared with the standard singular value decomposition (SVD) method. New optimization problem was defined according to the proposed matrix equation, and solved by an iterative algorithm with low computational complexity. The proposed method is tested using speech, Gaussian, and ECG signals. The performance measures used in this work are the signal-to-interference ratio, signal-to-distortion ratio, and signal-to-artifact ratio. Simulation results show that the proposed algorithm significantly separate the source signals with better performance measures as compared with the state of the art approaches such as the BSE-PLP, second order blind identification (SOBI), Principal Component Analysis (PCA), and fast independent component analysis (FastICA). The work has been published in Circuits, Systems, and Signal Processing [34].

1.5.4 Detection and extraction of fetal electrocardiogram signals using null space transformation matrices

A new algorithm of FECG extraction based on null space transformation matrix, named as Null space idempotent transformation matrix (NSITM), has been designed. First, the ECG mixture signals are used to compute the transformation matrix based on the mixture covariance matrix. Then, the fetal ECG signal is extracted from the null space of the ITM. The algorithm is tested to extract the FECG and maternal ECG (MECG) signals, as well as to detect the R peaks. Real ECG Data considered in this paper are collected from DAISY and Physionet databases. The synthesized ECG data are collected from Physionet/Fetal ECG Synthetic database. Results from real database indicate improvement in average FECG heart rate estimation and in R peaks evaluation metrics, as compared with values from principal component analysis (PCA) and fast independent component analysis (FastICA) algorithms. Results from synthesized ECG data show successful extracting of both FECG and MECG signals from all data. The extraction performances of the synthesized ECG data show considerable improvement over other algorithms used in this work, when signal-to-noise ratio (SNR) increases from 0 dB to 12 dB. The work has been submitted for publication.

1.6 Dissertation structure

The rest of this dissertation is organized as follows:

- Chapter 2 presents a paper on blind source extraction of a noisy mixture using a class of parallel linear predictor filters, oriented to speech and Gaussian signal extraction. This work has been published in IET signal processing, 2018, vol. 12, issue 8, pp, 1009-1016.
- Chapter 3 presents another work on using the parallel linear predictor filters, oriented to ECG extraction. The work has been accepted for publication in the proceedings of the 2018 IEEE international symposium on signal processing and information technology (ISSPIT), Dec. 6-8, 2018, Louisville, KY, USA.
- Chapter 4 presents a paper on Blind Source Extraction Using Idempotent Transformation Matrix. The work has been published in Circuits, Systems, and Signal Processing, Oct 2018, pages 1-21, Springer publisher.
- Chapter 5 presents a work on using the null space method, oriented to ECG signal separation. The work has been submitted for publication.
- Chapter 6 outlines the summary of this work, conclusions and the future work.
- Appendix A contains the list of published journal and conference papers.

Bibliography

[1] Yu, X., Hu, D. and Xu, J., 2013. Blind source separation: theory and applications. John Wiley and Sons.

[2] Naik, G.R. and Wang, W., 2014. Blind source separation. Springer: Berlin/Heidelberg, Germany.

[3] Liu, W., Mandic, D.P. and Cichocki, A., 2007. Blind source extraction based on a linear predictor. IET Signal Processing, 1(1), pp.29-34.

[4] Hyvärinen, A., Karhunen, J. and Oja, E., 2001. Independent Component Analysis. John Willey and Sons. Inc. New York.

[5] Bousse, M., Debals, O. and De Lathauwer, L., 2017. A tensor-based method for large-scale blind source separation using segmentation. IEEE Transactions on Signal Processing, 65(2), pp.346-358.

[6] Loghmari, M.A., Naceur, M.S. and Boussema, M.R., 2014. A new sparse source separation-based classification approach. IEEE Transactions on Geoscience and Remote Sensing, 52(11), pp.6924-6936.

[7] Osterwise, C. and Grant, S.L., 2014. On over-determined frequency domain BSS. IEEE/ACM Transactions on Audio, Speech, and Language Processing, 22(5), pp.956-966.

[8] Joho, M., Mathis, H. and Lambert, R.H., 2000, June. Overdetermined blind source separation: Using more sensors than source signals in a noisy mixture. In Proc. ICA (pp. 81-86).

[9] Puntanen, S., 2007. Matrix Algebra: Theory, Computations, and Applications in Statistics by James E. Gentle. International Statistical Review, 75(3), pp.435-435.

[10] He, X.S., He, F. and Cai, W.H., 2016. Underdetermined BSS based on K-means and AP clustering. Circuits, Systems, and Signal Processing, 35(8), pp.2881-2913.

[11] Kim, S. and Yoo, C.D., 2009. Underdetermined blind source separation based on subspace representation. IEEE Transactions on Signal processing, 57(7), pp.2604-2614.

[12] Hyvärinen, A., 1999. Fast and robust fixed-point algorithms for independent component analysis. IEEE transactions on Neural Networks, 10(3), pp.626-634.

[13] Cardoso, J.F. and Souloumiac, A., 1993, December. Blind beamforming for non-Gaussian signals. In IEE proceedings F (radar and signal processing) (Vol. 140, No. 6, pp. 362-370). IET Digital Library.

[14] Bell, A.J. and Sejnowski, T.J., 1995. An information-maximization approach to blind separation and blind deconvolution. Neural computation, 7(6), pp.1129-1159.

[15] Belouchrani, A., Abed-Meraim, K., Cardoso, J.F. and Moulines, E., 1997. A blind source separation technique using second-order statistics. IEEE Transactions on signal processing, 45(2), pp.434-444.

[16] Hwang, W.L., Lu, K.S. and Ho, J., 2018. Constrained null space component analysis for semiblind source separation problem. IEEE transactions on neural networks and learning systems, 29(2), pp.377-391.

[17] Meganem, I., Deville, Y., Hosseini, S., Deliot, P. and Briottet, X., 2014. Linear-quadratic blind source separation using NMF to unmix urban hyperspectral images. IEEE Transactions on Signal Processing, 62(7), pp.1822-1833.

[18] Kaftory, R. and Zeevi, Y.Y., 2013. Blind separation of time/position varying mixtures. IEEE Transactions on Image Processing, 22(1), pp.104-118.

[19] Omologo, M., Svaizer, P. and Matassoni, M., 1998. Environmental conditions and acoustic transduction in hands-free speech recognition. Speech Communication, 25(1-3), pp.75-95.

[20] Kokkinakis, K. and Loizou, P.C., 2008. Using blind source separation techniques to improve speech recognition in bilateral cochlear implant patients. The Journal of the Acoustical Society of America, 123(4), pp.2379-2390.

[21] Osterwise, C. and Grant, S.L., 2014. On over-determined frequency domain BSS. IEEE/ACM Transactions on Audio, Speech, and Language Processing, 22(5), pp.956-966.

[22] Arberet, S. and Vandergheynst, P., 2014. Reverberant audio source separation via sparse and low-rank modeling. IEEE Signal Processing Letters, 21(4), pp.404-408.

[23] Asaei, A., Taghizadeh, M., Haghighatshoar, S., Raj, B., Bourlard, H. and Cevher, V., 2016. Binary sparse coding of convolutive mixtures for sound localization and separation via spatialization. IEEE Transactions on Signal Processing, 64(EPFL-ARTICLE-211543), pp.567-579.

[24] Kokkinakis, K. and Loizou, P.C., 2010. Advances in modern blind signal separation algorithms: Theory and applications. Synthesis lectures on algorithms and software in engineering, 2(1), pp.1-100.

[25] Da Poian, G., Bernardini, R. and Rinaldo, R., 2016. Separation and analysis of fetal-ECG signals from compressed sensed abdominal ECG recordings. IEEE Transactions on Biomedical Engineering, 63(6), pp.1269-1279.

[26] Sutha, P. and Jayanthi, V.E., 2018. Fetal electrocardiogram extraction and analysis using adaptive noise cancellation and wavelet transformation techniques. Journal of medical systems, 42(1), p.21.

[27] Ma, Y., Xiao, Y., Wei, G. and Sun, J., 2017. Foetal ECG extraction using non-linear adaptive noise canceller with multiple primary channels. IET Signal Processing, 12(2), pp.219-227.

[28] Hsu, S.H., Mullen, T.R., Jung, T.P. and Cauwenberghs, G., 2016. Real-time adaptive EEG source separation using online recursive independent component analysis. IEEE transactions on neural systems and rehabilitation engineering, 24(3), pp.309-319.

[29] Martinek, R., Kahankova, R., Jezewski, J., Jaros, R., Mohylova, J., Fajkus, M., Nedoma, J., Janku, P. and Nazeran, H., 2018. Comparative Effectiveness of ICA and PCA in Extraction of Fetal ECG From Abdominal Signals: Toward Non-invasive Fetal Monitoring. Frontiers in physiology, 9.

[30] Behar, J., Andreotti, F., Zaunseder, S., Oster, J. and Clifford, G.D., 2016. A practical guide to non-invasive foetal electrocardiogram extraction and analysis. Physiological measurement, 37(5), p.R1.

[31] Dagher, I. and Nachar, R., 2006. Face recognition using IPCA-ICA algorithm. IEEE transactions on pattern analysis and machine intelligence, 28(6), pp.996-1000.

[32] Tonazzini, A., Gerace, I. and Martinelli, F., 2010. Multichannel blind separation and deconvolution of images for document analysis. IEEE Transactions on Image Processing, 19(4), pp.912-925.

[33] Taha, L. and Abdel-Raheem, E., 2018. Efficient blind source extraction of noisy mixture utilizing a class of parallel linear predictor filters. IET Signal Processing.

[34] Taha, L.Y. and Abdel-Raheem, E., 2018. A Computationally Efficient Blind Source Extraction Using Idempotent Transformation Matrix. Circuits, Systems, and Signal Processing, pp.1-21. Springer publisher.

Chapter 2

Blind Source Extraction Using Parallel Linear Predictor Filter (BSE-PLP)

2.1 Introduction

Blind source separation (BSS) is the reconstruction of some unobserved sources from a set of observed signals [1]. Blind source extraction (BSE) is a special type of BSS framework, that extracts one or limited source signals at a time, instead of recovering the entire source signals [2]. BSS/BSE applications can be found in telecommunications, signal processing, biomedical sciences and machine learning [3, 4].

In BSE, linear prediction (LP) technique has been recently used to extract the original source signals by estimating their autoregressive (AR) models from the knowledge of the input mixtures [5–9]. The prediction error can be minimized using different algorithms, such as the recursive least squares (RLS) [7, 8], Kalman filter [8, 10], and the standard gradient descent algorithm (GDA) [5, 11]. Due to the complex computations of RLS algorithms, only BSE-LP based GDA will be investigated in this chapter.

Ferdowsi *et al* proposed a joint BSE-LP model based on short-term and long-term prediction [5]. The GDA was used to estimate the demixing vector and the filter coefficients. However, the update of these terms require complex computations. Liu *et al.* proposed a class of BSE-LP algorithms of noiseless mixture based on a new cost function needed to solve the ambiguity associated with the power levels of the sources [12]. A similar approach was reported for noisy mixture using dual LP structure [13]. The noise effect was removed implicitly in the cost function. However, the cost function requires complex computations since it considers the ambiguity of the source signals power level. Also, the performance of the model with signal-to-noise ratio (SNR) variations is not investigated.

In addition to the complexity in updating the coefficients in the methods described in [5, 12, 13], these methods have another drawbacks in which the prediction filter length is unknown and being selected arbitrary. This affect the convergence speed and the extraction performance. Also, the convergence is slow and its learning rate is altered by the input mixture power.

In this chapter, we consider the above factors and propose a novel BSE system based on a new class of parallel linear predictor (PLP) filters. The new system model estimates the source AR temporal structure from the knowledge of the covariance matrix of the whitened data. Then, parallel adaptive filtering based on GDA is applied, by interchanging the rules of filter inputs, to estimate the input sources and the demixing matrix. The design factors considered in this work include the methods of updating PLP filter coefficients, the length and type of PLP filter, the noise level in mixture, and the separation performance measure [5, 7, 8, 14]. The work is also fortified with rigorous analysis and simulations to evaluate its performance. The proposed BSE-PLP method has several properties. (a) The filter input is taken from the covariance matrix of the whitened data. This has an important advantages of fixing the filter input power to unity.

Thus, there is no ambiguity associated with the power levels, as in [5, 12, 13], and the filter convergence becomes very fast to converge in few samples. (b) The estimated input sources are extracted from the predication filter coefficients. (c) The predication filters have a fixed length that is equal to the number of input samples. This resolves the unknown filter length problem associated in previous works [5, 7, 8, 14], and improves the extraction performance.

The remaining of this chapter is organized as follows. In Section 2, we briefly review the BSE-LP methods type GDA [5, 7, 8, 14] in the context of BSS. In Section 3, we present the BSE-PLP method, including its formulation, implementation, justification and mathematical proofs. The experimental results are demonstrated in Section 4. Finally, Section 5 concludes the chapter.

2.2 Brief review of BSE-LP type GDA

The general form of instantaneous Blind Source Separation (BSS) problem can be modeled by [1, 15]

$$\mathbf{X}(n) = \mathbf{A}\mathbf{S}(n) + \mathbf{G}(n), \tag{2.1}$$

where $\mathbf{X}(n) = [\mathbf{x}_1(n), \mathbf{x}_2(n), \ldots, \mathbf{x}_M(n)]^T \subset \mathbb{R}^{M\times N}$ is the mixture matrix, $\mathbf{x}_l(n) = [x_l(n), x_l(n-1), \ldots, x_l(n-N+1)], l = 1, 2, \ldots, M$, M is the number of mixtures, n is the sampling index, N is the number of samples, $\mathbf{A} \subset \mathbb{R}^{M\times L}$ is an unknown full rank mixing matrix, $\mathbf{S}(n) = [\mathbf{s}_1(n), \mathbf{s}_2(n), \ldots, \mathbf{s}_L(n)]^T \subset \mathbb{R}^{L\times N}$ is the unknown source matrix, $\mathbf{s}_k(n) = [s_k(n), s_k(n-1), \ldots, s_k(n-N+1)], k = 1, 2, \ldots, L$, L is the number of unknown sources, assumed less than or equal to M, and $\mathbf{G}(n) \subset \mathbb{R}^{M\times N}$ is the unknown additive noise matrix consisting of M uncorrelated noise vectors. Defining $\tilde{y}_k(n)$ as the estimated source signal of $s_k(n)$, and can be computed using the AR equation given by [5, 7, 13, 14]

$$\tilde{y}_k(n) = \sum_{i=1}^{N} b_{k,i} y_k(n-i), \tag{2.2}$$

where $b_{k,i}$ is the unknown linear predictor filter weight of index ki.
The main goal of BSE-LP is to estimate the source signal $s_k(n)$ by minimizing the k^{th} prediction error term, $e_k(n)$, given by

$$e_k(n) = y_k(n) - \tilde{y}_k(n). \tag{2.3}$$

Let assume that $\mathbf{A}^+ \subset \mathbb{R}^{L\times M}$ is the Moore-Penros inverse of $\mathbf{A}$, such that $A^+ = A^T(AA^T)^{-1}$, if $L \leq M$ [16, 17]. Defining $\mathbf{W}(n)$, equals to $\mathbf{A}^+$, as an unknown $L \times M$ demixing matrix with entries $[\mathbf{W}]_{kl} = w_{kl}, k = 1, 2, \ldots, L, l = 1, 2, \ldots, M$. Also, $\mathbf{W}(n)$ can be expressed by $\mathbf{W}(n) = [\mathbf{w}_1(n), \mathbf{w}_2(n), \ldots,\ \mathbf{w}_L(n)]^T$, where $\mathbf{w}_k(n) = [w_{k1}(n), w_{k2}(n), \ldots, w_{kM}(n)]$. Then, $y_k(n)$ can be expressed by

$$y_k(n) = \sum_{i=1}^{M} w_{k,i}(n)x_i(n). \tag{2.4}$$

From (2.2)-(2.4) we get [5, 7, 13, 14]

$$\begin{aligned} e_k(n) = &\sum_{i=1}^{M} w_{k,i}(n)x_i(n) \\ &- \sum_{i=1}^{N} b_{k,i} \sum_{j=1}^{M} w_{k,j}(n-i)x_j(n-i) \end{aligned} \tag{2.5}$$

Equation (2.5) can be optimized using GDA for the unknowns b_{ki} and $w_{kj}, k = 1, 2, \ldots, M, i = 1, 2, \ldots, N, j = 1, 2, \ldots, M$. For noisy mixture, another linear predictor filter may be required to cancel the effect of noise [13]. This is also required for BSE based short term and long term predictors [5]. These methods have several properties. (a) 1-2 predictors are required for source extraction. (b) The predictors weights and demixing vector are unknown and estimated after solving optimization problem. (c) The length of the predictor filter affect the extraction performance, thus must be carefully selected [5]. (d) The update equations for the predictors weights and demixing vector require variable learning rate due to the ambiguity of input power levels. This adds complexity to the update equations.

(e) The convergence of these method is slower than BSS techniques due to accumulation of error during deflation procedures [5]. Also, the variations of input power level affect the convergence. These drawbacks will be considered and solved in our proposed BSE-PLP technique discussed in next section.

2.3 Proposed BSE-PLP

2.3.1 System model

From (2.1), $\mathbf{S}(n)$ is given by

$$\mathbf{S}(n) = \mathbf{W}(n)\mathbf{X}(n) - \mathbf{W}(n)\mathbf{G}(n). \tag{2.6}$$

Let $\mathbf{C}_x$ be the sample covariance matrix of $\mathbf{X}(n)$ which is computed by [11]

$$\mathbf{C}_x = \frac{1}{N}\mathbf{X}(n)\mathbf{X}^T(n). \tag{2.7}$$

As $\mathbf{C}_x\mathbf{C}_x^{-1}$ is equal to an $N \times N$ identity matrix $\mathbf{I}_N$ then $\mathbf{W}(n)$ can be written as

$$\mathbf{W}(n) = \mathbf{W}(n)\mathbf{C}_x\mathbf{C}_x^{-1}. \tag{2.8}$$

Substituting $\mathbf{C}_x$ from (2.7) into (2.8) to obtain

$$\mathbf{W}(n) = \frac{1}{N}\mathbf{W}(n)\mathbf{X}(n)\mathbf{X}^T(n)\mathbf{C}_x^{-1}. \tag{2.9}$$

The matrix $\mathbf{C}_x$ can also be computed using singular value decomposition (SVD) [18]

$$\mathbf{C}_x = \mathbf{E}\mathbf{D}\mathbf{E}^T, \tag{2.10}$$

where $\mathbf{E}$ is a $M \times M$ matrix with the columns being the eigenvectors of $\mathbf{C}_x$, and $\mathbf{D}$ is a $M \times M$ diagonal matrix with the eigenvalues of $\mathbf{C}_x$. Multiplying (4.16) by

$\mathbf{X}(n)$ and considering (2.6) and (2.10), we have

$$\mathbf{S}(n) = \frac{1}{N}\left(\mathbf{S}(n) + \mathbf{W}(n)\mathbf{G}(n)\right)\left(\mathbf{X}^T(n)\mathbf{E}\mathbf{D}^{-1}\mathbf{E}^T\mathbf{X}(n)\right) - \mathbf{W}(n)\mathbf{G}(n). \quad (2.11)$$

Defining the whitened matrix $\widetilde{\mathbf{X}}(n) \subset \mathbb{R}^{M\times N}$ as [19]

$$\widetilde{\mathbf{X}}(n) = \mathbf{E}\mathbf{D}^{-1/2}\mathbf{E}^T\mathbf{X}(n), \quad (2.12)$$

then (2.11) can be easily written as

$$\mathbf{S}(n) = \mathbf{S}(n)\mathbf{R}(n) + \mathbf{W}(n)\mathbf{G}(n)\mathbf{Q}(n), \quad (2.13)$$

where $\mathbf{R}(n)$ is an $N \times N$ symmetrical matrix given by

$$\mathbf{R}(n) = \frac{1}{N}\widetilde{\mathbf{X}}^T(n)\widetilde{\mathbf{X}}(n), \quad (2.14)$$

with entries $[\mathbf{R}]_{p,q} = r_{p,q}, p, q = 1, 2, \ldots, N, \mathbf{Q}(n) = \mathbf{R}(n) - \mathbf{I}_N$. Moreover, $\mathbf{R} = [\mathbf{R}_1(n), \mathbf{R}_2(n), \ldots, \mathbf{R}_N(n)]$, where $\mathbf{R}_k(n)$ is a column vector equals to $[r_{1k}(n), r_{2k}(n), \ldots, r_{Nk}(n)]^T, k = 1, 2, \ldots, N$. Comparing (2.7) with (2.14), it is clear that $\mathbf{R}(n)$ is the covariance matrix of $\widetilde{\mathbf{X}}(n)$. Equation (2.13) can be rewritten as

$$\mathbf{S}(n) = \mathbf{S}(n)\mathbf{R}(n) + \mathbf{W}(n)\mathbf{T}_s(n), \quad (2.15)$$

where $\mathbf{T}_s(n) = \mathbf{G}(n)\mathbf{Q}(n)$. Since the entries of the noise matrix $\mathbf{G}(n)$ in (2.1) are not known, we generate a white noise matrix $\mathbf{V}(n)$ with known sample entries $[\mathbf{V}]_{lp} = \nu_{lp}, l = 1, 2, \ldots, M, p = 1, 2, \ldots, N$, such that a matrix equivalent to $\mathbf{T}_s(n)$ is generated and denoted as $\mathbf{T}(n)$, and is equal to $\mathbf{V}(n)\mathbf{Q}(n)$, $[\mathbf{T}]_{ln} = \tau_{ln} = \sum_{p=1}^{N}\nu_{lp}r_{pn} - \delta_{lp}, l = 1, 2, \ldots, M, n = 1, 2, \ldots, N$, δ_{lp} is Kronecker delta. Moreover, $\mathbf{T} = [\mathbf{T}_1(n), \mathbf{T}_2(n), \ldots, \mathbf{T}_N(n)]$, where $\mathbf{T}_k(n) = [\tau_{1k}(n), \tau_{2k}(n), \ldots, \tau_{Mk}(n)]^T, k = 1, 2, \ldots, N$.

Based on (2.15), the optimization problem may be defined to estimate $\mathbf{S}$ and $\mathbf{W}$.

However, BSE can also be used to extract one source signal at a time. This requires some modifications to (2.15). Defining $\tilde{y}_k(n-j), j = 0, 1, 2, \ldots, N-1$ as the k^{th} estimated source signal of $s_k(n-j)$, then from (2.15) we have

$$\tilde{y}_k(n-j) = \sum_{i=0}^{N-1} r_{i+1,j+1} y_k(n-i) + \sum_{l=1}^{M} w_{kl}(n) \tau_{lj+1}(n). \tag{2.16}$$

Thus, a set of N equations can be formulated from (2.16) to model the estimated source vector, defined by $\tilde{\mathbf{y}}_k(n-j) = [\tilde{y}_k(n), \tilde{y}_k(n-1), \ldots, \tilde{y}_k(n-N+1)]^T$. As these equations are independent to each other and can be computed in parallel, we propose the name parallel linear predictor (PLP). From (2.16), the j^{th} error term, defined as $e_k^j(n)$, is given by

$$\begin{aligned} e_k^j(n) &= y_k(n-j) - \tilde{y}_k(n-j) \\ &= y_k(n-j) - \sum_{i=0}^{N-1} r_{i+1,j+1} y_k(n-i) - \sum_{l=1}^{M} w_{kl}(n) \tau_{lj+1}(n). \end{aligned} \tag{2.17}$$

Equation (2.17) represents a new LP model that can be used for BSE of AR input sources. As the coefficients $r_{i+1,j+1}$ in (2.17) are known and computed from (2.14), we propose a new adaptive filtering approach to estimate $\tilde{y}_k(n-j)$ and $w_{kl}(n)$ from the knowledge of $r_{i+1,j+1}$ and $e_k^j(n)$. The proposed approach is based on interchanging the rules of inputs and the filter coefficients in (2.17). Thus, the filter coefficients are considered as the unknown source signals $\mathbf{y}_k(n) = [y_k(n), y_k(n-1), \ldots, y_k(n-N+1)]^T$. The coefficients $r_{i+1,j+1}$ are considered as the adaptive filter inputs which will be repeated every iteration till the filter converges. Figure 2.1 illustrates the proposed BSE-PLP model for extracting one source vector $\mathbf{y}_k(n)$ from the mixture $\mathbf{X}(n)$.

The proposed adaptive filter needs further investigation about the properties of the matrix $\mathbf{R}(n)$ whose elements represent the new filter input. In the following, two theorems are provided. The first theorem is a mathematical proof of the properties of $\mathbf{R}(n)$ and $\mathbf{Q}(n)$ matrices, related to their norms and their minimum

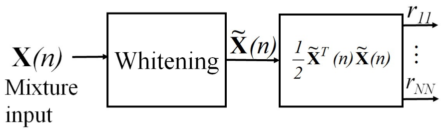

(a)

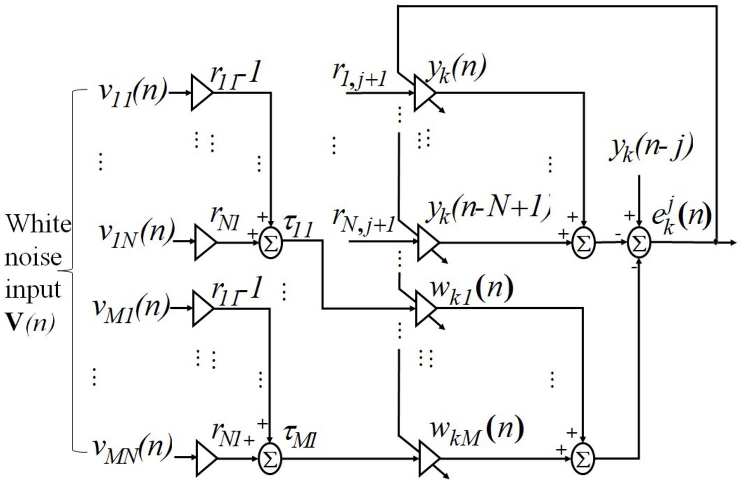

(a)

FIGURE 2.1: Structure of the j^{th} stage of the proposed BSE-PLP. (a) Whitening and $\mathbf{R}(n)$ matrix generation, (b) The proposed PLP filter

and maximum eigenvalues. The second theorem is a proof of the transformation property of the $\mathbf{R}(n)$ matrix.

Theorem 1: Given a whitened matrix $\widetilde{\mathbf{X}}(n)$ of an input mixture $\mathbf{X}(n)$, the matrices $\mathbf{R}(n)$ and $\mathbf{Q}(n)$ will have unity norm. The maximum and minimum eigenvalues of $\mathbf{R}(n)$ will be 1 and 0, respectively. The maximum and minimum eigenvalues of $\mathbf{Q}(n)$ are 0 and -1, respectively. The proof is established in the Appendix A.

Theorem 2: The $\mathbf{R}(n)$ matrix described in Theorem 1 has the following transformation properties

$$\mathbf{R}(n) = \begin{cases} \mathbf{R}(n)\mathbf{R}^T(n) & \text{for noiseless mixture ,} \\ \mathbf{R}(n)\mathbf{R}^T(n) + \Psi(n) & \text{for noisy mixture ,} \end{cases}$$

where $\Psi(n)$ is the noise error term. The proof is established in the Appendix B.

2.3.2 Optimization methodology

In this section, the GDA is applied to (2.17) to address the updates of $\mathbf{y}_k(n)$) and $\mathbf{w}_k(n)$. We propose a new cost function $J_k(\mathbf{w}_k(n), \mathbf{y}_k(n))$ using the mean squares prediction error (MSPE) [5, 7], we can write

$$J_k(\mathbf{w}_k(n), \mathbf{y}_k(n)) = \frac{1}{N}\sum_{j=0}^{N-1}\left[e_k^j(n)\right]^2, \tag{2.18}$$

First, the gradients are evaluated as

$$\nabla_{w_{kl}} J_k(\mathbf{w}_k(n), \mathbf{y}_k(n)) = -\sum_{i=0}^{N-1} e_k^i(n)\tau_{li+1}(n), \tag{2.19}$$

and

$$\nabla_{y_k(n-j)} J_k(\mathbf{w}_k(n), \mathbf{y}_k(n)) = e_k^j(n) - \sum_{i=0}^{N-1} r_{j+1,i+1} e_k^i(n), \tag{2.20}$$

then, the updates of $w_{kl}(n)$ and $y_k(n-j)$ now become

$$w_{kl}(n+1) = w_{kl}(n) + \mu_w \sum_{i=0}^{N-1} e_k^i(n)\tau_{li+1}(n), \tag{2.21}$$

and

$$y_k(n-j+1) = y_k(n-j) - \mu_y \left[e_k^j(n) - \sum_{i=0}^{N-1} r_{j+1,i+1} e_k^i(n) \right], \tag{2.22}$$

where μ_w and μ_y are the learning rates. From (2.21)-(2.22), the updates of $\mathbf{w}_k(n)$ and $\mathbf{y}_k(n-j)$ are obtained as follows

$$\mathbf{w}_k(n+1) = \mathbf{w}_k(n) + \mu_w \mathbf{T}(n)\mathbf{E}_r(n), \tag{2.23}$$

$$\mathbf{y}_k(n+1) = \mathbf{y}_k(n) + \mu_y \mathbf{Q}(n)\mathbf{E}_r(n), \tag{2.24}$$

where $\mathbf{E}_r(n) = [e_k^0(n), e_k^1(n), \ldots, e_k^{N-1}(n)]^T$.
To check the convergence of the method, let assume that $\mathbf{y}_{opt}(n)$ is the optimum solution having minimum noise contents. Then, subtracting $\mathbf{y}_{opt}(n)$ from both sides of (2.24) and multiplying by $\mathbf{R}(n)$ we get

$$\begin{aligned} \mathbf{R}(n)\left[\mathbf{y}_k(n+1) - \mathbf{y}_{opt}(n)\right] = \mathbf{R}(n)\left[\mathbf{y}_k(n) - \mathbf{y}_{opt}(n)\right] \\ + \mu_y \mathbf{R}(n)\mathbf{Q}(n)\mathbf{E}_r(n). \end{aligned} \tag{2.25}$$

From (2.15) and (2.25), and considering the optimum solution, we have $\mathbf{R}(n)\mathbf{y}_k(n+1) \approx \mathbf{y}_k(n+1)$, $\mathbf{R}(n)\mathbf{y}_k(n) \approx \mathbf{y}_k(n)$, $\mathbf{R}(n)\mathbf{y}_{opt}(n) \approx \mathbf{y}_{opt}(n)$. Furthermore, using theorem 2, the term $\mu_y \mathbf{R}(n)\mathbf{Q}(n)\mathbf{E}_r(n)$ in (2.25) approaches zero since $\mathbf{R}(n)\mathbf{Q}(n) = \mathbf{R}^2(n) - \mathbf{R}(n) \approx 0$, (see also the simulation results shown in Fig. 2.4). Then (2.25) is reduced to

$$\mathbf{y}_k(n+1) - \mathbf{y}_{opt}(n) \approx \mathbf{y}_k(n) - \mathbf{y}_{opt}(n). \tag{2.26}$$

From (2.26), we have

$$\mathbf{y}_k(n+1) \to \mathbf{y}_k(n), \tag{2.27}$$

thus (2.24) converges as $n \to \infty$. This conclusion is confirmed by simulation in Fig. 2.4.

To address the optimum values of μ_w and μ_y when $e_k^j(n+1)$ approaches zero, Taylor series expansion is used. Ignoring second and higher order derivatives, $e_k^j(n+1)$ is given by [14]

$$\begin{aligned} e_k^j(n+1) \approx e_k^j(n) &+ \sum_{i=0}^{N-1} \frac{\partial e_k^j(n)}{\partial y_k(n-i)} \Delta y_k(n-i) \\ &+ \sum_{l=1}^{M} \frac{\partial e_k^j(n)}{\partial w_{kl}(n)} \Delta w_{kl}(n). \end{aligned} \tag{2.28}$$

From (2.17), (2.21)-(2.22) the followings can be verified

$$\begin{aligned} \frac{\partial e_k^j(n)}{\partial y_k(n-i)} &= \delta_{ij} - r_{i+1,j+1}, \\ \frac{\partial e_k^j(n)}{\partial w_{kl}(n)} &= -\tau_{l,j+1}(n), \\ \Delta y_k(n-i) &= -\mu_y \left[e_k^j(n) - \sum_{i=0}^{N-1} r_{j+1,i+1} e_k^i(n) \right], \\ \Delta w_{kl}(n) &= \mu_w \sum_{i=0}^{N-1} e_k^i(n) \tau_{l,i+1}(n), \end{aligned} \tag{2.29}$$

where $j = 0, 1, \ldots, N-1$. From (2.28)-(2.29), and assuming $j = 0$, then $e_k^0(n+1)$ can be simplified to

$$\begin{aligned} e_k^0(n+1) =& e_k^0(n) - \mu_y \sum_{i=0}^{N-1} e_k^i(n) + \mu_y \mathbf{R}_1(n) \mathbf{E}_r(n) \\ & - \mu_w e_k^0(n) \sum_{l=1}^{M} \tau_{ll}^2(n). \end{aligned} \tag{2.30}$$

For optimum case, the noise term is minimized. Thus, $\sum_{i=0}^{N-1} e_k^i(n) \approx 0$ and $\mathbf{R}_1(n)\mathbf{E}_r(n) \approx e_k^0(n)$ then (2.30) can be further simplified to

$$e_k^0(n+1) \approx e_k^0(n)\left(1 + \mu_y - \mu_w \|\mathbf{T}_1(n)\|_2^2\right). \tag{2.31}$$

Assuming $\mu_y \approx \mu_w = \mu_{opt}$, where μ_{opt} is the optimum value of μ. As $e_k^0(n+1) \to 0$ then (2.31) can be minimized, and μ_{opt} will be equal to

$$\mu_{opt} = \frac{1}{\|\mathbf{T}_1(n)\|_2^2 - 1}. \tag{2.32}$$

Similar equation to (2.32) can be found, for $j > 0$, if $\mathbf{T}_1(n)$ is replaced by $\mathbf{T}_{j+1}(n)$. As $\mathbf{T}(n) = \mathbf{V}(n)\mathbf{Q}(n)$ then from (A.14) in theorem 1, and using the norm inequality

$$\|\mathbf{T}(n)\|_2 \leq \|\mathbf{V}(n)\|_2 \|\mathbf{Q}(n)\|_2, \tag{2.33}$$

we have

$$\begin{aligned} \|\mathbf{T}(n)\|_2 &\leq \|\mathbf{V}(n)\|_2, \\ \|\mathbf{T}_j(n)\|_2 &< \|\mathbf{V}(n)\|_2. \end{aligned} \tag{2.34}$$

From (2.32)-(4.4), μ_{opt} is inversely proportional to the input noise power only. The estimation of noise power requires further investigation and is beyond the scope of this dissertation. For noise free case, μ_{opt} is constant and is equal to -1. In both cases, μ_{opt} is independent on the mixture input $\mathbf{X}(n)$. This solves the problem in previous works such as [5, 12, 13].

2.3.3 Algorithm of the proposed BSE-PLP

The BSE-PLP Algorithm is designed based on the proposed optimization methodology described in Section 2.3.2. The algorithm extracts $\mathbf{w}_k(n)$, $\mathbf{y}_k(n)$, and $e_k^j(n)$,

$j = 0, 1, \ldots, N-1$ from the input mixture $\mathbf{X}(n)$. Maximum number of iterations is denoted by $maxiter$. We present the following algorithmic procedure:

Algorithm 1 Proposed BSE-PLP algorithm

1: Set the values of N, k, M, $\mathbf{w}_k(n)$, $\mathbf{y}_k(n)$ and $\mathbf{V}(n)$.

2: Set the value of $maxiter$.

3: Update $\widetilde{\mathbf{X}}(n)$, $\mathbf{R}(n)$, $\mathbf{T}(n)$, and μ by (2.12), (2.14), (2.15), and (2.32), respectively.

4: for $iteration = 1$ to $maxiter$

5: Update $e_k^j(n)$, $\mathbf{w}_k(n)$, and $\mathbf{y}_k(n)$, in each iteration, by (2.17), (2.23) and (2.24), respectively.

6: end for

7: Return $e_k^j(n+1)$, $\mathbf{w}_k(n+1)$, and $\mathbf{y}_k(n+1)$.

2.4 Experiments

In this section, three different simulations are provided. They are: the signal extraction versus $maxiter$ variations, the error analysis of $\Psi(n)$ in (B.5) and $e_k^j(n)$ in (2.17), and the extraction performance of the proposed BSE-PHP algorithm and comparison with SOBI and FastICA algorithms [16, 21]. These algorithms are selected because they have become benchmark methods due to their popularity and their success in extracting signals from input mixture [1, 3, 22, 23].

2.4.1 Signal extraction

To check the signal extraction versus $maxiter$ variations, we use the algorithm shown in Section 2.3.3 and set first $maxiter = 2$. Two independent simulation sets are performed to extract white Gaussian noise (WGN) and speech signals. Three uncorrelated WGN signals $[s_1(n), s_2(n), s_3(n)]$, shown in Fig. 2.2(a), are mixed by a randomly generated mixing matrix **A** then adding a non stationary WGN to each source signal such that the SNR = 30 dB. Number of samples is selected as $N = 80$. The added noise is uncorrelated with source signals. The simulation extracts one source signal at a time, then is repeated to extract other signals. Figure 2.2(b) illustrates the mixture signals $[x_1(n), x_2(n), x_3(n)]$. Figure 2.2(c) illustrates the extracted signals $[y_1(n), y_2(n), y_3(n)]$ which match the signals $[s_1(n), s_2(n), s_3(n)]$ in Fig. 2.2(a).

The previous simulation is repeated to extract three uncorrelated clean speech signals $[s_1(n), s_2(n), s_3(n)]$, shown in Fig. 2.3(a), corresponding to three English numbers $'One'$, $'Two'$, and $'Eight'$, respectively. The signals are sampled at 8 kHz. Number of samples is selected as $N = 6000$. Figure 2.3(b) illustrates the mixture signals $[x_1(n), x_2(n), x_3(n)]$. Figure 2.3(c) illustrates the extracted signals $[y_1(n), y_2(n), y_3(n)]$ which match the original source signals $[s_1(n), s_2(n), s_3(n)]$ in Fig. 2.3(a).

The above two simulations are repeated for $maxiter = 4, 6, \ldots, 10$. Results from simulations, regarding the extracted Gaussian and speech signals, are almost the same as in Fig. 2.2(c) and Fig. 2.3(c), respectively. For example, the results of the extracted signals for $maxiter = 6$ are shown in Fig. 2.2(d) and Fig. 2.3(d), respectively. The similarities between the extracted signals and the original source signals will be investigated in Section 2.4.3.

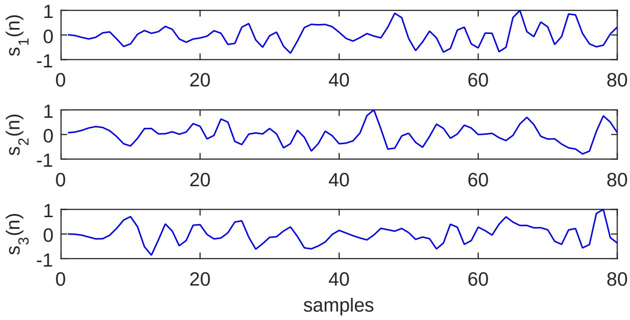

(a)

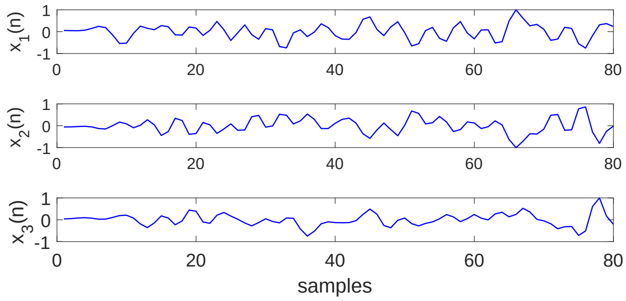

(b)

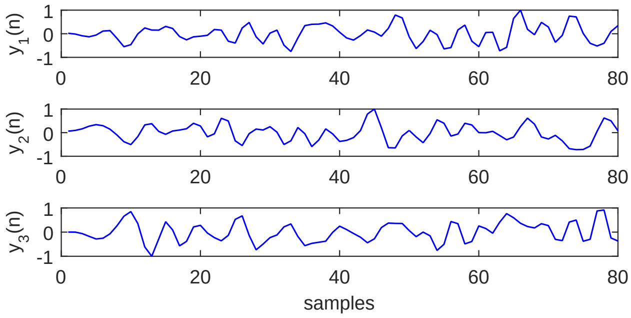

(c)

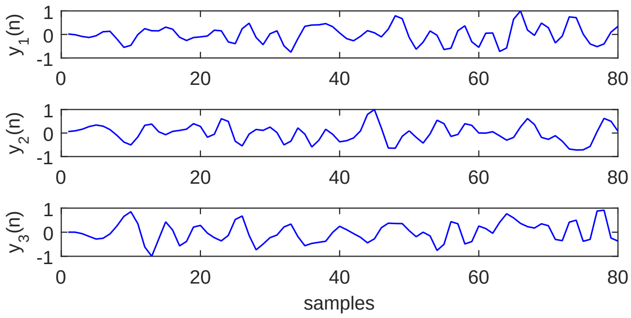

(d)

FIGURE 2.2: Extraction of Gaussian signals(a)Input Gaussian source signals (b)Mixture signals (c)Extracted signals, considering $maxiter = 2$ (d)Extracted signals, considering $maxiter = 6$

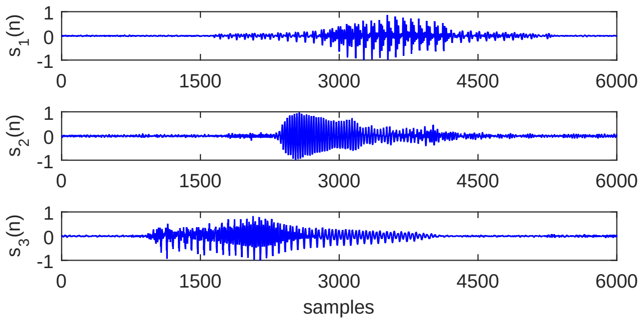

(a)

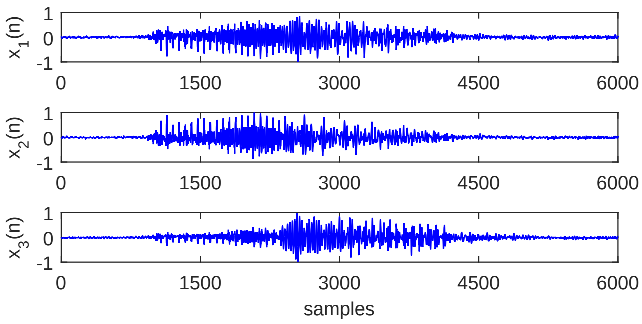

(b)

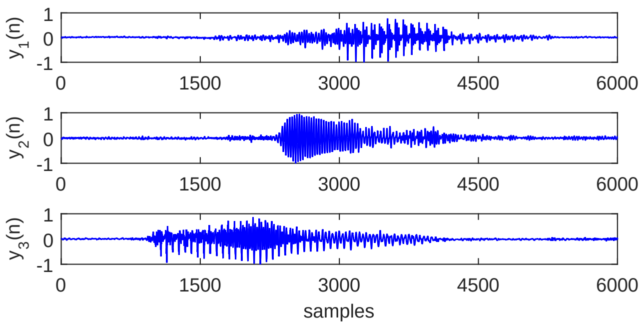

(c)

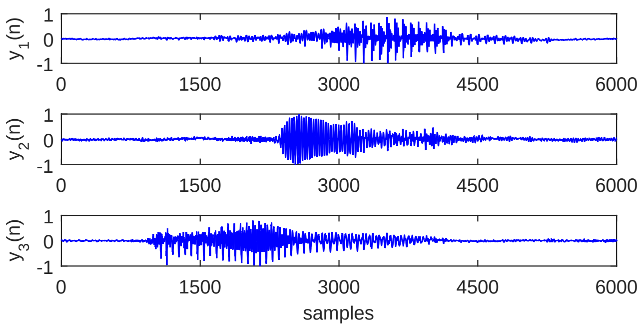

(d)

FIGURE 2.3: Extraction of Speech signals(a)Input clean speech signals (b)Mixture signals (c)Extracted signals, considering $maxiter = 2$ (d)Extracted signals, considering $maxiter = 6$

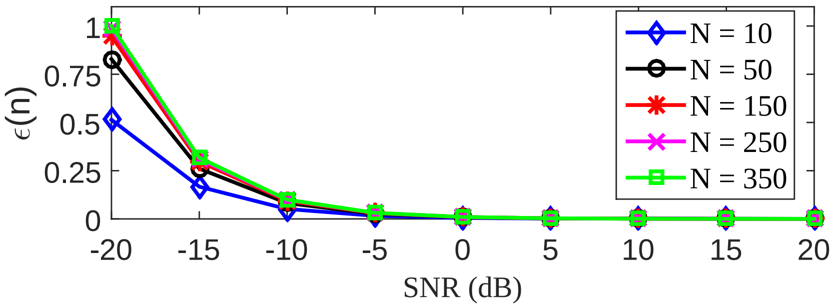

FIGURE 2.4: Variations of $\epsilon(n)$ with SNR

2.4.2 Error analysis

The same simulation steps in Section 2.4.1 are used to measure the mean squares error (MSE) of $\Psi(n)$, denoted by $\epsilon(n)$, when N varies from 50-350. This error was analyzed in Appendix B. Figure 2.4 illustrates the results; for any value of N, the results show that $\epsilon(n)$ decreases to zeros as the SNR approaches 0 dB. Thus, the error can be ignored to simplify (B.5) by (B.3), as shown in appendix B.
The simulation is repeated to measure the MSE of $e_k^j(n)$, denoted by $\gamma(n)$, and considering the noiseless and the stationary and non stationary WGN case (SNR $= 20$ dB). Results are shown in Fig. 2.5; All MSE curves converge fast to minimum values in 2 iterations. This proves the conclusion drawn in (2.27). Also, $maxiter = 2$ justifies the results in Section 2.4.1. Thus, the proposed BSE-PLP can be considered as a class of deterministic BSE methods. This point will be further justified using performance analysis in Section 2.4.3.

2.4.3 Extraction performance

The last simulation has four parts. The first part is used to investigate the effect of varying $maxiter$, used in Algorithm 1, on the similarity performance index (SPI), that is based on the correlations between $\mathbf{s}_k(n)$ and $\mathbf{y}_k(n)$ [5, 6], given by the

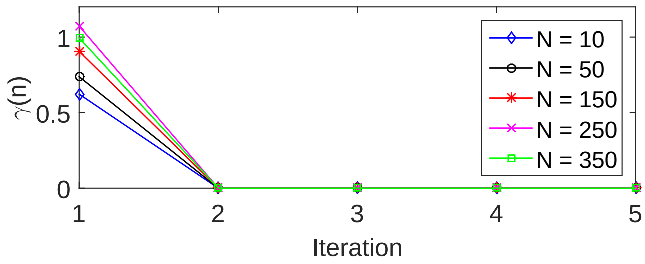

(a)

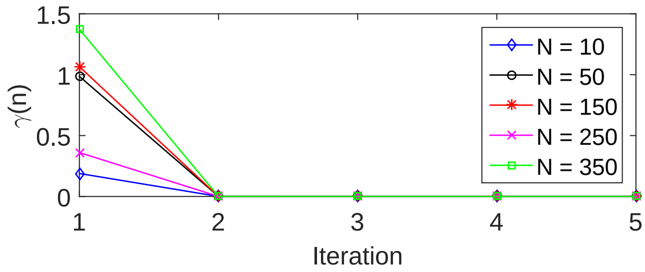

(b)

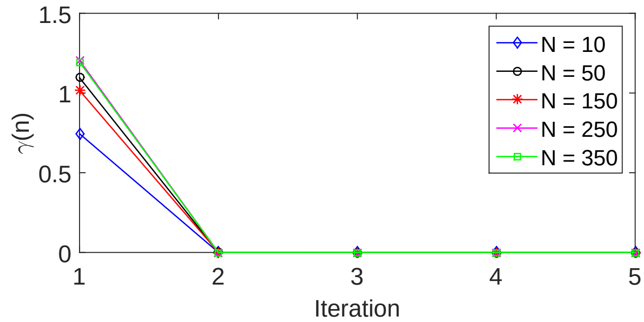

(c)

FIGURE 2.5: Variations of $\gamma(n)$ with number of iterations(a)noiseless case(b)with stationary noise, SNR = 20 dB (c)with non stationary noise, SNR = 20 dB

relation

$$\text{SPI} = \frac{1}{M}\sum_{i=1}^{M} 10log_{10}\left|\frac{\langle \mathbf{y}_k(n), \mathbf{s}_k(n)\rangle}{\sqrt{\langle \mathbf{y}_k(n), \mathbf{y}_k(n)\rangle \langle \mathbf{s}_k(n), \mathbf{s}_k(n)\rangle}} - 1\right|,$$

where $\langle . \rangle$ denotes the inner product. We follow the same simulation procedure steps in Section 2.4.1 by setting first $maxiter = 2$ then recording the mean values of SPI after 1000 trials of independent simulations. The process is repeated by varying $maxiter$ from 2 to 10. The unknown signals used for extractions are

Gaussian, Speech (the same used in Section 2.4.1) and three uncorrelated sawtooth, sinusoidal, and square signals, with number of samples taken as 100, and having frequencies of 3 kHz, 5 kHz, and 10 kHz, respectively. The additive WGN considered in this experiment is of non stationary type. Results of simulation are illustrated in Fig. 2.6. It is clear from the results that increasing the value of *maxiter* will not give considerable advantages in remarkably enhancing SPI performances. Thus, we can select $maxiter = 2$ in Algorithm 1. This conclusion is also obtained in Section 2.4.1 and Section 2.4.2. Thus, Algorithm 1 can be presented without the iteration loop, by removing steps 2, 4, and 6, and writing step 5 twice. The simplified algorithmic procedure is shown in Algorithm 2.

Algorithm 2 The simplified BSE-PLP algorithm

1: Set the values of N, k, M, $\mathbf{w}_k(n)$, $\mathbf{y}_k(n)$ and $\mathbf{V}(n)$.

2: Update $\widetilde{\mathbf{X}}(n)$, $\mathbf{R}(n)$, $\mathbf{T}(n)$, and μ by (2.12), (2.14), (2.15), and (2.32), respectively.

3: Update $e_k^j(n)$, $\mathbf{w}_k(n)$, and $\mathbf{y}_k(n)$ by (2.17), (2.23) and (2.24), respectively.

4: Update $e_k^j(n)$, $\mathbf{w}_k(n)$, and $\mathbf{y}_k(n)$ by (2.17), (2.23) and (2.24), respectively.

5: Return $e_k^j(n+1)$, $\mathbf{w}_k(n+1)$, and $\mathbf{y}_k(n+1)$.

The second part is intended to apply Algorithm 2 by following the same simulation procedure steps in Section 2.4.1 (for extracting the WGN) then recording the mean values of SPI after 1000 trials of independent simulations. The simulation is repeated for $N = 10, 50, 150, 250, 350$. Results are shown in Fig. 2.7 and indicate that with $N = 10$ and at low SNR, the SPI is better than that with $N = 50$ to 350. At high SNR, all plots show good SPI, below -20 dB.

The third part is similar to the second part but used to compare the SPI measured from the proposed BSE-PLP (Algorithm 2), with the SPI measured using SOBI and FastICA algorithms. The source signals considered in this simulation are sawtooth, sinusoidal, and square signals, with the same simulation settings

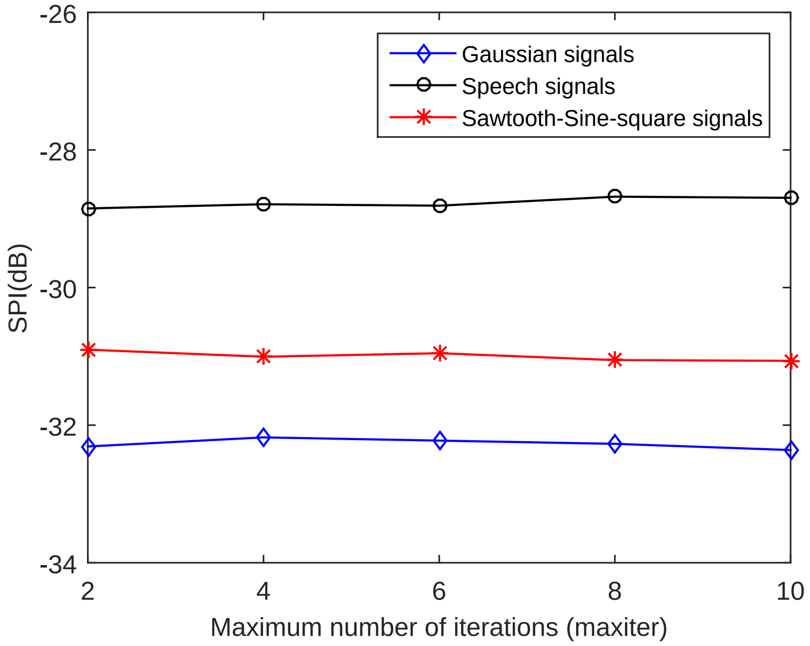

FIGURE 2.6: Variations of SPI with *maxiter*

used in part 1 of this section. The additive WGN is of stationary and non stationary type. The same data was also used by SOBI and FastICA algorithms, for comparison purposes. Comparing the results in Fig. 2.8, it is clear that the proposed method has better SPI than the other two algorithms, when the SNR is varied according to the specified ranges in Fig. 2.8. The SPI remains almost constant for all three algorithms at high SNR (above 60 dB for stationary additive WGN case and above 40 dB for stationary additive WGN case). However, the proposed BSE-PLP algorithm still shows better SPI.

The fourth part is similar to the third part but includes the estimation of the source-to-interference ratio (SIR), the source-to-artifacts ratio (SAR), and the source-to-distortion ratio (SDR) [8]. The computation of these terms involves first the decomposition of the extracted signals $\mathbf{y}_k(n)$ according to [25]

$$\mathbf{y}_k(n) = \mathbf{s}_{target} + \mathbf{e}_{interf} + \mathbf{e}_{noise} + \mathbf{e}_{artif}, \tag{2.35}$$

where $\mathbf{s}_{target}$ is the component of $\mathbf{s}_k(n)$ in $\mathbf{y}_k(n)$, $\mathbf{e}_{interf}$, $\mathbf{e}_{noise}$, and $\mathbf{e}_{artif}$ are the

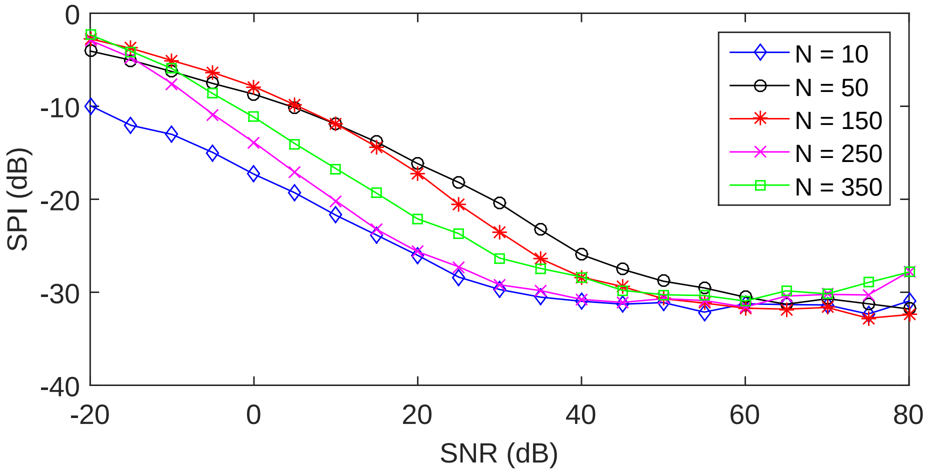

FIGURE 2.7: Variations of SPI with SNR, using Algorithm 2

interference, noise and artifact error terms, respectively. Second, the SIR, SAR, and SDR terms are computed using the BSS EVAL toolbox [25–27]

$$\mathrm{SIR} = 10log_{10}\frac{\|\mathbf{s}_{target}\|_2^2}{\|\mathbf{e}_{interf}\|_2^2}, \tag{2.36}$$

$$\mathrm{SAR} = 10log_{10}\frac{\|\mathbf{s}_{target} + \mathbf{e}_{interf} + \mathbf{e}_{noise}\|_2^2}{\|\mathbf{e}_{artif}\|_2^2}, \tag{2.37}$$

$$\mathrm{SDR} = 10log_{10}\frac{\|\mathbf{s}_{target}\|_2^2}{\|\mathbf{e}_{interf} + \mathbf{e}_{noise} + \mathbf{e}_{artif}\|_2^2}. \tag{2.38}$$

As above performance measures are inspired by the usual definition of the SNR, their higher values reflect better separation algorithm [8, 25–27]. Comparing the results in Tables (2.1-2.2), it is clear that the proposed method has better SIR, SAR, and SDR, than the other two algorithms, when the SNR is varied according to the specified ranges in Tables 2.1 and 2.1.

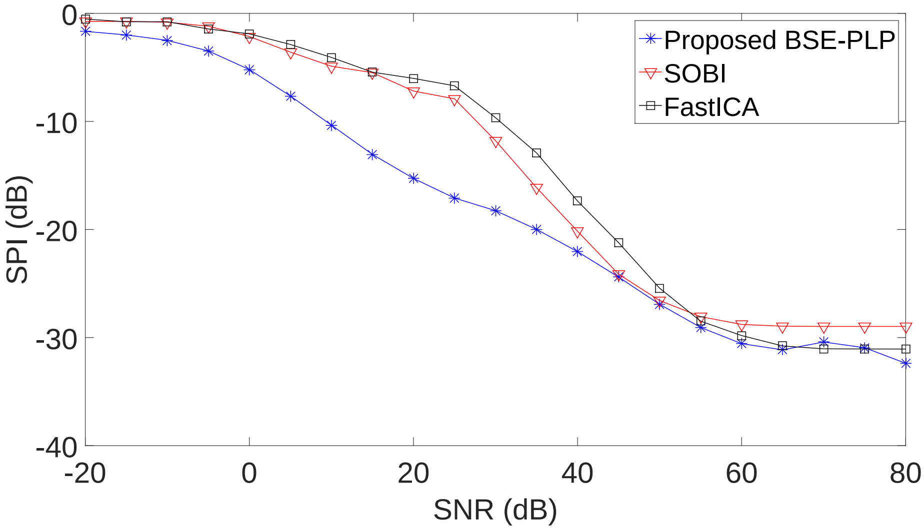

(a)

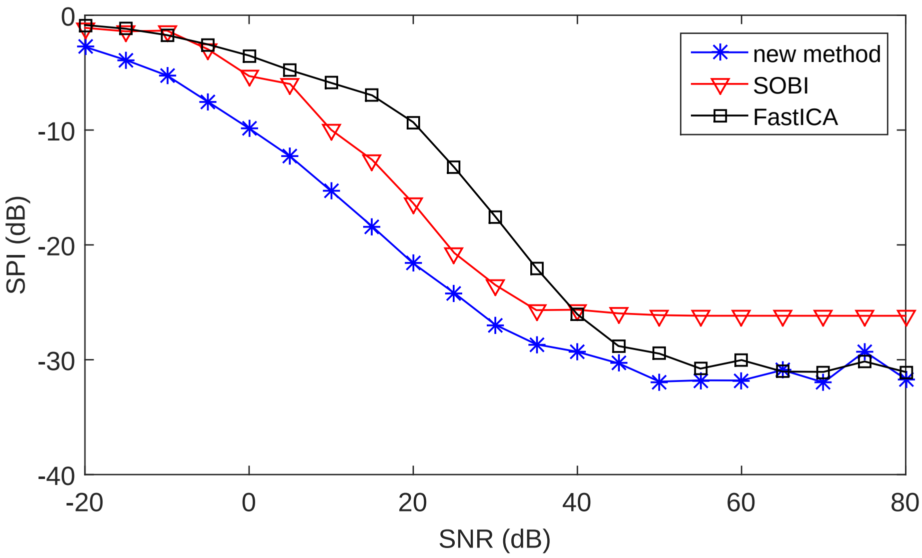

(b)

FIGURE 2.8: SPI versus SNR for the Proposed BSE-PLP (Algorithm 2), SOBI, and FastICA methods (a)Assuming stationary additive WGN (b)Assuming non stationary additive WGN

TABLE 2.1: Comparison between SIR, SAR, and SDR, using the proposed BSE-PLP (Algorithm 2), SOBI, and FastICA algorithms. Assuming stationary additive WGN

	Algorithm	SNR = 10 dB	SNR = 20dB	SNR = 40 dB	Noiseless case
SIR (dB)	SOBI	1.56	20.6	28.5	28.7
	FastICA	−4.6	10.04	33.5	33.9
	Proposed BSE-PLP	7.99	24.7	34.03	34.1
SAR (dB)	SOBI	9.2	8.5	31.04	180.1
	FastICA	−0.89	4.5	22.7	55.08
	Proposed BSE-PLP	10.6	14.6	34.1	183.6
SDR (dB)	SOBI	0.356	8.09	26.39	28.3
	FastICA	−9.14	2.61	21.69	31.24
	Proposed BSE-PLP	2.65	14.2	30.8	32.3

TABLE 2.2: Comparison between SIR, SAR, and SDR, using the proposed BSE-PLP (Algorithm 2), SOBI, and FastICA algorithms. Assuming non stationary additive WGN

	Algorithm	SNR = 10 dB	SNR = 20dB	SNR = 40 dB	Noiseless case
SIR (dB)	SOBI	24.9	26.9	27.01	27.13
	FastICA	5.75	22.1	35.3	35.76
	Proposed BSE-PLP	25.89	27.03	35.74	36.8
SAR (dB)	SOBI	12.7	12.71	41.36	179.02
	FastICA	2.67	7.12	26.2	41.17
	Proposed BSE-PLP	17.7	23.22	44.84	181.14
SDR (dB)	SOBI	12.3	12.46	26.41	27.13
	FastICA	−2.57	6.9	25.5	30.6
	Proposed BSE-PLP	16.53	21.66	29.01	30.88

2.5 Conclusion

A novel BSE algorithm, referred to as BSE-PLP, has been presented. The model combined the source extraction and noise cancellation in one framework. The design problem has been formulated and an analysis has also been provided, with mathematical proofs. The interchangeability between the mixture input $\mathbf{X}(n)$ (the normal BSE input) with the $\mathbf{R}(n)$ matrix has an impact on fixing the eigenvalues and power input to the filter, thus making the learning rate μ constant for noiseless case, or dependable only on the input noise power, for noisy case. The proposed algorithm converged very fast in 2 iterations for different filter lengths. Simulation results have shown that the proposed algorithm significantly separated the source signals when the SNR varied from -20 dB to 80 dB. The algorithm performance indices SPI, SIR, SAR and SDR were provided and were shown considerable improvement as compared to SOBI and FastICA algorithms.

Bibliography

[1] Bousse, M., Debals, O. and De Lathauwer, L., 2017. A tensor-based method for large-scale blind source separation using segmentation. IEEE Transactions on Signal Processing, 65(2), pp.346-358.

[2] Debals, O., Van Barel, M. and De Lathauwer, L., 2016. Löwner-Based Blind Signal Separation of Rational Functions With Applications. IEEE Trans. Signal Processing, 64(8), pp.1909-1918.

[3] Lu, X., Li, X., Fu, M.S. and Wang, H., 2017. Robust maximum signal fraction analysis for blind source separation. IET Signal Processing, 11(8), pp.969-974.

[4] Lu, S., Wang, W. and Wang, G., 2017. Stationary Points of a Kurtosis Maximization Criterion for Noisy Blind Source Extraction. IEEE Access, 5, pp.8736-8740.

[5] Ferdowsi, S., Sanei, S., Abolghasemi, V., Nottage, J. and O'Daly, O., 2013. Removing ballistocardiogram artifact from EEG using short-and long-term linear predictor. IEEE Transactions on Biomedical Engineering, 60(7), pp.1900-1911.

[6] Wang, G., Zhang, Y., He, B. and Chong, K.T., 2016. A framework of target detection in hyperspectral imagery based on blind source extraction. IEEE journal of selected topics in applied earth observations and remote sensing, 9, pp.835-844.

[7] Ayon, J.J. and Narasimhan, S., 2015, July. Using an on-line BSE technique for wide-area oscillations monitoring. In Power and Energy Society General Meeting, 2015 IEEE (pp. 1-5). IEEE.

[8] Liu, B., Reju, V.G. and Khong, A.W., 2014. A linear source recovery method for underdetermined mixtures of uncorrelated AR-model signals without sparseness. IEEE Transactions on Signal Processing, 62(19), pp.4947-4958.

[9] Tengtrairat, N., Woo, W.L., Dlay, S.S. and Gao, B., 2016. Online Noisy Single-Channel Source Separation Using Adaptive Spectrum Amplitude Estimator and Masking. IEEE Trans. Signal Processing, 64(7), pp.1881-1895.

[10] Li, G. and Lyu, S., 2015. Extracting chaotic signal from noisy environment: a random searching method. Chinese Journal of Electronics, 24(3), pp.584-589.

[11] Cichocki, A. and Amari, S.I., 2002. Adaptive blind signal and image processing: learning algorithms and applications (Vol. 1). John Wiley and Sons.

[12] Liu, W., Mandic, D.P. and Cichocki, A., 2007. Blind source extraction based on a linear predictor. IET Signal Processing, 1(1), pp.29-34.

[13] Liu, W., Mandic, D.P. and Cichocki, A., 2008, July. A dual-linear predictor approach to blind source extraction for noisy mixtures. In Sensor Array and Multichannel Signal Processing Workshop, 2008. SAM 2008. 5th IEEE (pp. 515-519). IEEE.

[14] Mandic, D.P. and Cichocki, A., 2003, April. An online algorithm for blind extraction of sources with different dynamical structures. In Proc. of the 4th Int. Conf. on Independent Component Analysis and Blind Signal Separation (ICA 2003)(pp. 645-650).

[15] Hyvärinen, A., 2001. Complexity pursuit: separating interesting components from time series. Neural computation, 13(4), pp.883-898.

[16] Ahmadian, P., Sanei, S., Ascari, L., González-Villanueva, L. and Umiltà, M.A., 2013. Constrained blind source extraction of readiness potentials from EEG. IEEE Transactions on Neural Systems and Rehabilitation Engineering, 21(4), pp.567-575.

[17] Puntanen, S., 2007. Matrix Algebra: Theory, Computations, and Applications in Statistics by James E. Gentle. International Statistical Review, 75(3), pp.435-435.

[18] Bose, T. and Meyer, F., 2003. Digital signal and image processing. John Wiley and Sons, Inc..

[19] Romano, J.M.T., Attux, R., Cavalcante, C.C. and Suyama, R., 2016. Unsupervised signal processing: channel equalization and source separation. CRC Press.

[20] Johnson, R.A. and Wichern, D.W., 2002. Applied multivariate statistical analysis (Vol. 5, No. 8). Upper Saddle River, NJ: Prentice hall.

[21] Taha, A.L., Taha, L.Y. and Abdel-Raheem, E., 2015, December. FastICA architecture utilizing FPGA and iterative symmetric orthogonalization for multivariate signals. In Signal Processing and Information Technology (ISSPIT), 2015 IEEE International Symposium on (pp. 279-284). IEEE.

[22] Hsu, S.H., Mullen, T.R., Jung, T.P. and Cauwenberghs, G., 2016. Real-time adaptive EEG source separation using online recursive independent component analysis. IEEE transactions on neural systems and rehabilitation engineering, 24(3), pp.309-319.

[23] Albera, L., Kachenoura, A., Comon, P., Karfoul, A., Wendling, F., Senhadji, L. and Merlet, I., 2012. ICA-based EEG denoising: a comparative analysis of fifteen methods. Bulletin of the Polish Academy of Sciences: Technical Sciences, 60(3), pp.407-418.

[24] Javidi, S., Mandic, D.P. and Cichocki, A., 2010. Complex blind source extraction from noisy mixtures using second-order statistics. IEEE Transactions on Circuits and Systems I: Regular Papers, 57(7), pp.1404-1416.

[25] Vincent, E., Gribonval, R. and Févotte, C., 2006. Performance measurement in blind audio source separation. IEEE transactions on audio, speech, and language processing, 14(4), pp.1462-1469.

[26] Fevotte, C., Gribonval, R. and Vincent, E., 2005. BSS-EVAL toolbox user guide–Revision 2.0.

[27] Kemiha, M. and Kacha, A., 2017. Complex blind source separation. Circuits, Systems, and Signal Processing, 36(11), pp.4670-4687.

Chapter 3

Extraction of Fetal Electrocardiogram Signals Using BSE Based PLP

3.1 Introduction

The Fetal Electrocardiogram (FECG) have been used to provide description on the electrical activity of the fetal heart. Monitoring FECG is useful to early diagnosis the cardiovascular disorder states[1–3].
Different approaches of FECG extraction were reported in the literature such as principle component analysis (PCA), independent component analysis (ICA), singular value decomposition (SVD), wavelet transform, blind source separation (BSS), blind source extraction (BSE), least mean squares (LMS), artificial neural networks (ANN), and Kalman filters[3–7]. Some of existing works used LMS with adaptive noise cancellation techniques and the wavelet transform technique. Also the accuracy, sensitivity and positive predictive value are also determined for fetal QRS detection technique [2]. The work in [7] proposed using the compressive

sensing (CS) theory, for the compression and joint detection and classification of mother and fetal heart beats. The scheme was based on the sparse representation of the components derived from ICA. In [8], a non-linear multi-sensory adaptive noise canceller (ANC, MsANC) with both multi-primary and multi-reference channels was proposed for FECG extraction. The primary channels are connected by a linear combiner (LC) whose output serves as a primary signal for the whole MsANC. A new method of using the kernel non-linear PCA was proposed in [9] to extract the non-linear PCs from multidimensional data then estimate the foetal ECG signal precisely. The work in [10] presented a new method of FECG extraction by subtracting the mapped thoracic signal from an abdominal signal. The singular value decomposition (SVD) and smooth window (SW) techniques were combined to build a reference signal in an ANC and used for FECG signal extraction in [11]. The work in [12] presented a method of estimating the fetal heart rate (FHR) using sequential total variation denoising and compare its performance with that of other single-channel fetal ECG extraction methods via simulation using the Fetal ECG Synthetic Database.

The aim of this chapter is to investigate the FECG extraction using our proposed BSE-PLP method [13], presented in chapter 2. The method is tested by simulation using synthesized and real ECG signals.

3.2 Simulation and results

Three different simulations are provided in this section. The fist simulation synthesizes the ECG signal using [15] then extracts the FECG signals using BSE-PLP algorithm. The second simulation uses real data from DAISY (Database for the Identification of Systems) [16] as ECG mixture signals, then extracts the FECG signals. Both simulations use four ECG source signals, two MECG and two FECG signals. The second simulation is repeated using PCA, FastICA, and SOBI, for comparison purposes. These algorithms are popular and are successful in extracting signals from input mixture [14]. The third simulation is similar to the second simulation but intended to evaluate the extracting metrics of all algorithms used in this chapter. All simulations were carried out using Matlab.

3.2.1 FECG extraction using synthesized ECG data

Four ECG signals (two MECG and two FECG) are generated using MatLab so that the MECG and the FECG frequencies are 82 Hz and 140 Hz, respectively. Number of samples is selected as $N = 500$. Then, the signals are mixed by a randomly generated mixing matrix $\mathbf{A}$. BSE-PLP algorithm is then applied to extract the FECG signals.
Fig. 3.1 illustrates the synthesized MECG and FECG signals that models the QRS complexes. Fig. 3.2 illustrates the synthesized ECG mixture. Fig. 3.3 illustrates the extracted signals. Comparing the results from Fig. 3.1 and Fig. 3.3, its is clear that the BSE-PLP algorithm is successfully extracting MECG and FECG signals from their mixture, since the extracted signals $\mathbf{y}_1(n), \mathbf{y}_2(n), \mathbf{y}_3(n)$ match the original signals $\mathbf{s}_1(n), \mathbf{s}_2(n), \mathbf{s}_3(n)$.

3.2.2 FECG extraction using real ECG data

A 9 channels data (three from abdominal and 6 from thorax) were recorded from pregnant women for 10s. The sampling frequency was 250 Hz. However, only the first 500 samples were used for simulation. Also, only four mixture ECG signals (three abdominal and one thorax) were used in this simulation. Then, BSE-PLP, PCA, FastICA, and SOBI algorithms were applied to extract the FECG signals.

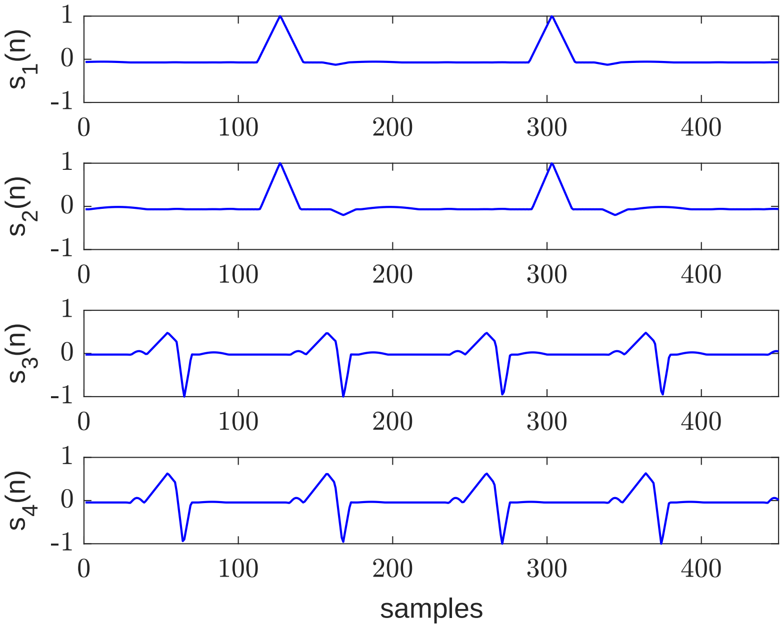

FIGURE 3.1: Synthesized MECG and FECG signals.

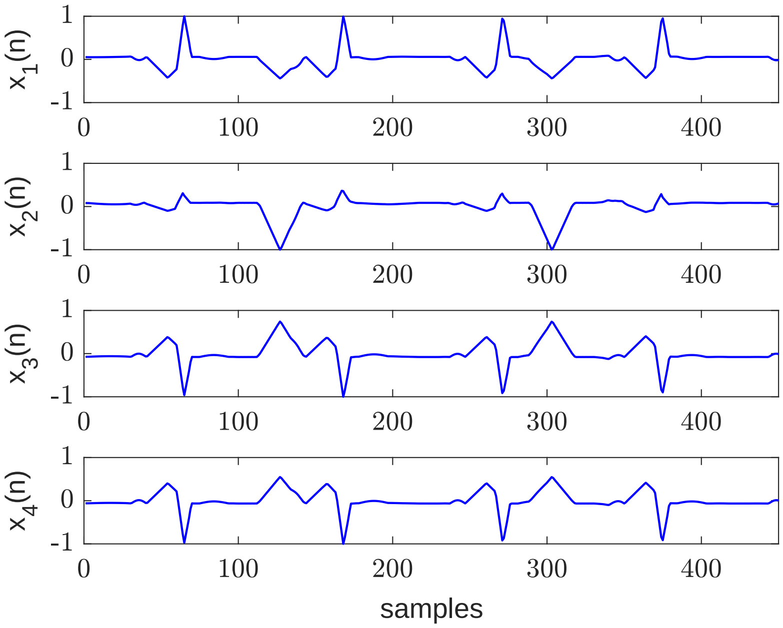

FIGURE 3.2: Synthesized ECG mixture.

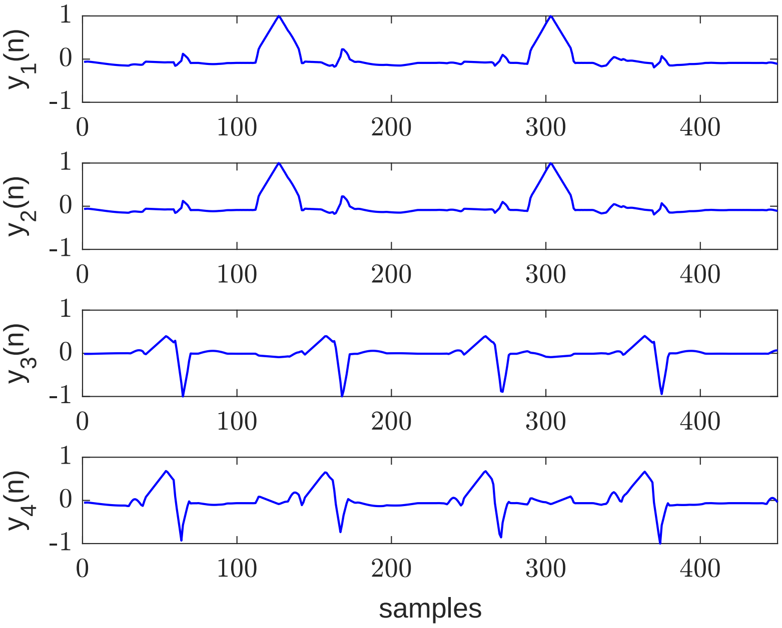

FIGURE 3.3: Extracted MECG and FECG signals using BSE-PLP algorithm.

Fig. 3.4 illustrates the recorded ECG signals. Fig. 3.5–3.8 illustrate the extracted ECG signals using all selected algorithms. Several conclusions were recorded from the results. First, from Fig. 3.4–3.5, its is clear that the BSE-PLP algorithm is successfully extracting all MECG and FECG signals from their mixture. This conclusion was also drawn in Section 5.5.1. Thus, the BSE-PLP algorithm can be used to extract both MECG and FECG signals from synthesized and real ECG data. Second, from Fig. 3.4, 3.6, the PCA algorithm shows also a successful extraction of the ECG signals. However, the extracted signal $\mathbf{y}_1(n)$ contains large amount of noise. Thus, $\mathbf{y}_1(n)$ cannot be considered as an extracted signal without further denoising process. Third, from Fig. 3.4, 3.7–3.8, both FastICA and SOBI algorithms are able to extract the three signals $\mathbf{y}_1(n)$–$\mathbf{y}_3(n)$. However, they failed in extracting the FECG signal $\mathbf{y}_4(n)$. Forth, the BSE-PLP algorithm shows a considerable improvement, in signal extraction, as compared with PCA, FastICa, and SOBI algorithms.

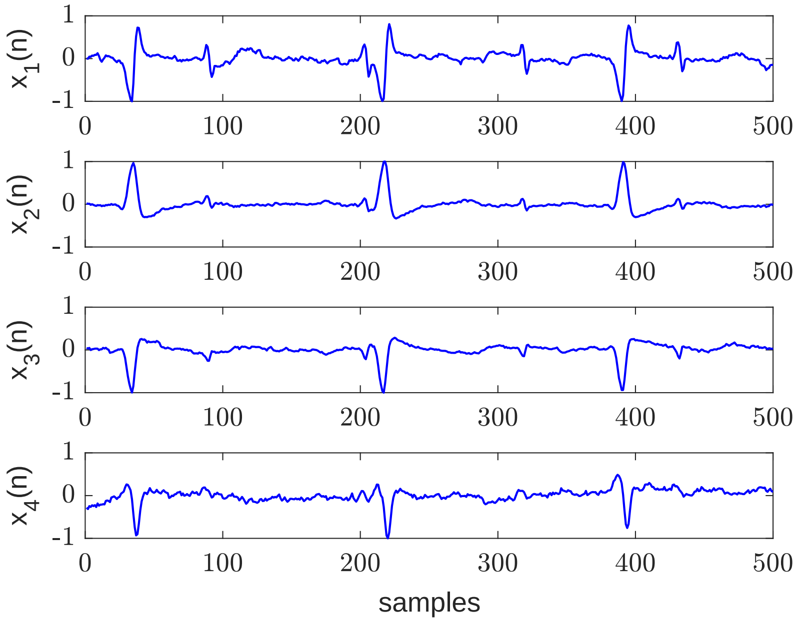

FIGURE 3.4: Recorded ECG signals.

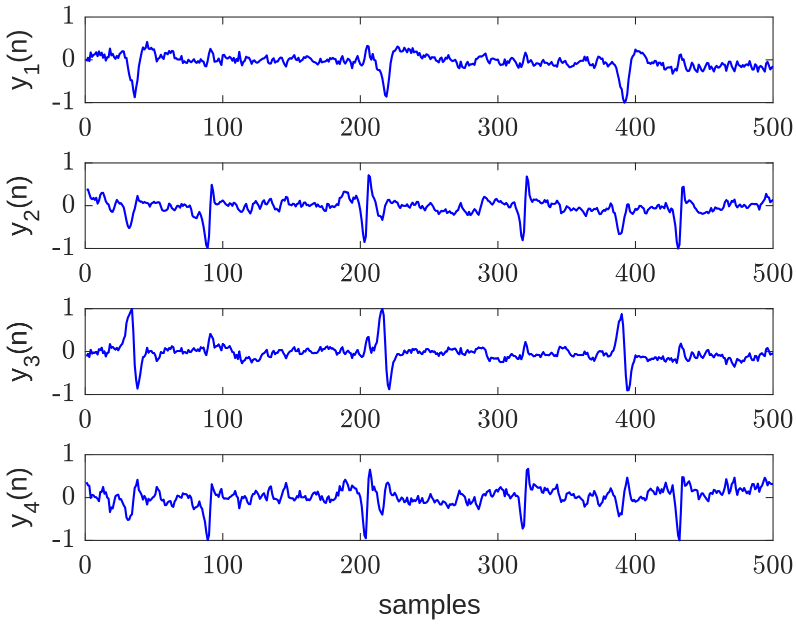

FIGURE 3.5: Extracted ECG signals using BSE-PLP algorithm.

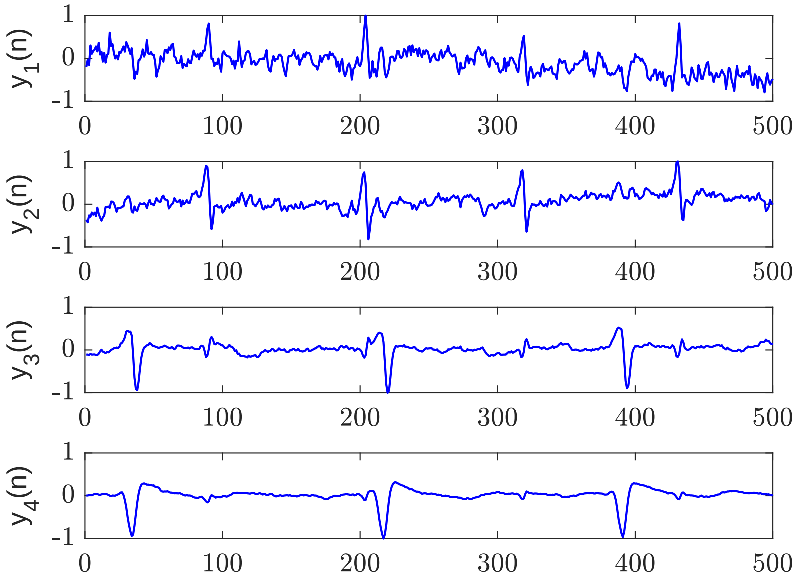

FIGURE 3.6: Extracted ECG signals using PCA.

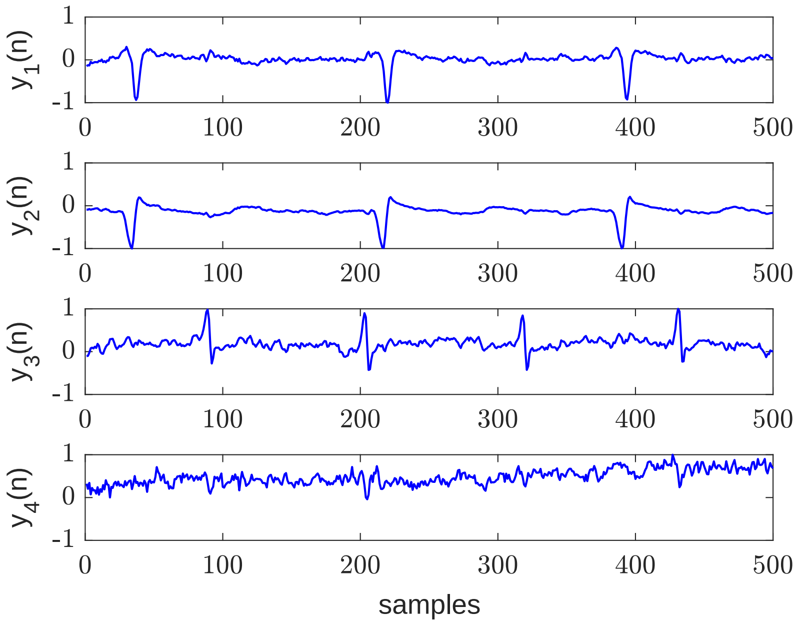

FIGURE 3.7: Extracted ECG signals using FastICA.

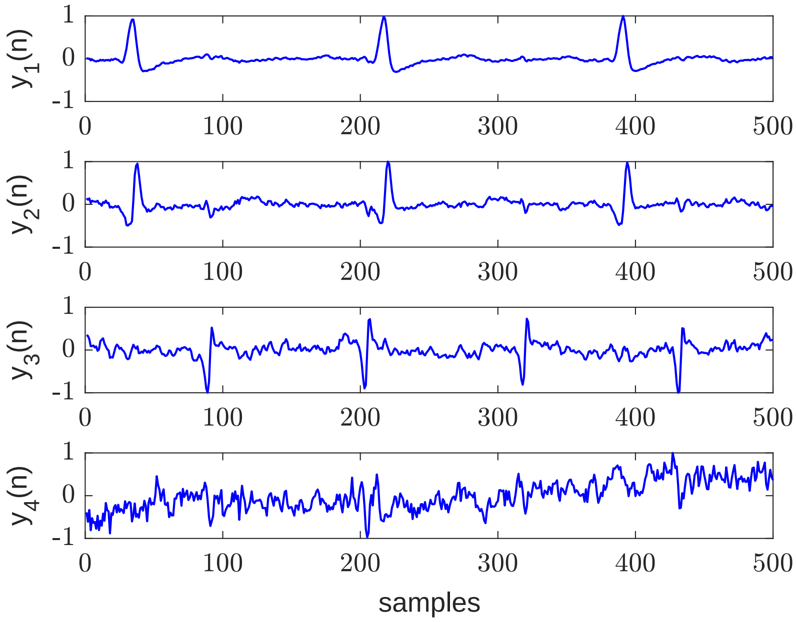

FIGURE 3.8: Extracted ECG signals using SOBI.

3.2.3 FECG evaluation metrics

In this simulation, we used the same ECG data in Section 3.2.2 with $N = 2500$, i.e, covers all the 10s data length. To evaluate extracting process, the sensitivity (SE) and accuracy (ACC) are being used for R-peaks detection [2, 3]. Defining NOP, TP, FN, and FP as number of peaks, true positive, false negative, and false positive, respectively, the SE and Acc are computed as follows:

$$SE\ \% = \frac{TP}{TP + FN} \times 100\% \tag{3.1}$$

$$ACC\ \% = \frac{TP}{TP + FN + FP} \times 100\% \tag{3.2}$$

We follow the same simulation procedure as in Section 3.2.2 then measure SE and ACC using (3.1) and (3.2), respectively. The NOP in the extracted FECG is found to be 22 using all algorithms. Results are show in Table 3.1. From the results, it is clear that the BSE-PLP algorithm scores the highest values in SE and ACC. Thus, BSE-PLP algorithms has significant improve in FECG signal detection as compared with other algorithms used in this chapter.

TABLE 3.1: Evaluation of detected peaks

Algorithm	**NOP**	**TP**	**FP**	**FN**	**SE(%)**	**Acc(%)**
PCA	22	19	3	3	86.36	76
FastICA	22	20	2	2	90.9	83.3
SOBI	22	20	3	2	90.9	80
BSE-PLP	22	21	1	1	95.45	91.3

3.3 Conclusion

The BSS linear model has been used in this chapter to model the ECG signal. The design problem has been formulated and the mathematical equations used for FECG extraction and evaluation have also been provided. The BSE-PLP algorithm is applied to extract the FECG signals using both synthesized and real ECG data. A successful extraction of FECG and MECG signals have recorded for four synthesized ECG data consisting of two MECG and two FECG data. The success was also recorded when applying four real ECG data (three from abdominal and one from thorax). The evaluation of R-peaks using BSE-PLP algorithm has been investigated in this chapter, and based on the SE and ACC extracing metrics. Results have shown considerable improvement as compared to PCA, FastICA, and SOBI algorithms.

Bibliography

[1] Da Poian, G., Rozell, C.J., Bernardini, R., Rinaldo, R. and Clifford, G.D., 2018. Matched filtering for heart rate estimation on compressive sensing ECG measurements. IEEE Transactions on Biomedical Engineering, 65(6), pp.1349-1358.

[2] Sutha, P. and Jayanthi, V.E., 2018. Fetal electrocardiogram extraction and analysis using adaptive noise cancellation and wavelet transformation techniques. Journal of medical systems, 42(1), p.21.

[3] Martinek, R., Kahankova, R., Skutova, H., Koudelka, P., Zidek, J. and Koziorek, J., 2016, July. Adaptive signal processing techniques for extracting abdominal fetal electrocardiogram. In 2016 10th International Symposium on Communication Systems, Networks and Digital Signal Processing (CSNDSP)(pp. 1-6). IEEE.

[4] Taha, A.L., Taha, L.Y. and Abdel-Raheem, E., 2015, December. FastICA architecture utilizing FPGA and iterative symmetric orthogonalization for multivariate signals. In 2015 IEEE International Symposium on Signal Processing and Information Technology (ISSPIT) (pp. 279-284). IEEE.

[5] Jagannath, D.J. and Selvakumar, A.I., 2014. Issues and research on foetal electrocardiogram signal elicitation. Biomedical signal processing and control, 10, pp.224-244.

[6] Ferdowsi, S., Sanei, S., Abolghasemi, V., Nottage, J. and O'Daly, O., 2013. Removing ballistocardiogram artifact from EEG using short-and long-term linear predictor. IEEE Transactions on Biomedical Engineering, 60(7), pp.1900-1911.

[7] Da Poian, G., Bernardini, R. and Rinaldo, R., 2016. Separation and analysis of fetal-ECG signals from compressed sensed abdominal ECG recordings. IEEE Transactions on Biomedical Engineering, 63(6), pp.1269-1279.

[8] Ma, Y., Xiao, Y., Wei, G. and Sun, J., 2017. Foetal ECG extraction using non-linear adaptive noise canceller with multiple primary channels. IET Signal Processing, 12(2), pp.219-227.

[9] Xueyun, W. and Wei, Z., 2018. Application of kernel PCA for foetal ECG estimation. Electronics Letters, 54(6), pp.340-342.

[10] Wei, Z., Xiaolong, L., Xueyun, W. and Hongxing, L., 2015. Foetal ECG extraction by support vector regression. Electronics Letters, 52(7), pp.506-507.

[11] Zhang, N., Zhang, J., Li, H., Mumini, O., Samuel, O., Ivanov, K. and Wang, L., 2017. A novel technique for fetal ECG extraction using single-channel abdominal recording. Sensors, 17(3), p.457.

[12] Lee, K. and Lee, B., 2016. Sequential total variation denoising for the extraction of fetal ECG from single-channel maternal abdominal ECG. Sensors, 16(7), p.1020.

[13] Taha, L.Y. and Abdel-Raheem, E., 2018. Efficient blind source extraction of noisy mixture utilising a class of parallel linear predictor filters. IET Signal Processing, 12(8), pp.1009-1016.

[14] Hyvarinen, A., Karhunen, J. and Oja, E., 2001. Independent component analysis and blind source separation.

[15] https://www.mathworks.com/matlabcentral/leexchange/10858-ecg-simulation-usingmatlab

[16] http://homes.esat.kuleuven.be/smc/daisy/daisydata.html

Chapter 4

Blind Source Extraction Using Idempotent Transformation Matrix (BSE-ITM)

4.1 Introduction

Blind source separation (BSS) is aimed to reconstruct some unobserved sources from a set of observed signals without prior knowledge of the source signals or the mixture [1, 2]. In many applications, one or limited source signals are only required for extractions. Thus, Blind source extraction (BSE) is used for these purposes [3, 4]. BSE has the merits of low computation complexity and greater flexibility [3]. Applications of BSS/BSE can be found in telecommunications, speech signal processing, astronomical imaging, biomedical sciences, machine learning, audio signal separation, mechanical signal separation and machine fault diagnosis [5–13].

Different approaches of BSS and BSE were reported in the literature, such as independent component analysis (ICA) [7, 9, 11, 14], linear prediction [15–18], SOBI [19], Null Space Component analysis (NCA) [5], non-negative matrix factorization

(NMF) [20], and sparse component analysis (SCA) [21].

In BSS/ICA technique, the observed data are whitened to make the data uncorrelated.Then, higher-order statistics are used to minimized the cost function and address the independent sources. FastICA uses non-Gaussianity measures to minimize the statistical independence of the estimated source data [14].

The computational complexity is a challenging factor that must be considered in these approaches. Furthermore, in BSE type linear prediction, the input source signals power, the methods of updating filter coefficients and the length of adaptive filter must also be considered [4, 6, 15, 18, 22, 23].

BSS algorithm complexity is also affected by number of unknown sources and mixture. If the later is greater than the former, the problem is denoted as over determined BSS problem and can be solved by all BSS approaches. Otherwise, the problem becomes complex and denoted as under-determined BSS problem since the mixing matrix becomes non-invertible [23].

This work presents a method of BSE-based on idempotent transformation matrix (ITM). First, a computationally efficient algorithm is designed to compute the matrix without using SVD. Next, optimization is carried out by an iterative algorithm based on least mean squares (LMS) and block LMS (BLMS) [24], with low computational complexity. The filter coefficients are updated from the elements of the ITM, and not from the output error. This drastically reduces the filter length problems, increases its error convergence, and reduces the system complexity. The proposed method is applied to separate speech and white Gaussian signals. Simulation is provided to investigate the performance measure of extraction.

The paper is organized as follows. Section 4.2 presents the theory of the BSE problem that is based on linear prediction. The computational complexity of the proposed ITM using new iterative algorithm based on ITM properties is provided in Section 4.3, and compared with SVD. Section 4.4 explains full analysis of the proposed BSE-ITM model and a comparison with the state of the arts models in terms of the length of the filter and the methods of using the predication error in updating the filter coefficient. A computationally efficient BSE-ITM algorithm using BLMS is also provided, and compared with LMS algorithm. The performance of the proposed BSE-ITM model using BLMS algorithm is tested for evaluation in Sect. 4.5. This includes error analysis of computing the ITM using SVD and the proposed algorithm, quality of separation, and convergence analysis of the proposed algorithm. Section 4.6 is devoted to concluding remarks.

4.2 BSE-based linear prediction

In BSS/BSE problem, the instantaneous noiseless mixture equation can be modeled by [1, 25]

$$\mathbf{X}(m) = \mathbf{AS}(m), \tag{4.1}$$

where $\mathbf{X}(m)$ is the mixture matrix, equal to $[\mathbf{x}_1(m), \mathbf{x}_2(m), \ldots, \mathbf{x}_M(m)]^T$, m is the sampling index, M is the number of mixture vectors, $\mathbf{x}_i(m)$ is the i^{th} zero mean mixture vector such that $\mathbf{x}_i(m) = [x_i(m), x_i(m-1), \ldots, x_i(m-N+1)], i = 1, 2, \ldots, M$; N is the number of samples, $\mathbf{A}$ is an unknown full rank $M \times L$ mixing matrix, L is the number of unknown sources, and $\mathbf{S}(m)$ is the unknown source matrix consisting of L zero mean vectors, equal to $[\mathbf{s}_1(m), \mathbf{s}_2(m), \ldots, \mathbf{s}_L(m)]^T$, $\mathbf{s}_j(m)$ is the j^{th} source vector such that $\mathbf{s}_j(m) = [s_j(m), s_j(m-1), \ldots, s_j(m-N+1)], j = 1, 2, \ldots, L$. The goal of the BSS problem is to estimate $\mathbf{A}$ and $\mathbf{S}(m)$ from the knowledge of $\mathbf{X}(m)$. However, and as mentioned in Section 5.1, BSE can be used to extract one or limited source signals. In this paper, only BSE-based algorithms will be considered.

In BSE-based linear predication, the goal is to find one source signal, defined by $y_j(m)$ as the extracted (also called the desired) source signal of $s_j(m)$. Then, the general linear prediction problem can be expressed as [6]

$$\begin{aligned} e_j(m) &= y_j(m) - \hat{y}_j(m) \\ &= \sum_{l=1}^{M} z_{jl}(m) x_l(m) - \sum_{p=1}^{K} b_{jp} y_j(m-p) \end{aligned} \tag{4.2}$$

where $e_j(m)$ is the j^{th} prediction error term, $y_j(m)$ is the j^{th} extracted source signal, computed from the unknown demixing vector $[z_{j1}(m), z_{j2}(m), \ldots, z_{jM}(m)]$ and $x_l(m)$, and $\hat{y}_j(m)$ is the j^{th} predicted source signal, computed from b_{jp}, the unknown linear predictor filter weight of index jp, and the delayed $y_j(m)$ signal, with K being the unknown prediction order. Equation (4.2) can be optimized for the unknowns $z_{jl}(m)$ and b_{jp}, $l = 1, 2, \ldots, M, p = 1, 2, \ldots, K$. This method has some challenges. First, the value of the unknown K must be assumed prior to optimization. This affects the performance of the method in extracting signals. Second, the optimization is carried out for two unknowns, $z_{jl}(m)$ and b_{jp}. This adds complexity to both computations and realizations. Thus, developing a new BSE method with fixed prediction filter length and having only one unknown parameter ($z_{jl}(m)$ or b_{jp}) is crucial. These challenges will be considered in our proposed BSE-ITM method discussed in Sections 4.3 -4.4.

4.3 The proposed Idempotent Transformation Matrix (ITM)

4.3.1 Motivation

In this section, we propose a new ITM, named $\mathbf{W}(m)$, that can be efficiently computed from the mixture $\mathbf{X}(m)$ using the algorithm proposed in Section 4.3.2. The $\mathbf{W}(m)$ matrix has a fixed size equal to $N \times N$. Thus, the length of the linear prediction filter K in (4.2) is constant that is equal to N. The q^{th} row, $q = 1, 2, \ldots, N$, in the matrix $\mathbf{W}(m)$ holds the q^{th} linear prediction filter coefficients. Once the $\mathbf{W}(m)$ matrix is computed, the BSE optimization problem will be simplified to a one unknown parameter, named $z_{jl}(m)$. The proposed BSE algorithm based on $\mathbf{W}(m)$ will be discussed in Section 4.4.

4.3.2 Properties and computation of W(m) matrix

Assume that there exists a square matrix $\mathbf{W}(m) \subset \mathbb{R}^{N \times N}$, with entries $[\mathbf{W}]_{q,k} = w_{q,k}, q, k = 1, 2, \ldots, N$, such that $\mathbb{R}$

$$\mathbf{S}(m) = \mathbf{S}(m)\mathbf{W}(m), \tag{4.3}$$

then using the norm inequality

$$\|\mathbf{S}(m)\|_2 \leq \|\mathbf{S}(m)\|_2 \|\mathbf{W}(m)\|_2,$$

hence

$$\|\mathbf{W}(m)\|_2 \leq 1. \tag{4.4}$$

Without loss of generality, we shall assume that $\|\mathbf{W}(m)\|_2 = 1$. Thus, the maximum eigenvalue of $\mathbf{W}(m)$, denoted by $\lambda_{max}[\mathbf{W}(m)]$, is given by

$$\lambda_{max}[\mathbf{W}(m)] = 1. \tag{4.5}$$

Multiplying (4.3) by $\mathbf{S}^T(m)$, we have

$$\mathbf{S}(m)\mathbf{S}^T(m) = \mathbf{S}(m)\mathbf{W}(m)\mathbf{W}^T(m)\mathbf{S}^T(m),$$

hence

$$\mathbf{S}(m) = \mathbf{S}(m)\mathbf{W}(m)\mathbf{W}^T(m), \tag{4.6}$$

and from (4.3) and (4.6), we obtain

$$\mathbf{W}(m) = \mathbf{W}(m)\mathbf{W}^T(m) = \mathbf{W}^2(m), \tag{4.7}$$

thus, $\mathbf{W}$(m) is an idempotent matrix, satisfying also the followings

$$\lambda_q\left[\mathbf{W}(m)\right] = \begin{cases} 1 & \text{for} \quad q = 1, 2, \ldots, L \\ 0 & \text{for} \quad q = L+1, L+2, \ldots, N \end{cases} \tag{4.8}$$

$$\mathbf{tr}[\mathbf{W}(m)] = L, \tag{4.9}$$

where $\mathbf{tr}[.]$ is the trace operator. Next, the summation of row and column elements of $\mathbf{W}(m)$ are investigated. From (4.3), the j^{th} source signal $s_j(m-k+1)$, $j = 1, 2, \ldots, L$, $k = 1, 2, \ldots, N$, is given by

$$s_j(m-k+1) = \sum_{q=1}^{N} w_{q,k} s_j(m-q+1), \tag{4.10}$$

hence

$$\sum_{k=1}^{N} s_j(m-k+1) = \sum_{q=1}^{N}\sum_{k=1}^{N} w_{q,k} s_j(m-q+1). \tag{4.11}$$

Since we assumed that the individual source vectors have zero mean, then $\sum_{k=1}^{N} s_j(m-k+1) = 0$. Thus, using (4.11) and considering that $\mathbf{W}(m)$ is a symmetrical matrix, we have

$$\sum_{k=1}^{N} w_{q,k} = \sum_{k=1}^{N} w_{k,q} = 0, \quad q = 1, 2, \ldots, N, \tag{4.12}$$

thus, each row and column in $\mathbf{W}(m)$ has zero mean value.

Next, we compute the $\mathbf{W}(m)$ matrix. Assume that $\mathbf{A}^{-1}$ is the generalized inverse of $\mathbf{A}$, then from (4.1), $\mathbf{S}(m)$ is given by

$$\mathbf{S}(m) = \mathbf{A}^{-1}\mathbf{X}(m). \tag{4.13}$$

To compute $\mathbf{W}(m)$ matrix, it is required to find a similarity between (4.3) and (4.13). Equation (4.13) can be written as

$$\mathbf{S}(m) = \mathbf{A}^{-1}\mathbf{I}_N\mathbf{X}(m) = \mathbf{A}^{-1}\sigma_x\sigma_x^{-1}\mathbf{X}(m). \tag{4.14}$$

where $\mathbf{I}_N$ is an $N \times N$ identity matrix and σ_x is the $M \times M$ covariance matrix of $\mathbf{X}(m)$, which is computed as in [25]

$$\sigma_x = \mathbf{U}_x\mathbf{D}_x\mathbf{U}_x^T = \frac{1}{N}\mathbf{X}(m)\mathbf{X}^T(m), \tag{4.15}$$

where $\mathbf{U}_x\mathbf{D}_x\mathbf{U}_x^T$ is the SVD of σ_x, $\mathbf{U}_x$ is the $M \times M$ unitary matrix whose columns being the eigenvectors of σ_x, and $\mathbf{D}_x$ is the $M \times M$ diagonal matrix whose diagonal elements are the eigenvalues of σ_x. Then from (4.13)-(4.15) we obtain

$$\mathbf{S}(m) = \frac{1}{N}\mathbf{A}^{-1}\mathbf{X}(m)\mathbf{X}^T(m)\mathbf{U}_x\mathbf{D}_x^{-1}\mathbf{U}_x^T\mathbf{X}(m), \tag{4.16}$$

$$= \mathbf{S}(m)\frac{1}{N}\mathbf{X}^T(m)\sigma_x^{-1}\mathbf{X}(m). \tag{4.17}$$

Comparing (4.3) with (4.17), the matrix $\mathbf{W}(m)$ is given by

$$\mathbf{W}(m) = \frac{1}{N}\mathbf{X}^T(m)\sigma_x^{-1}\mathbf{X}(m). \tag{4.18}$$

It is clear from (4.18) that the computation of $\mathbf{W}$(m) involves the product of three matrices with a computational complexity equal to $\mathcal{O}(M^4N^2)$. Also, σ_x^{-1} requires the estimation of the matrices $\mathbf{U}_x$ and $\mathbf{D}_x$ using SVD approach. For example, the computational complexity of SVD using Golub-Reinsch algorithm is $\mathcal{O}(6N^3 +$

$\frac{14}{3}N^3$) [26]. Various methods for reducing the SVD computational complexity were reported in the literature [27, 28]. However, the reduction is not significant and still the computational burden for implementing SVD is a challenging task. In [29], the BSS-null space approach was used to compute $\mathbf{W}(m)$. The null space involves the computations of eigenvalues and eigenvectors of $\mathbf{W}(m)$ using SVD. This method has the same computational complexity encountered in (4.18). Thus, finding an alternative method of computing $\mathbf{W}(m)$ with less computational complexity is crucial.

In this paper, we propose an iterative method for estimating $\mathbf{W}(m)$ without using SVD. The method applies the properties of this matrix, depicted in this section, using the following derivations:

From (4.1)-(4.3), we can write

$$\begin{aligned}
\mathbf{X}(m) &= \mathbf{A}\mathbf{S}(m)\mathbf{W}(m), \\
&= \mathbf{X}(m)\mathbf{W}(m), && (4.19) \\
\mathbf{E}_r^x &= \mathbf{X}(m) - \mathbf{X}(m)\mathbf{W}(m), && (4.20) \\
\epsilon_x(m) &= \frac{1}{MN}\sum_{i=1}^{M}\sum_{k=1}^{N}\upsilon_{ik}^2(m), && (4.21)
\end{aligned}$$

where $\mathbf{E}_r^x$ is the $M \times N$ error matrix between $\mathbf{X}(m)$ and $\mathbf{X}(m)\mathbf{W}(m)$, with entries $[\mathbf{E}]_{i,k} = \upsilon_{i,k}, i = 1, 2, \ldots, M, k = 1, 2, \ldots, N$, and $\epsilon_x(m)$ is the mean squares error (MSE) of $\mathbf{E}_r^x(m)$. The computational complexity of (4.21) is $\mathcal{O}(M^2N^2)$.

Next, we define $\mathbf{W}(m)$ using SVD, as follows

$$\mathbf{W}(m) = \mathbf{U}_w\mathbf{D}_w\mathbf{V}_w^T, \tag{4.22}$$

where $\mathbf{U}_w$ and $\mathbf{V}_w$ are $N \times N$ unitary matrices, and $\mathbf{D}_w$ is a $N \times N$ diagonal matrix, whose diagonal elements being the eigenvalues of $\mathbf{W}(m)$ according to (4.8). Then, from (4.7)-(4.8), (4.22), and considering that $\mathbf{V}_w^T\mathbf{V}_w = I_N$, $\mathbf{D}_w^2 = \mathbf{D}_w$, the matrix

$\mathbf{W}(m)$ can be written as

$$\mathbf{W}(m) = \mathbf{U}_w \mathbf{D}_w \mathbf{U}_w^T. \tag{4.23}$$

As the elements of $\mathbf{D}_w$ are either 0 or 1, the product $\mathbf{U}_w \mathbf{D}_w$ requires no multiplications, and all its columns, whose index is greater than M, have zero elements. Thus, the computational complexity of (4.23) is reduced to $\mathcal{O}(MN^2)$.

Next, we assume that $\mathbf{W}(m) = [\mathbf{w}_1(m), \mathbf{w}_2(m), \ldots, \mathbf{w}_N(m)]$, where $\mathbf{w}_q(m)$ is the q^{th} row of $\mathbf{W}(m)$, $q = 1, 2, \ldots, N$. Algorithm 3 illustrates the iterative method of computing $\mathbf{W}(m)$. In this algorithm, we assume that the maximum values of $\epsilon_x(m)$ and number of iterations are ϵ_{max} and i_{max}, respectively. In each iteration, $\mathbf{W}(m)$ rows are adjusted such that their mean values become zero. Another update is needed by converting $\mathbf{W}(m)$ to a symmetrical unity norm matrix to satisfy (4.4). The iteration will be repeated till the error $\epsilon_x(m)$ becomes less than ϵ_{max}. Then, the estimated $\mathbf{W}(m)$ and $\epsilon_x(m)$ are recorded as $\widehat{\mathbf{W}}(m)$ and $\hat{\epsilon}_x(m)$, respectively. This algorithm has a computational complexity equal to $\mathcal{O}(M^2N^2 + MN^2)$. Thus, there is a considerable reduction in computations when using this algorithm, as compared with the SVD method in (4.18). Figure 4.1 illustrates a comparison between the variations of numerical complexities of SVD and iterative methods, with N. We assumed that $\epsilon_{max} < 10^{-4}$ and $q_{max} = 3$. The iterative method shows considerable reduction in complexity for all values of N.

4.4 The proposed BSE-ITM algorithm

4.4.1 Motivation

Once the transformation matrix $\mathbf{W}(m)$ is computed, optimization method will be carried out to extract $\mathbf{A}$ and $\mathbf{S}(m)$. In this paper, we use (4.10), (4.18), and Algorithm 3, to develop a new BSE algorithm that extracts one source at a time. The

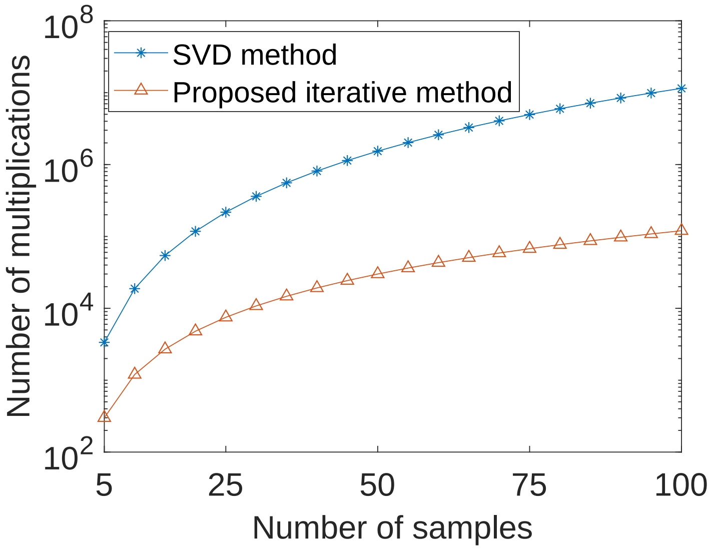

FIGURE 4.1: Numerical complexities of computing $\mathbf{W}(m)$ using SVD and the proposed iterative methods.

Algorithm 3 the proposed iterative method of computing $\mathbf{W}(m)$

Initials N, L, M, m,ϵ_{max}, q_{max}
Read the values of the $M \times N$ mixture matrix $\mathbf{X}$(m).
Compute $\mathbf{D}_w$ by (4.8).
Set $\mathbf{U}_w$ as a random $N \times N$ unitary matrix.
Compute $\mathbf{W}(m)$ by (4.23), as an initial guess.
$q = 1$.
while $q < q_{max}$ **do**
for $j = 1$ to L
    Compute $\mu_w^j(m)$, the mean value of $\mathbf{w}_j(m)$,
    $\mathbf{w}_j(m) = \mathbf{w}_j(m) - \mu_w^j(m)$.
end for
$\|\mathbf{W}(m)\|_2 = \mathbf{tr}[\mathbf{W}(m)]/L$,
$\mathbf{W}(m) = \frac{1}{2}\frac{\mathbf{W}(m)+\mathbf{W}^T(m)}{\|\mathbf{W}(m)\|_2}$
update $\mathbf{E}_r^x$ by (4.20).
update $\epsilon_x(m)$ by (4.21).
if $\epsilon_x(m) < \epsilon_{max}$
    $\widehat{\mathbf{W}}(m) = \mathbf{W}(m)$,
    $\hat{\epsilon}_x(m) = \epsilon_x(m)$,
    exit while.
endif
$q = q + 1$.
end while
Return $\widehat{\mathbf{W}}(m), \hat{\epsilon}_x(m)$

process is repeated to extract another signal. The similarity (correlation) between the two extracted signals is checked to avoid duplication in the extraction. If duplication exists, the extraction and similarity checking is repeated until no similarity is recorded. Similar procedure will be followed for extracting third, fourth, ... signals. Once all source signals are extracted, the process is terminated. Figure 4.2(a) illustrates the block diagram of the proposed BSE-ITM model. We define the de-mixing matrix as $\mathbf{Z}(m) = [\mathbf{z}_1(m), \mathbf{z}_2(m), \ldots, \mathbf{z}_M(m)]^T$, with entries $[\mathbf{Z}]_{jl} = z_{jl}, j = 1, 2, \ldots, L, l = 1, 2, \ldots, M$, where $\mathbf{z}_j(m) = [z_{j1}(m), z_{j2}(m), \ldots, z_{jM}(m)]$ is the j^{th} de-mixing vector. Then from [23], we can write

$$\mathbf{Y}(m) = \mathbf{Z}(m)\mathbf{X}(m), \tag{4.24}$$

where $\mathbf{Y}(m)$ is the $L \times N$ estimated source matrix, which is equal to $[\mathbf{y}_1(m), \mathbf{y}_2(m), \ldots, \mathbf{y}_L(m)]^T$, $\mathbf{y}_j(m)$ is the j^{th} estimated source vector such that $\mathbf{y}_j(m) = [y_j(m), y_j(m-1), \ldots, y_j(m-N+1)], j = 1, 2, \ldots, L$.

The coefficients of the j^{th} FIR filter in Fig. 4.2(a) is assigned by the j^{th} row of the matrix $\mathbf{W}(m)$. As $\mathbf{W}(m)$ has N rows and N columns, the FIR filter has N coefficients, as well. The difference between the j^{th} desired signal $y_j(m)$ (which is the extracted signal) and the predicted signal $\hat{y}_j(m)$ is denoted by the error $e_j(m)$, and used to update $\mathbf{z}_j(m)$. The proposed model is compared with the noiseless BSE models in [15, 17, 25]. These models can be simplified as illustrated in Fig. 4.2(b). The error $e_j(m)$ is used to update both $\mathbf{z}_j(m)$ and the FIR filter coefficients. This adds complexity to the algorithm and needs long iterations till the filter converges. Furthermore, the filter requires different lengths for different extracted signals. However, in the proposed BSE-ITM model, the FIR coefficients are fixed by N and are computed directly from $\mathbf{W}(m)$. This reduces the complexity of the FIR filter.

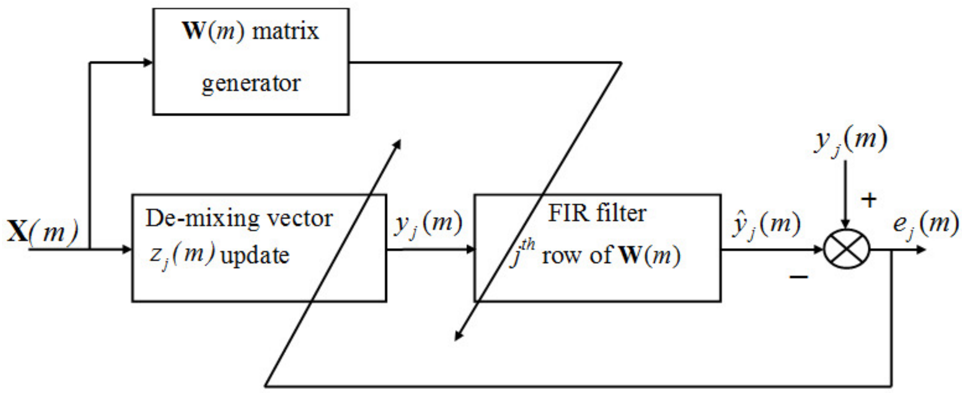

(a) The proposed BSE-ITM model.

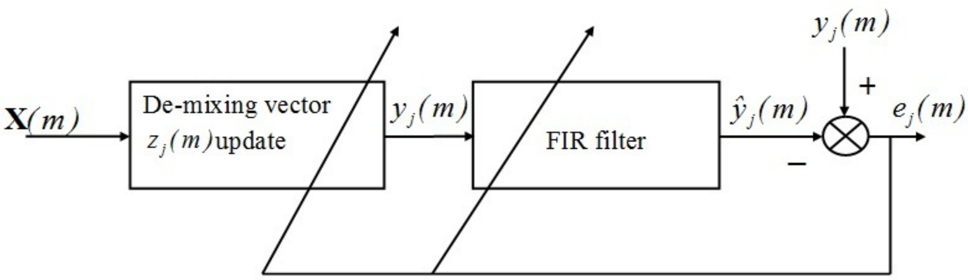

(b) BSE model in [15, 17, 25].

FIGURE 4.2: Comparison between the proposed BSE model and the simplified model for [15, 17, 25]

4.4.2 Optimization analysis

From (4.10) and Fig. 4.2(a), $\hat{y}_j(m)$ can be written as

$$\hat{y}_j(m) = \sum_{q=1}^{N} w_{q,1} y_j(m - q + 1), \tag{4.25}$$

and from (4.24), $y_j(m)$ can be written as

$$y_j(m) = \sum_{l=1}^{M} z_{jl}(m) x_l(m). \tag{4.26}$$

From (4.25) and (4.26), $e_j(m)$ can be evaluated as

$$\begin{aligned} e_j(m) &= y_j(m) - \hat{y}_j(m) \\ &= \sum_{l=1}^{M} z_{jl}(m) x_l(m) - \sum_{q=1}^{N} w_{q,1} \sum_{l=1}^{M} z_{jl}(m-q+1) x_l(m-q+1) \end{aligned} \tag{4.27}$$

Defining the cost function $\mathcal{J}[\mathbf{z}_j(m)]$ using the mean squares prediction error (MSPE) [17], we have

$$\mathcal{J}[\mathbf{z}_j(m)] = \frac{1}{2} e_j^2(m), \tag{4.28}$$

then the weight updates of $\mathbf{z}_j(m)$ can be found by applying the LMS technique [23, 24]. First, the gradient is evaluated as

$$\nabla_{z_{jl}} \mathcal{J}[\mathbf{z}_j(m)] = x_l(m) e_j(m), \tag{4.29}$$

then the update of $\mathbf{z}_j(m)$ is as follows

$$\mathbf{z}_j(m+1) = \mathbf{z}_j(m) - \mu_z \mathbf{x}(m) e_j(m), \tag{4.30}$$

where $\mathbf{x}(m)$ is the mixture vector, equals to $[x_1(m), x_2(m), \ldots, x_M(m)]^T$, and μ_z is the LMS learning rate of $\mathbf{z}_j(m)$, and can be computed as [23]

$$\mu_z = \frac{\alpha}{\|\mathbf{x}(m)\|_2}, \tag{4.31}$$

where α is any number that can be chosen between 0 and 1.

4.4.3 Computational complexity

Assume that the LMS algorithm processes $\mathbf{X}(m)$ mixture which is formed as a block of N samples. Then, from (4.27) and (4.30), the LMS algorithm requires number of real multiplications, denoted as C_{LMS}, given by

$$C_{LMS} = MN^2 + 2MN + N = \mathcal{O}(MN^2). \tag{4.32}$$

To reduce the computational complexity, BLMS technique is used since $\mathbf{z}_j(m)$ will be updated only once per block, instead of at every sample [24]. Following the same procedure as in LMS technique, the coefficient updates will be

$$\mathbf{z}_j(r+1) = \mathbf{z}_j(r) - \frac{\mu_z}{N}\sum_{k=1}^{N} \mathbf{x}_k(rN+k-1)e_j(rN+k-1), \tag{4.33}$$

where the sampling index r is replaced by $rN + k - 1, r = 0, 1, 2, \ldots,$ is the block index, $k = 1, 2, 3, \ldots, N$, is the sampling index defined in each block. From (4.27) and (4.33), the BLMS model requires number of real multiplications, denoted as C_{BLMS}, given by

$$C_{BLMS} = C_{LMS} = 2MN + 2M = \mathcal{O}(MN). \tag{4.34}$$

Comparing (4.32) with (4.34), it is clear that the computational complexity has been drastically decreased if BLMS model is used.

4.4.4 The proposed algorithm

Based on the proposed model discussed in Section 4.4, Algorithm 4 will be applied to extract the $\mathbf{z}_j(m)$ and $\mathbf{y}_j(m), j = 1, 2, \ldots, L$. Maximum number of data samples is assumed to be N_{max}. The input mixture $\mathbf{X}(m)$ is segmented into blocks of length N. First, the algorithm sets the values of N_{max}, j, N, M, $\mathbf{z}_j(m)$, μ_z. Then, iteration starts and the data from the r^{th} block of the mixture, denoted by $\boldsymbol{X}^r$, is captured. $\mathbf{X}^r$ is given by

$$\mathbf{X}^r, r = 0, 1, 2, \cdots = \begin{bmatrix} x_1(rN) & x_1(rN+1) & \cdots & x_1(rN+N-1) \\ x_2(rN) & x_2(rN+1) & \cdots & x_2(rN+N-1) \\ \vdots & \vdots & \vdots & \vdots \\ x_M(rN) & x_M(rN+1) & \cdots & x_M(rN+N-1) \end{bmatrix}. \quad (4.35)$$

Next, steps (6-7) update $\mathbf{W}(m)$, $\mathbf{y}_j(m)$, $\hat{\mathbf{y}}_j(m)$, and $e_j(m)$. steps (8-13) update $\mathbf{z}_j(m)$ according to the type of selected optimization technique (LMS or BLMS). Finally, $\mathbf{z}_j(r+1)$ is normalized to a unit length in step (14) to avoid the critical case where the norm of $\mathbf{z}_j(r+1)$ become too small [30]. Steps (4-16) are repeated till all input blocks are processed.

Algorithm 4 Proposed BSE-ITM algorithm using LMS and BLMS techniques

1: **Initials** N_{max}, j, N, M, $\mathbf{z}_j(m)$, μ_z.
2: **Enter** select.
3: $r = 0$.
4: **while** $r < N_{max}$ **do**
5: Read the r^{th} block of $\mathbf{X}(m)$ by (4.35).
6: update $\mathbf{W}(m)$ by Algorithm 3.
7: update $\mathbf{y}_j(m)$, $\hat{\mathbf{y}}_j(m)$, and $e_j(m)$ in each iteration by (4.26), (4.25), and (4.27), respectively.
8: **if** select = LMS
9: update $\mathbf{z}_j(m)$ in each iteration by (4.30).
10: **elseif** select = BLMS
11: update $\mathbf{z}_j(m)$ in each iteration by (4.33).
12: **else** (wrong selection, go to step 2).
13: **endif**
14: normalize $\mathbf{z}_j(r+1)$.
15: $r = r + 1$.
16: **end while**
17: **Return** $\mathbf{y}_j(m), e_j(m), \mathbf{z}_j(r+1)$.

4.5 Simulation results

In this section, a detailed simulation is provided to test the performance of the proposed algorithms 3-4, used for BSE-ITM. Results of extraction signals were compared with other BSS algorithms such as Principal Component Analysis (PCA) [14], SOBI and FastICA. These algorithms are selected because they become benchmark methods due to their popularity and their success in extracting signals from input mixture [31–33]. The results were also compared with the BSE-parallel linear predictor (PLP) algorithm. The BSE-PLP algorithm is based on interchanging the rules of filter inputs such that the transformation matrix becomes the filter input while the estimated source signals are considered as the parallel filter coefficients [34]. The Results are recorded as the mean values of 100 independent simulations. In all simulation experiments, the mixing matrix $\mathbf{A}$ is randomly generated. Three types of input source signals are used, speech, white Gaussian, and electrocardiogram (ECG) signals, and chosen according to the experiment. The mixture $\mathbf{X}(m)$ is computed by (4.1). The proposed Algorithm 4 is used to extract the sources based on BLMS. All experiments are simulated in MATLAB.

4.5.1 Experiment 1

In this experiment, we test the error in computing $\mathbf{W}(m)$ matrix by two approaches, (4.18) and Algorithm 3. The $\mathbf{W}(m)$ computed by (4.18) is considered as the reference matrix. We use three uncorrelated randomly generated white Gaussian signals as the input sources. The signals are mixed by a randomly generated mixing matrix $\mathbf{A}$. Then, $\mathbf{W}(m)$ matrix is computed by the two approaches. Defining $\mathbf{E}_r^w(m)$ as the error matrix $\mathbf{W}_{\mathrm{SVD}}(m) - \mathbf{W}_{iter}(m)$, where $\mathbf{W}_{\mathrm{SVD}}(m)$ and $\mathbf{W}_{iter}(m)$ are the numerical values of $\mathbf{W}(m)$, computed by (4.18) and algorithm

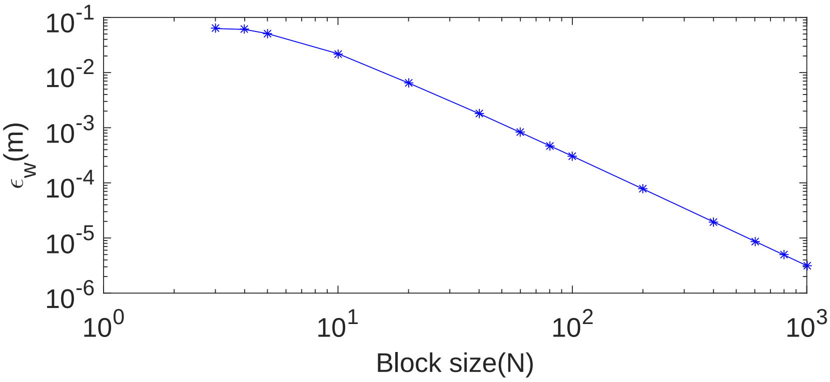

FIGURE 4.3: ϵ_w versus block size.

3, respectively. Then, $\mathbf{E}_r^w(m)$ can be written as

$$\mathbf{E}_r^w(m) = \begin{bmatrix} \hat{w}_{11}(m) & \hat{w}_{12}(m) & \cdots & \hat{w}_{1N}(m) \\ \hat{w}_{21}(m) & \hat{w}_{22}(m) & \cdots & \hat{w}_{2N}(m) \\ \vdots & \vdots & \vdots & \vdots \\ \hat{w}_{N1}(m) & \hat{w}_{N2}(m) & \cdots & \hat{w}_{NN}(m) \end{bmatrix}, \tag{4.36}$$

where $\hat{w}_{qk}(m), q, k = 1, 2, \ldots, N$ is the difference between $w_{qk}(m)$, computed by (4.18), and $w_{qk}(m)$, computed by Algorithm 3. The MSE of $\mathbf{E}_r^w(m)$, defined by $\epsilon_w(m)$, can be computed as

$$\epsilon_w(m) = \frac{1}{N^2} \sum_{q=1}^{N} \sum_{k=1}^{N} \hat{w}_{qk}^2(m). \tag{4.37}$$

The simulation is repeated for different values of the block size N. Results are illustrated in Fig. 4.3. Results indicate that $\epsilon_w(m)$ decreases as N increases. For $N \geq 50$, $\epsilon_w(m)$ will be less than 10^{-3}, which is an acceptable error value. For better accuracy, we may choose $N \geq 100$, thus $\epsilon_w(m)$ will be less than 10^{-4} .

4.5.2 Experiment 2

In this experiment, we investigate the performance of Algorithm 4 for signal extraction. We use three uncorrelated clean speech signals $\mathbf{s}_1(m), \mathbf{s}_2(m)$, and $\mathbf{s}_3(m)$, correspond to three English words $'How'$, $'Seven'$, and $'Electrical'$, respectively. The signals are sampled at 8 kHz, and mixed by a randomly generated mixing matrix $\mathbf{A}$. The values of N_{max} and N are selected to be 12,000 and 200, respectively. The resultant mixture $\mathbf{X}(m)$ is used as an input to Algorithm 4. The $\mathbf{z}_j(m)$ vector is randomly initialized. The simulation extracts one source signal at a time then is repeated to extract other signals. Figure 4.4(a) illustrates the input source signals, while the extracted signals are shown in Fig. 4.4(b).

The simulation is repeated to extract three uncorrelated randomly generated white Gaussian signals, with $N_{max} = 4000$ and $N = 100$. Figure 4.5(a) illustrates portion of the input source signals, while the extracted signals are shown in Figure 4.5(b).

The simulation is also repeated to extract a fetal ECG (FECG) and maternal ECG (MECG) signals, with $N_{max} = 500$ and $N = 100$. As a comparison between the ECG source signals (MECG and FECG) and the extracted signals is required in this experiment, the ECG source signals must be first synthesized [35–37]. The synthesized ECG signals were then mixed by a randomly generated mixing matrix $\mathbf{A}$. We selected in this experiment one MECG signal and one FECG signal. The heart beats of the FECG was assumed to be 140 beats per minute (BPM) while 80 BPM was selected for the MECG signal. We assume that some of the heart beats coincide [4]. The ECG signals were simulated using Matlab [38]. Figure 4.6(a) illustrates the synthesized ECG source signals, while the extracted signals are shown in Fig. 4.6(b).

Results from Fig. 4.4−4.6 indicate that the new algorithm is successfully extracting signals from their mixture.

Next, we test the performance of speech, Gaussian, and ECG signal extraction. We

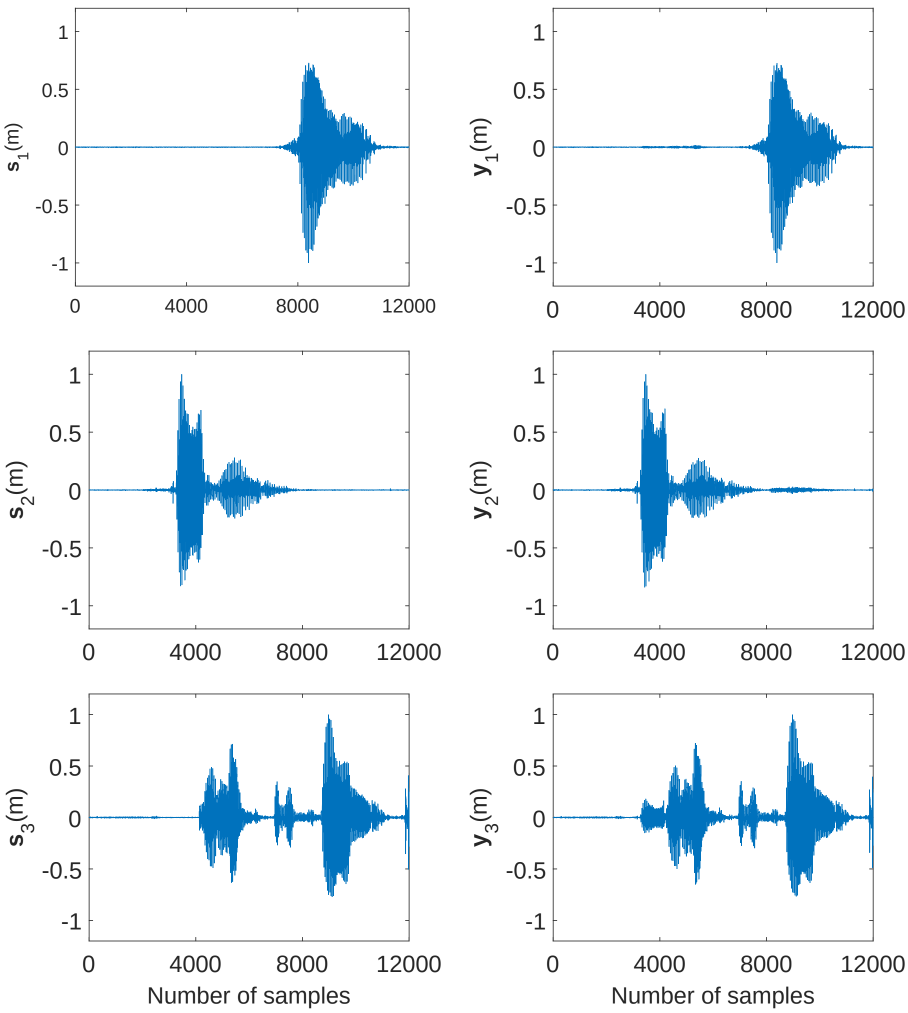

(a) Input source signals $\mathbf{s}_j(m)$, $j = 1, 2, 3$.

(b)Extracted signals $\mathbf{y}_j(m)$, $j = 1, 2, 3$.

FIGURE 4.4: Results of extracting speech signals using the proposed BSE-ITM algorithm based BLMS.

use the same simulation settings for speech, Gaussian and ECG signal extraction as explained in section 4.5.2. In the case of ECG signal extraction, we added one more MECG signal having the same beat rate used in 4.5.2. The extraction performance includes the estimation of the source-to-interference ratio (SIR), the source-to-artifacts ratio (SAR), the source-to-distortion ratio (SDR), and the signal-to-noise ratio (SNR) [22, 39]. These performance measures require first the decomposition

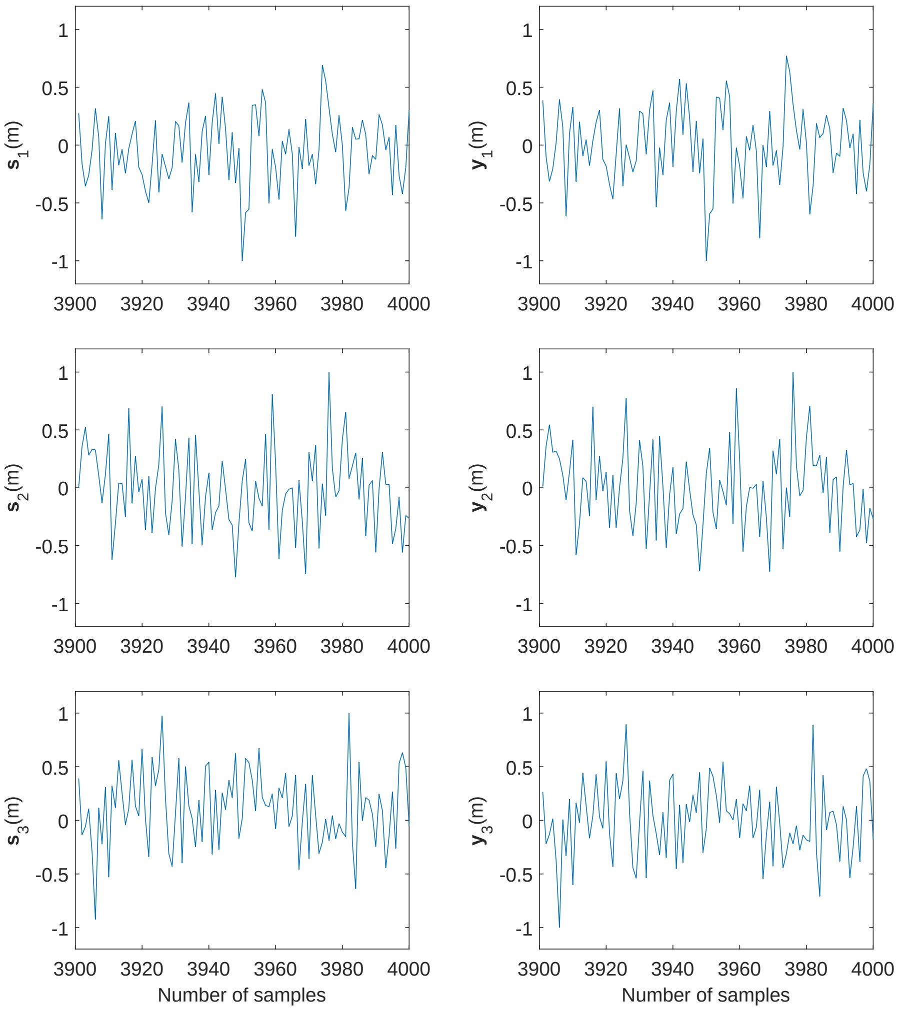

(a) Input source signals $\mathbf{s}_j(m)$, $j = 1, 2, 3$.

(b)Extracted signals $\mathbf{y}_j(m)$, $j = 1, 2, 3$.

FIGURE 4.5: Results of extracting white Gaussian signals using the proposed BSE-ITM algorithm based BLMS.

of the extracted signals $\mathbf{y}_j(m)$, as follows [40]

$$\mathbf{y}_j(m) = \mathbf{s}_{target} + \mathbf{e}_{interf} + \mathbf{e}_{noise} + \mathbf{e}_{artif}, \tag{4.38}$$

where $\mathbf{s}_{target}$ is the component of $\mathbf{s}_k(n)$ in $\mathbf{y}_k(n)$, $\mathbf{e}_{interf}$, $\mathbf{e}_{noise}$, and $\mathbf{e}_{artif}$ are the interference, noise and artifact error terms, respectively. Second, the terms are

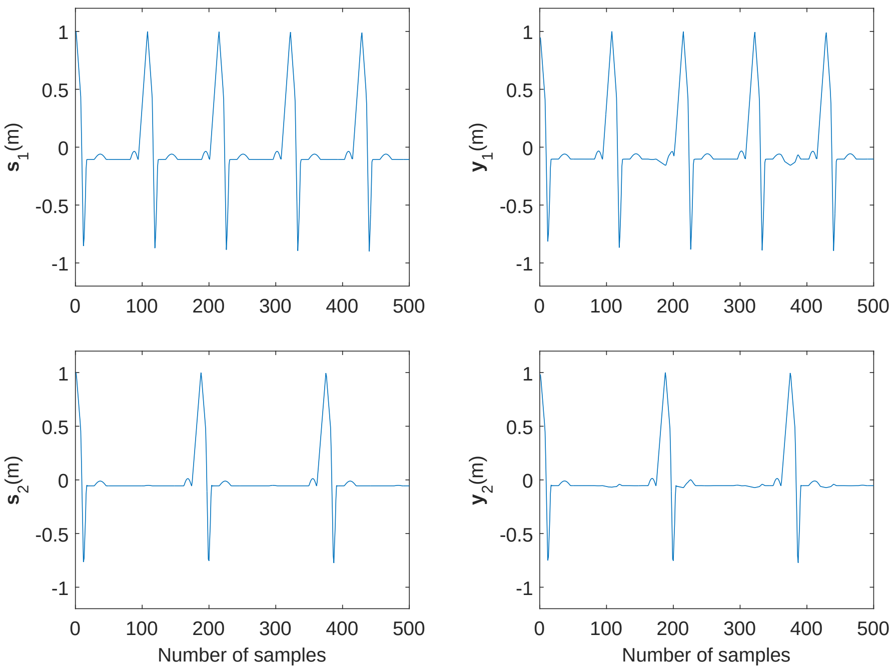

(a) Synthesized ECG signals $\mathbf{s}_j(m)$, $j = 1, 2$.

(b)Extracted signals $\mathbf{y}_j(m)$, $j = 1, 2$.

FIGURE 4.6: Results of extracting ECG signals using the proposed BSE-ITM algorithm based BLMS. $\mathbf{s}_1(m)$ and $\mathbf{s}_2(m)$ are the synthesized FECG and MECG, respectively. $\mathbf{y}_1(m)$ and $\mathbf{y}_2(m)$ are the extracted FECG and MECG, respectively.

computed using BSS EVAL toolbox, as follows [40–42]

$$\text{SIR} = 10log_{10}\frac{\|\mathbf{s}_{target}\|_2^2}{\|\mathbf{e}_{interf}\|_2^2}, \tag{4.39}$$

$$\text{SAR} = 10log_{10}\frac{\|\mathbf{s}_{target} + \mathbf{e}_{interf} + \mathbf{e}_{noise}\|_2^2}{\|\mathbf{e}_{artif}\|_2^2}, \tag{4.40}$$

$$\text{SDR} = 10log_{10}\frac{\|\mathbf{s}_{target}\|_2^2}{\|\mathbf{e}_{interf} + \mathbf{e}_{noise} + \mathbf{e}_{artif}\|_2^2}, \tag{4.41}$$

$$\text{SNR} = 10log_{10}\frac{\|\mathbf{s}_k(n)\|_2^2}{\|\mathbf{s}_k(n) - \mathbf{y}_k(n)\|_2^2}. \tag{4.42}$$

To compare the results with other BSS methods, the experiment is repeated using PCA [14, 39], BSE-PLP, SOBI and FastICA algorithms. Results of simulation are shown in Tables 4.1-4.3. The proposed BSE-ITM based BLMS algorithm, provided

TABLE 4.1: Comparison between the proposed BSE-ITM based BLMS with PCA, BSE-PLP, SOBI, and FastICA, in terms of SIR, SAR, SDR, and SNR. Assuming that the unknown sources are three speech signals

	Algorithm	Input source signals			Average
		$\mathbf{s}_1(m)$	$\mathbf{s}_2(m)$	$\mathbf{s}_3(m)$	
SIR (dB)	PCA [14, 39]	9.647	4.653	3.736	6.012
	BSE-PLP [34]	5.146	8.614	8.3364	7.365
	SOBI [19]	20.588	17.568	25.736	21.297
	FastICA [7, 9, 11, 14]	19.337	24.837	20.689	21.621
	BSE-ITM based BLMS	23.787	23.484	18.078	21.783
SAR (dB)	PCA [14, 39]	9.211	9.055	9.540	9.268
	BSE-PLP [34]	18.641	26.593	24.792	23.342
	SOBI [19]	9.3196	13.352	7.8809	10.184
	FastICA [7, 9, 11, 14]	15.316	17.204	22.033	18.184
	BSE-ITM based BLMS	38.842	34.511	32.861	35.405
SDR (dB)	PCA [14, 39]	9.647	4.653	3.736	6.012
	BSE-PLP [34]	5.146	8.614	8.336	7.365
	SOBI [19]	8.9717	11.903	7.7989	9.5577
	FastICA [7, 9, 11, 14]	15.299	17.129	21.475	17.967
	BSE-ITM based BLMS	23.653	23.152	17.934	21.58
SNR (dB)	PCA [14, 39]	19.697	10.187	9.995	13.293
	BSE-PLP [34]	48.632	26.645	61.349	45.543
	SOBI [19]	50.403	45.708	41.417	45.943
	FastICA [7, 9, 11, 14]	54.133	49.290	38.073	47.165
	BSE-ITM based BLMS	67.915	63.124	66.752	65.93

in bold letters in Tables 4.1-4.3, shows better average performance in terms of the three performance measures (SIR, SAR and SDR), with SIR parameter only slightly improved, compared to other methods. However, a considerable improve in SNR are recorded, as compared with all other algorithms.

TABLE 4.2: Comparison between the proposed BSE-ITM based BLMS with PCA, BSE-PLP, SOBI, and FastICA, in terms of SIR, SAR, SDR, and SNR. Assuming that the unknown sources are three uncorrelated Gaussian signals)

	Algorithm	Input source signals			Average
		$\mathbf{s}_1(m)$	$\mathbf{s}_2(m)$	$\mathbf{s}_3(m)$	
SIR (dB)	PCA [14, 39]	0.950	1.588	4.414	2.317
	BSE-PLP [34]	1.683	3.232	10.986	5.300
	SOBI [19]	1.587	3.507	8.348	4.481
	FastICA [7, 9, 11, 14]	-1.74	12.427	-1.0992	3.195
	BSE-ITM based BLMS	7.603	11.373	19.398	12.791
SAR (dB)	PCA [14, 39]	14.847	14.922	14.749	14.839
	BSE-PLP [34]	16.226	16.238	17.49	16.651
	SOBI [19]	15.018	15.2	15.021	15.08
	FastICA [7, 9, 11, 14]	14.926	15.291	14.852	15.023
	BSE-ITM based BLMS	19.85	19.223	17.232	18.762
SDR (dB)	PCA [14, 39]	0.950	1.588	4.414	2.317
	BSE-PLP [34]	1.683	3.232	10.986	5.300
	SOBI [19]	1.587	3.507	8.348	4.481
	FastICA [7, 9, 11, 14]	-1.740	12.427	-1.099	3.195
	BSE-ITM based BLMS	6.735	9.451	11.427	9.204
SNR (dB)	PCA [14, 39]	10.144	9.926	11.692	10.588
	BSE-PLP [34]	10.047	11.596	23.954	15.199
	SOBI [19]	9.596	11.8	16.28	12.559
	FastICA [7, 9, 11, 14]	7.232	26.186	7.602	13.673
	BSE-ITM based BLMS	12.631	20.307	22.14	18.359

4.5.3 Experiment 3

In this experiment, we test the convergence of error $e_j(m)$ in (4.27). Defining $\mathbf{E}_r^e(m)$ as $\mathbf{Y}(m) - \mathbf{S}(m)$, and can be written as

$$\mathbf{E}_r^e(m) = \begin{bmatrix} e_1(m) & e_1(m-1) & \cdots & e_1(m-N+1) \\ e_2(m) & e_2(m-1) & \cdots & e_2(m-N+1) \\ \vdots & \vdots & \vdots & \vdots \\ e_L(m) & e_L(m-1) & \cdots & e_L(m-N+1) \end{bmatrix}, \tag{4.43}$$

then, the MSE of $\mathbf{E}_r^e(m)$, defined by $\epsilon_e(m)$, can be computed as

$$\epsilon_e(m) = \frac{1}{LN} \sum_{j=1}^{L} \sum_{k=1}^{N} e_j^2(m-k+1), \tag{4.44}$$

TABLE 4.3: Comparison between the proposed BSE-ITM based BLMS with PCA, BSE-PLP, SOBI, and FastICA, in terms of SIR, SAR, SDR, and SNR. Assuming that the unknown sources are three ECG signals (two from a mother and one from its fetus)

	Algorithm	Input source signals			Average
		$\mathbf{s}_1(m)$	$\mathbf{s}_2(m)$	$\mathbf{s}_3(m)$	
SIR (dB)	PCA [14, 39]	10.778	7.132	-12.699	1.7369
	BSE-PLP [34]	5.146	8.614	8.3364	7.365
	SOBI [19]	16.957	0.386	14.52	10.621
	FastICA [7, 9, 11, 14]	22.885	11.529	13.284	15.899
	BSE-ITM based BLMS	19.141	9.652	20.228	16.341
SAR (dB)	PCA [14, 39]	29.905	30.085	29.611	29.867
	BSE-PLP [34]	86.399	82.594	84.835	84.609
	SOBI [19]	11.494	13.857	298.99	108.11
	FastICA [7, 9, 11, 14]	27.236	23.038	190.54	80.271
	BSE-ITM based BLMS	13.441	17.938	293.1	108.16
SDR (dB)	PCA [14, 39]	18.538	7.1161	-12.084	4.523
	BSE-PLP [34]	9.167	4.961	14.519	9.549
	SOBI[19]	10.34	0.027	14.52	8.295
	FastICA [7, 9, 11, 14]	16.546	11.213	13.284	13.681
	BSE-ITM based BLMS	12.656	9.5071	20.228	14.13
SNR (dB)	PCA [14, 39]	22.188	17.064	0.9784	13.41
	BSE-PLP [34]	31.552	24.793	60.581	38.975
	SOBI [19]	64.682	38.261	38.261	44.046
	FastICA [7, 9, 11, 14]	86.776	33.447	30.552	50.258
	BSE-ITM based BLMS	58.761	44.106	80.168	61.012

We use the same simulation settings in Experiment 2, for white Gaussian signal extraction. Figure 4.7 illustrate the simulation results. Results show that $\epsilon_e(m)$ convergences very fast for all values of N. Also, all errors for $N > 50$ are below 10^{-4}, which is an acceptable error level.

4.6 Conclusion

This work introduced a new method for BSE using the ITM that is computed by the input mixture. The matrix has good properties in terms of its unity norm and

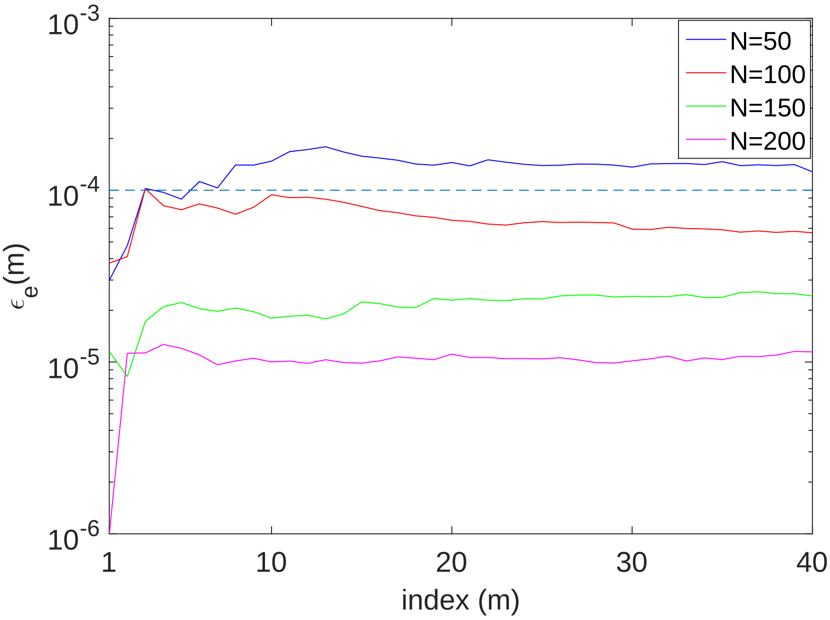

FIGURE 4.7: Convergence of $\epsilon_e(m)$ using the proposed BSE-ITM algorithm based BLMS.

zero mean (rows and columns). New iterative algorithm was presented to compute the ITM with less computational complexity as compared to the standard SVD method. New optimization problem was defined according to the proposed ITM, and solved using BLMS algorithm with low computational complexity. The impact of scaling down the real multiplications using the new algorithm has been investigated. Also, the proposed algorithm used the ITM as a filter coefficients. Thus, the filter coefficients are controlled by the mixture input, not by the output error signals. This has the merits of fixing the filter length and improving the output error convergence. The proposed algorithm was evaluated using speech, white Gaussian, and ECG signals. Simulation results have shown that the proposed algorithm significantly separating the source signals with better performance measures in terms of SIR, SAR, SDR, and SNR.

Bibliography

[1] Bousse, M., Debals, O. and De Lathauwer, L., 2017. A tensor-based method for large-scale blind source separation using segmentation. IEEE Transactions on Signal Processing, 65(2), pp.346-358.

[2] Li, G. and Lyu, S., 2015. Extracting chaotic signal from noisy environment: a random searching method. Chinese Journal of Electronics, 24(3), pp.584-589.

[3] Ren, Y., Song, Y. and Su, X., 2015. Low-complexity channel reconstruction methods based on SVD-ZF precoding in massive 3D-MIMO systems. China Communications, 12(Supplement), pp.49-57.

[4] Debals, O., Van Barel, M. and De Lathauwer, L., 2016. Löwner-based blind signal separation of rational functions with applications. IEEE Transactions on Signal Processing, 64(8), pp.1909-1918.

[5] Hwang, W.L., Lu, K.S. and Ho, J., 2018. Constrained null space component analysis for semiblind source separation problem. IEEE transactions on neural networks and learning systems, 29(2), pp.377-391.

[6] Ferdowsi, S., Abolghasemi, V. and Sanei, S., 2012, September. Blind separation of ballistocardiogram from EEG via short-and-long-term linear prediction filtering. In 2012 IEEE International Workshop on Machine Learning for Signal Processing (pp. 1-6). IEEE.

[7] Chai, R., Naik, G.R., Nguyen, T.N., Ling, S.H., Tran, Y., Craig, A. and Nguyen, H.T., 2017. Driver fatigue classification with independent component

by entropy rate bound minimization analysis in an EEG-based system. IEEE journal of biomedical and health informatics, 21(3), pp.715-724.

[8] Liu, B., Reju, V.G. and Khong, A.W., 2014. A linear source recovery method for underdetermined mixtures of uncorrelated AR-model signals without sparseness. IEEE Transactions on Signal Processing, 62(19), pp.4947-4958.

[9] Naik, G.R., Al-Timemy, A.H. and Nguyen, H.T., 2016. Transradial amputee gesture classification using an optimal number of sEMG sensors: an approach using ICA clustering. IEEE Transactions on Neural Systems and Rehabilitation Engineering, 24(8), pp.837-846.

[10] Chi, Y., 2016. Guaranteed blind sparse spikes deconvolution via lifting and convex optimization. IEEE Journal of Selected Topics in Signal Processing, 10(4), pp.782-794.

[11] Meganem, I., Deville, Y., Hosseini, S., Deliot, P. and Briottet, X., 2014. Linear-quadratic blind source separation using NMF to unmix urban hyperspectral images. IEEE Transactions on Signal Processing, 62(7), pp.1822-1833.

[12] Naik, G.R., Selvan, S.E. and Nguyen, H.T., 2016. Single-channel EMG classification with ensemble-empirical-mode-decomposition-based ICA for diagnosing neuromuscular disorders. IEEE Transactions on Neural Systems and Rehabilitation Engineering, 24(7), pp.734-743.

[13] Wang, H., Su, Z. and Fang, H., 2017, July. Simulating Normal and Abnormal ECG Signals in Children Age 0-16. In 2017 IEEE/ACM International Conference on Connected Health: Applications, Systems and Engineering Technologies (CHASE) (pp. 282-283). IEEE.

[14] Taha, L.Y. and Abdel-Raheem, E., 2018. A Computationally Efficient Blind Source Extraction Using Idempotent Transformation Matrix. Circuits, Systems, and Signal Processing, pp.1-21.

[15] Liu, H., Liu, S., Huang, T., Zhang, Z., Hu, Y. and Zhang, T., 2016. Infrared spectrum blind deconvolution algorithm via learned dictionaries and sparse representation. Applied Optics, 55(10), pp.2813-2818.

[16] Kumar, V.A., Rao, C.V.R. and Dutta, A., 2018. Performance analysis of blind source separation using canonical correlation. Circuits, Systems, and Signal Processing, 37(2), pp.658-673.

[17] Ferdowsi, S., Sanei, S., Abolghasemi, V., Nottage, J. and O'Daly, O., 2013. Removing ballistocardiogram artifact from EEG using short-and long-term linear predictor. IEEE Transactions on Biomedical Engineering, 60(7), pp.1900-1911.

[18] https://www.mathworks.com/matlabcentral/fileexchange/10858-ecg-simulation-using-matlab (2006). Accessed Sep 2018

[19] Ahmadian, P., Sanei, S., Ascari, L., González-Villanueva, L. and Umiltà, M.A., 2013. Constrained blind source extraction of readiness potentials from EEG. IEEE Transactions on Neural Systems and Rehabilitation Engineering, 21(4), pp.567-575.

[20] Mandic, D.P. and Cichocki, A., 2003, April. An online algorithm for blind extraction of sources with different dynamical structures. In Proc. of the 4th Int. Conf. on Independent Component Analysis and Blind Signal Separation (ICA 2003)(pp. 645-650).

[21] Javidi, S., Mandic, D.P. and Cichocki, A., 2010. Complex blind source extraction from noisy mixtures using second-order statistics. IEEE Transactions on Circuits and Systems I: Regular Papers, 57(7), pp.1404-1416.

[22] Li, Y., Nie, W., Ye, F. and Lin, Y., 2016. A mixing matrix estimation algorithm for underdetermined blind source separation. Circuits, Systems, and Signal Processing, 35(9), pp.3367-3379.

[23] Lu, X., Li, X., Fu, M.S. and Wang, H., 2017. Robust maximum signal fraction analysis for blind source separation. IET Signal Processing, 11(8), pp.969-974.

[24] Bose, T. and Meyer, F., 2003. Digital signal and image processing. John Wiley and Sons, Inc..

[25] Cichocki, A. and Amari, S.I., 2002. Adaptive blind signal and image processing: learning algorithms and applications (Vol. 1). John Wiley and Sons.

[26] Albera, L., Kachenoura, A., Comon, P., Karfoul, A., Wendling, F., Senhadji, L. and Merlet, I., 2012. ICA-based EEG denoising: a comparative analysis of fifteen methods. Bulletin of the Polish Academy of Sciences: Technical Sciences, 60(3), pp.407-418.

[27] Pendharkar, G., Naik, G.R. and Nguyen, H.T., 2014. Using blind source separation on accelerometry data to analyze and distinguish the toe walking gait from normal gait in ITW children. Biomedical Signal Processing and Control, 13, pp.41-49.

[28] Zhou, L. and Li, C., 2016. Outsourcing eigen-decomposition and singular value decomposition of large matrix to a public cloud. IEEE Access, 4, pp.869-879.

[29] Taha, A.L., Taha, L.Y. and Abdel-Raheem, E., 2015, December. FastICA architecture utilizing FPGA and iterative symmetric orthogonalization for multivariate signals. In 2015 IEEE International Symposium on Signal Processing and Information Technology (ISSPIT) (pp. 279-284). IEEE.

[30] Liu, W., Mandic, D.P. and Cichocki, A., 2008, July. A dual-linear predictor approach to blind source extraction for noisy mixtures. In 2008 5th IEEE Sensor Array and Multichannel Signal Processing Workshop (pp. 515-519). IEEE.

[31] Becker, H., Albera, L., Comon, P., Kachenoura, A. and Merlet, I., 2017. A penalized semialgebraic deflation ICA algorithm for the efficient extraction of interictal epileptic signals. IEEE journal of biomedical and health informatics, 21(1), pp.94-104.

[32] Liu, W., Mandic, D.P. and Cichocki, A., 2007. Blind source extraction based on a linear predictor. IET Signal Processing, 1(1), pp.29-34.

[33] Hsu, S.H., Mullen, T.R., Jung, T.P. and Cauwenberghs, G., 2016. Real-time adaptive EEG source separation using online recursive independent component analysis. IEEE transactions on neural systems and rehabilitation engineering, 24(3), pp.309-319.

[34] Taha, L.Y. and Abdel-Raheem, E., 2017, April. A null space approach for complete and over-complete blind source separation of autoregressive source signals. In 2017 IEEE 30th Canadian Conference on Electrical and Computer Engineering (CCECE) (pp. 1-4). IEEE.

[35] Rongjie, W., Yiju, Z. and Haifeng, Z., 2016. A class of sequential blind source separation method in order using swarm optimization algorithm. Circuits, Systems, and Signal Processing, 35(9), pp.3220-3243.

[36] Sutha, P. and Jayanthi, V.E., 2018. Fetal electrocardiogram extraction and analysis using adaptive noise cancellation and wavelet transformation techniques. Journal of medical systems, 42(1), p.21.

[37] Vincent, E., Gribonval, R. and Févotte, C., 2006. Performance measurement in blind audio source separation. IEEE transactions on audio, speech, and language processing, 14(4), pp.1462-1469.

[38] Wang, L. and Chi, Y., 2016. Blind deconvolution from multiple sparse inputs. IEEE Signal Processing Letters, 23(10), pp.1384-1388.

[39] Kemiha, M. and Kacha, A., 2017. Complex blind source separation. Circuits, Systems, and Signal Processing, 36(11), pp.4670-4687.

[40] Taha, L.Y. and Abdel-Raheem, E., 2018. Efficient blind source extraction of noisy mixture utilising a class of parallel linear predictor filters. IET Signal Processing, 12(8), pp.1009-1016.

[41] Févotte, C., Gribonval, R. and Vincent, E., 2005. BSS_EVAL toolbox user guide–Revision 2.0.

[42] Kaftory, R. and Zeevi, Y.Y., 2013. Blind separation of time/position varying mixtures. IEEE Transactions on Image Processing, 22(1), pp.104-118.

Chapter 5

Detection and Extraction of FECG signals Using Null Space Approach

5.1 Introduction

The electrocardiogram (ECG) signal, in non-invasive method, incorporates of the maternal ECG (MECG) signal, the fetal ECG (FECG) signal, and several sources of interference such power line interference, baseline wander, motion artifact, fetal brain activity, muscle artifact, and instrumentation noise [1–3]. FECG signal is used to monitor the health status of the fetus by determining its maturity level, reactivity, development and existence of fetal distress [4].

FECG extraction and enhancement method requires the elimination of the MECG as well as optimal detection of the FECG. The frequencies of both signals are few Hertz's and are possibly overlapping. Thus, separating them using the conventional linear filter fails. To address this problem, large number of FECG extraction algorithms have been proposed over the past decades. Some of these algorithms were based on the blind source separation (BSS) or blind source extraction (BSE) techniques [6, 7]. In general, the extraction algorithms can be classified as either spatial (non adaptive) or temporal (adaptive) algorithms [7]. Examples of the BSS/BSE based non adaptive algorithms include principal component analysis (PCA) [8], null space component (NCA)[9], independent component analysis (ICA) [10], and parallel linear predictor (PLP) filters [11, 12]. Examples of the adaptive algorithms include the multi-sensory adaptive noise canceller (MSANC) [7], fast adaptive orthogonal group ICA [13], adaptive Volterra filter (AVF) [14], adaptive neuro fuzzy inference system (ANFIS) and wavelet transform [15], and Kalman filtering [16].

The comparison between the relative performances of these algorithms is a challenging task due to the absence of a large public database and of also the absence of a defined evaluation methodology. However, It is possible to highlight the strengths and weaknesses of limited algorithms, evaluated on the same database and using the same methodology [17].

It has been reported that NCA and ICA algorithms represent the smallest amount of information that can be adopted for solving the BSS problem [9]. Note that ICA algorithm requires data whitening prior to applying the algorithm. This is necessary to minimize the correlation between the mixture signals. The PCA approach may be used for data whitening. The NCA approach assumes that the sources are linearly independents. However, the ICA approach considers that the sources are statistically independents.

The NCA was proposed in 2007 by R. B. Chena and Y. NianWub [18] to solve the over-complete BSS problem. The solution space of the source signals were characterized by the null space of the mixing matrix using singular value decomposition (SVD). The problem were formulated in the framework of Bayesian latent variable model. The work was only applied to three sound signals. There is no information about the performance of this approach when the number of signals is increased. The computational complexity of this algorithm was not provided. Also, there were no comparisons with other methods. Another NCA algorithm was presented in [19] for noisy mixture. This algorithm used a transformation matrix to resolve the rotation ambiguity and extract the source signals that were assumed to be linearly independent. The initial guess of this algorithm depends more heavily on the solutions as compared with ICA. Also, it has higher complexity than many existing ICA methods. The work in [9] presented an extension of NCA framework, named constraint NCA (c-NCA) approach. This approach was considered as an alternative approach to the c-ICA. The c-NCA used signal-dependent semidefinite operators, which is a bilinear mapping, as signatures for operator design. A prior knowledge of how the data are prepared, collected, and mixed, is needed in this approach. This method has many issues. First, the algorithm requires a little knowledge about the sources during initialization. This is not suitable for real-life cases. Second, the condition for convergence requires the calculation of maximal eigenvalues of the Hessian matrix of the objective function. The calculation of eigenvalues is numerically intractable. Third, the complexity of the algorithm is high and approaches $\mathcal{O}(N_1N_2N^3)$, where N_1 is the number of iterations, N_2 is the number of proximal splitting iterations, and N is the number of samples. Thus, designing new null space separating operator with less computational complexity, with no initialization constraint, and fast convergence, is crucial.

This paper is aimed to develop a non-adaptive FECG detection and extraction algorithm, based on using the null space approach in estimating the FECG and MECG signals from the ITM. The algorithm first minimizes the effect of noise then extracts the FECG and MECG signals, and detects the fetal heart rate. A comparison between the proposed algorithms and other similar algorithms will be provided.

The rest of this paper is organized as follows. In Section 5.2, we briefly define the BSS problem and how it can be used in FECG extraction. The ECG signal is also illustrated in this section. A review on the popular FECG extraction methods (PCA and FastICA), in the context of BSS, is shown in Section 5.3. In

Section 5.4, we present the proposed FECG and MECG extraction algorithms, and how to detect the R peaks in the QRS complex. The experimental results are demonstrated in Section 5.5. Finally, Section 5.6 concludes the paper.

5.2 Problem formulation

The biological ECG signal of a pregnant woman is a composite signal between the FECG, MECG, and the noise. It has been proven that the noiseless ECG signals can be modelled using the linear BSS model expressed by [8]:

$$\boldsymbol{X} = \boldsymbol{A}\boldsymbol{S}, \tag{5.1}$$

where $\boldsymbol{X}$ is the $M \times N$ zero mean recorded ECG mixture signals, from the thorax and the abdominal channels, $\boldsymbol{A}$ is the $M \times L$ unknown full rank mixing matrix, $\boldsymbol{S}$ is the $L \times N$ unknown source signals (the FECG and the MECG signals), recalling that M is the number of recorded ECG signals, L is the number of the unknown source signals, and N is the number of samples of each measurement. We assume that both M and L are less than N. The matrices $\boldsymbol{X}$ and $\boldsymbol{S}$ have M and L row vector signals, respectively. A typical ECG signal for $N = 500$ is illustrated in Fig. 5.1, [17]. It is clear from Fig. 5.1 that the ECG signal is composed of P wave, QRS complex, S wave, and T wave. Both FECG and MECG signals are periodic and take the same shape shown in Fig. 5.1. However, the amplitude and duration of P, QRS, and T waves are different. Also, the FECG signal has higher frequency than the MECG signal [2, 4]. The ECG signal is captured by appropriate electrodes placed at the abdominal and thorax.

The estimation of $\boldsymbol{S}$ and $\boldsymbol{A}$ from $\boldsymbol{X}$ is the main goal of the BSS problem. To estimate $\boldsymbol{S}$, we denote matrix $\boldsymbol{Y}$, having the same dimension of $\boldsymbol{S}$, as the estimated source matrix, given by

$$\boldsymbol{Y} = \boldsymbol{H}\boldsymbol{X}, \tag{5.2}$$

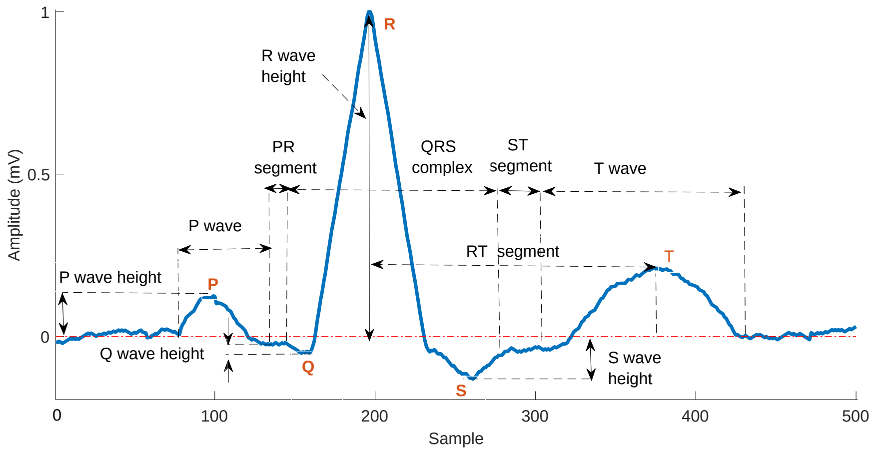

FIGURE 5.1: Typical ECG signals, $N = 500$.

where $\boldsymbol{H}$ is the $L \times M$ estimated transformation matrix.

As the BSS model shown in (5.1) is affected by scaling, permutation, and rotation ambiguities [22], several methods has been developed to extract $\boldsymbol{S}$ using (5.2). This will be discussed in Section 5.3.

5.3 FECG extraction methods

In this section, we discus some important extraction approaches, such as PCA and ICA.

5.3.1 PCA approach

Different methods were reported in the literature to estimate $\boldsymbol{H}$ based on PCA [23]. The PCA whitening method is one of the popular methods, in which the matrix $\boldsymbol{H}$ is equal to $\boldsymbol{C}_x^{-\frac{1}{2}}$, where $\boldsymbol{C}_x$ is the $M \times M$ whitening matrix. This matrix is estimated from covariance matrix of $\boldsymbol{X}$. From (5.2), the estimated source matrix

$\boldsymbol{Y}$, using PCA approach, is given by:

$$\boldsymbol{Y} = \boldsymbol{C}_x^{-\frac{1}{2}} \boldsymbol{X}. \tag{5.3}$$

The output signals (the row vectors) from $\boldsymbol{Y}$, after applying PCA whitening, has the property of being uncorrelated. However, these vectors do not necessarily represent independent sources [23]. Thus, the PCA method is weak in signal extraction. Despite this weakness, the PCA algorithm has less amount of computations as compared with other methods, and shows acceptable detection of FECG R peaks. Thus, the PCA method is still showing interest by researchers in the field of FECG detection and extraction [25, 26].

5.3.2 ICA approach

In ICA approach, the matrix $\boldsymbol{H}$ is equal to $\boldsymbol{A}^+$ which is the Moore-Penros inverse of $\boldsymbol{A}$, such that $\boldsymbol{A}^+ = \boldsymbol{A}^T(\boldsymbol{A}\boldsymbol{A}^T)^{-1}$, if $L \leq M$ [11]. The resultant estimated row vectors in $\boldsymbol{Y}$ must be statistically independents. In many ICA algorithms, whitening process is needed. Denoting $\hat{\boldsymbol{x}}(n)$ as the output of the PCA whitening process at sample n, the $\boldsymbol{Y}$ matrix can be estimated by first solving the optimization problem [24]

$$\begin{aligned} \text{minimize} \quad & \|\boldsymbol{z}(n) - \boldsymbol{s}(n)\|_2 \\ \text{subject to} \quad & \boldsymbol{z}(n) = \boldsymbol{A}^+ \hat{\boldsymbol{x}}(n), \end{aligned} \tag{5.4}$$

where

$$\boldsymbol{z}(n) = \begin{bmatrix} z_1(n) \\ z_2(n) \\ \vdots \\ z_L(n) \end{bmatrix}, \boldsymbol{A}^+ = \begin{bmatrix} p_{11} & p_{12} & \cdots & p_{1M} \\ p_{21} & a_{22} & \cdots & p_{2M} \\ \vdots & \vdots & \vdots & \vdots \\ p_{L1} & a_{L2} & \cdots & p_{LM} \end{bmatrix},$$

$$\hat{\boldsymbol{x}}(n) = \begin{bmatrix} \hat{x}_1(n) \\ \hat{x}_2(n) \\ \vdots \\ \hat{x}_M(n) \end{bmatrix}, \boldsymbol{s}(n) = \begin{bmatrix} s_1(n) \\ s_2(n) \\ \vdots \\ s_L(n) \end{bmatrix}, \tag{5.5}$$

then, for a block of N samples, the $\boldsymbol{Y}$ matrix is computed as follows

$$\boldsymbol{Y} = \begin{bmatrix} z_1(n) & z_1(n-1) & \cdots & z_1(n-N+1) \\ z_2(n) & z_2(n-1) & \cdots & z_2(n-N+1) \\ \vdots & \vdots & \vdots & \vdots \\ z_L(n) & z_L(n-1) & \cdots & z_L(n-N+1) \end{bmatrix}, \tag{5.6}$$

The ICA based FECG extraction has some challenges. First, it assumes independent sources and its performance is directly affecting the quality and speed of FECG signal extraction. Second, The background noise has a considerable affect on its performance [3]. Some works were reported to combine the ICA approach with other approaches such as wavelet decomposition [10] and adaptive noise cancellation (ANC) [27].

5.4 The proposed FECG extraction and detection method

The null space idempotent transformation matrix (NSITM) algorithm is explained in this section. A proposed R peak detection method is also presented in this section.

5.4.1 FECG extraction using Null Space ITM (NSITM)

Define the j^{th} signal $y_j(n-k+1)$, $j = 1, 2, \ldots, L$, $k = 1, 2, \ldots, N$, as the extracted FECG or MECG source signal, and expressed by the following N prediction filter [20, 21, 28]

$$y_j(n-k+1) = \sum_{q=1}^{N} w_{q,k} y_j(n-q+1), \tag{5.7}$$

where $w_{q,k}$ is the AR coefficients of $y_j(n-k+1)$. where $i = 1, 2, \ldots, L$ and w_{ik} is the AR coefficients of $y_i(n)$. Re-writing (5.7) in matrix form, we obtain

$$\boldsymbol{Y} = \boldsymbol{Y}\boldsymbol{W}, \tag{5.8}$$

where $\boldsymbol{Y}$ is the extracted source matrix of dimension $L \times N$, and can be written as

$$\boldsymbol{Y} = \begin{bmatrix} y_1(n) & y_1(n-1) & \cdots & y_1(n-N+1) \\ y_2(n) & y_2(n-1) & \cdots & y_2(n-N+1) \\ \vdots & \vdots & \vdots & \vdots \\ y_L(n) & y_L(n-1) & \cdots & y_L(n-N+1) \end{bmatrix}, \tag{5.9}$$

and $\boldsymbol{W}$ is the $N \times N$ symmetrical idempotent transformation matrix, and is given by

$$\boldsymbol{W} = \begin{bmatrix} w_{1,1} & w_{1,2} & \cdots & w_{1,N} \\ w_{2,1} & w_{2,2} & \cdots & w_{2,N} \\ \vdots & \vdots & \vdots & \vdots \\ w_{N,1} & w_{N,2} & \cdots & w_{N,N} \end{bmatrix}. \tag{5.10}$$

The matrix $\boldsymbol{W}$ can be computed as follows [21]

$$\boldsymbol{W} = \frac{1}{N}\boldsymbol{X}^T\boldsymbol{C}_x^{-1}\boldsymbol{X}, \tag{5.11}$$

where $\boldsymbol{C}_x$ is the covariance matrix of $\boldsymbol{X}$. Equation (5.8) can be rewritten as

$$\boldsymbol{Q}\boldsymbol{Y}^T = \boldsymbol{0}_{N\times L}, \tag{5.12}$$

$$\boldsymbol{Q} = \boldsymbol{W} - \boldsymbol{I}_N, \tag{5.13}$$

where $\boldsymbol{Q}$ is the required $N \times N$ separation matrix, and $\boldsymbol{0}_{N\times L}$ is an $N \times L$ zero matrix. Equation (5.12) can be solved for the unknown $\boldsymbol{Y}$ using the null space of $\boldsymbol{Q}$, as follows:

$$\boldsymbol{Y} = Null(\boldsymbol{Q}). \tag{5.14}$$

Since the extracted signals of the $\boldsymbol{Y}$ matrix are computed based on (5.14), i.e, the Null space (NS) of $\boldsymbol{Q}$, and since $\boldsymbol{W}$ is an ITM, we name this method as NSITM. The solution of (5.14) can be obtained using SVD. First, we express $\boldsymbol{Q}$ by

$$\boldsymbol{Q} = \boldsymbol{U}_q\boldsymbol{D}_q\boldsymbol{V}_q^T, \tag{5.15}$$

where $\boldsymbol{U}_q$ is an $N \times N$ unitary matrix, $\boldsymbol{D}_q$ is an $N \times N$ diagonal matrix with the eigenvalues of $\boldsymbol{Q}$, and $\boldsymbol{V}_q$ is an $N \times N$ matrix with the columns being the eigenvectors of $\boldsymbol{Q}$. Assume that $\boldsymbol{V}_q$ is expressed by

$$\boldsymbol{V}_q = \begin{bmatrix} v_{1,1} & v_{1,2} & \cdots & v_{1,N} \\ v_{2,1} & v_{2,2} & \cdots & v_{2,N} \\ \vdots & \vdots & \vdots & \vdots \\ v_{N,1} & v_{N,2} & \cdots & v_{N,N} \end{bmatrix}, \tag{5.16}$$

then, from (5.14), (5.15) and (5.16), and since $L < N$, the solution $\boldsymbol{Y}$ will be taken from the last L column vectors of $\boldsymbol{V}_q$, and is given by

$$\boldsymbol{Y} = \begin{bmatrix} v_{1,N-L+1} & v_{1,N-L+2} & \cdots & v_{1,N} \\ v_{2,N-L+1} & v_{2,N-L+2} & \cdots & v_{2,N} \\ \vdots & \vdots & \vdots & \vdots \\ v_{N,N-L+1} & v_{N,N-L+2} & \cdots & v_{N,N} \end{bmatrix}^T \tag{5.17}$$

From (5.11), (5.14), (5.15), and (5.17), we propose the NSITM algorithm 5 that extracts the FECG signals from the ECG mixture signals. The algorithm needs first a prepossessing stage to remove the noises since the ECG signals are contaminated with different types of noise, as declared in Section 5.1. A second order notch filter having cutoff frequency of 50 Hz or 60 Hz is needed to remove the 50 Hz or the 60 Hz power line interference, respectively. The selection of cutoff frequency depends upon the power line standard which is either European or US standard [10]. The baseline wander is reduced using high pass filter of 0.5 Hz cutoff frequency [17]. A low pass Butterworth filter with 100 Hz cutoff frequency is applied to limit the frequency band of the ECG signals. Other noise sources are minimized using LMS based adaptive noise cancellation (ANC) algorithm [4].

Algorithm 5 The proposed NSITM algorithm

1: **Initials** N, L, M
2: Read the ECG signals $\boldsymbol{X}$.
3: Prepossessing by denoising filters (low pass, high pass, notch) and ANC.
4: Compute $\boldsymbol{W}$ by (5.11).
5: Compute $\boldsymbol{Q}$ by (5.13)
6: Compute $\boldsymbol{V}_q$ by (5.15) using SVD method.
7: Compute $\boldsymbol{Y}$ by (5.17).
8: **Return** $\boldsymbol{Y}$.

5.4.2 FECG R peaks detection

The R peak in the fetal QRS complex, shown in Fig. 5.1, are detected by searching for FECG signal values between 50% – 100% of the global maximum. This threshold level minimizes the searching error. Due to the periodic nature of the FECG signal, and since the time needed to record ECG signals is typically long and contains many periods of the signals, we define $\boldsymbol{p}$ as a vector that contains the sampling indices of all detected peaks, and H as the number of detected peaks, then the difference in sampling indices between two consecutive peaks, defined as $\boldsymbol{dp}$, is given by

$$\boldsymbol{dp}(k) = \boldsymbol{p}(k+1) - \boldsymbol{p}(k), k = 1, 2, \ldots, H-1. \tag{5.18}$$

The k^{th} fetal heart rate (FHR_k) can be calculated from (5.18) as follows

$$\mathrm{FHR}_k = 60 f_s / \boldsymbol{dp}(k). \tag{5.19}$$

5.5 Experiments

Four different simulations are provided in this section. The first simulation uses real ECG signals from Database for the Identification of Systems (DAISY) [29]. Then, the FECG signal is extracted using our proposed NSITM algorithm. The simulation is repeated using PCA and FastICA algorithms, for comparison purposes. The R peak detection of FECG signal is also provided. The second simulation is similar to the first simulation but using another real data from Physionet/-Computing in Cardiology Challenge 2013 database [30, 31]. The third simulation is intended to evaluate the R peaks detection metrics of the proposed NSITM algorithm by comparing the results from the first and second simulation, with the results obtained from PCA and FastICA algorithms. The fourth simulation extracts the FECG signals from a synthesized ECG data then evaluates its performance. The synthesized data were taken from Physionet/Fetal ECG Synthetic Database (FECGSYNDB) [31, 32]. All simulations were conducted in Matlab.

5.5.1 FECG extraction and R peaks detection of real ECG data from DAISY database

A recorded real ECG signals, from pregnant women for 10s, were used from [29]. The signals were acquired from 8 channels sensors (five abdominal and three thorax channels). The sampling frequency f_s was selected to be 250 Hz. Then, the proposed NSITM algorithm was applied to extract the FECG signals. The PCA and FastICA algorithms were also applied to extract the FECG signals, and their results will be compared with the results from the proposed algorithm.
Fig. 5.2 illustrates the recorded ECG signals, with $N = 2500$ samples, and $M = 7$, using five abdominal signals $x_1(n)$-$x_5(n)$ and two thorax signals $x_6(n)$-$x_7(n)$. Figs. 5.3-5.4 illustrate the extracted FECG and MECG signals, respectively, using the selected algorithms. Figs. 5.5-5.6 illustrate the extracted FECG and MECG signals, respectively, using the selected algorithms, considering all mixture signals shown in Fig. 5.2. From Fig. 5.3 and Fig. 5.5 and applying (5.18)-(5.19), the mean values of the FHR are estimated and shown in Table 5.1. This table also illustrates the estimation of FHR by considering five different selections of abdominal and thorax signals. Several conclusions were recorded from the results. First, the

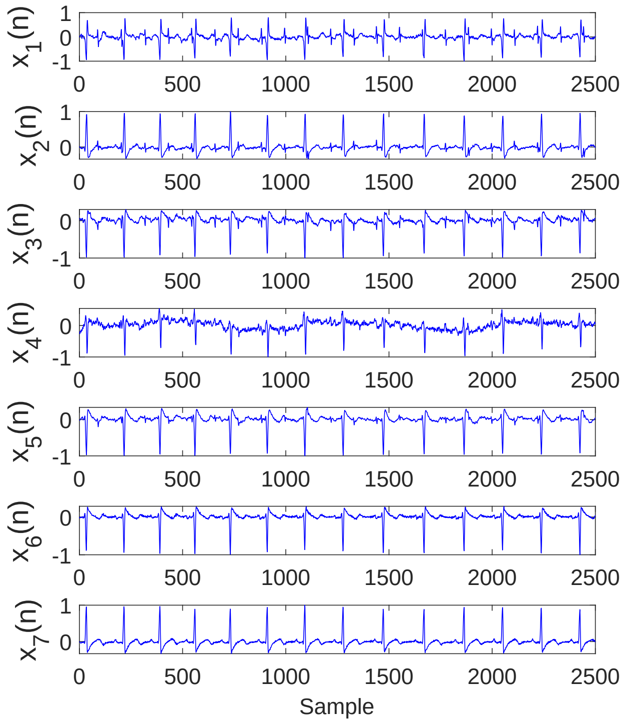

FIGURE 5.2: Recorded ECG signals using DAISY data set, $N = 2500$, $M = 7$, $f_s = 250$ Hz. The abdominal signals are the first 5 signals from the top while the remaining two are thorax signals.

proposed NSITM algorithm, the PCA algorithm, and the FastICA algorithm were successfully extracting the FECG and MECG signals from the ECG mixture. Second, The estimated FECG signals using NSITM and FastICA show less noise contents as compared with PCA. Third, the extraction using $M = 7$ is better than that with $M = 5$. Forth, the mean value of FHR using NSITM algorithm is equal to ≈134 beats per minute (bpm), which is almost the same as the result obtained in [4]. This provides confidence in the ability of the proposed algorithm to successfully detect the fetal R peaks.

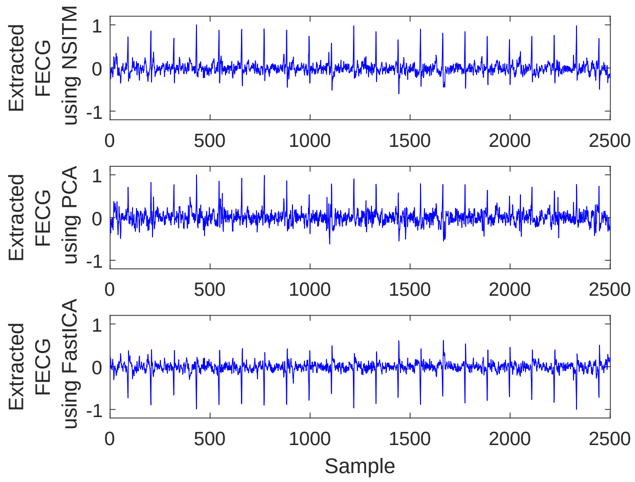

FIGURE 5.3: Extracted FECG signals from ECG signals in Fig. 5.2, using NSITM, PCA, and FastICA, assuming $M = 5$ (three abdominal signals $x_1(n)$-$x_3(n)$ and two thorax signals $x_6(n)$-$x_7(n)$)

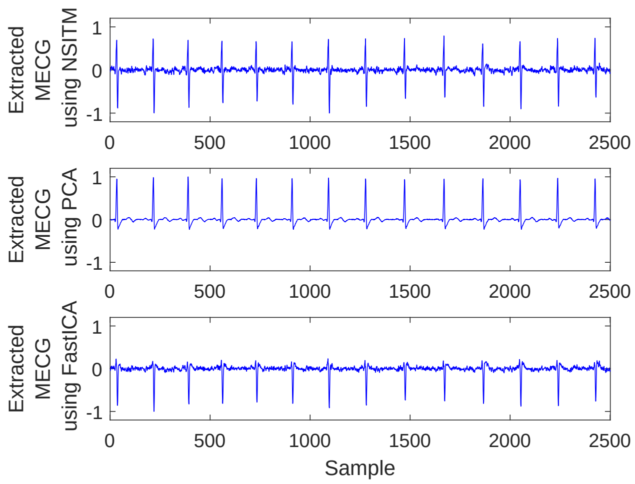

FIGURE 5.4: Extracted MECG signals from ECG signals in Fig. 5.2, using NSITM, PCA, and FastICA, assuming $M = 5$ (three abdominal signals $x_1(n)$-$x_3(n)$ and two thorax signals $x_6(n)$-$x_7(n)$)

5.5.2 FECG extraction and R peaks detection of real ECG data from Physionet Database

A recorded real ECG signals, from pregnant women for 1 minute, were used from Physionet Challenge 2013 data set a [30, 31]. Each recording includes four noninvasive abdominal signals. The data were obtained from multiple sources using a

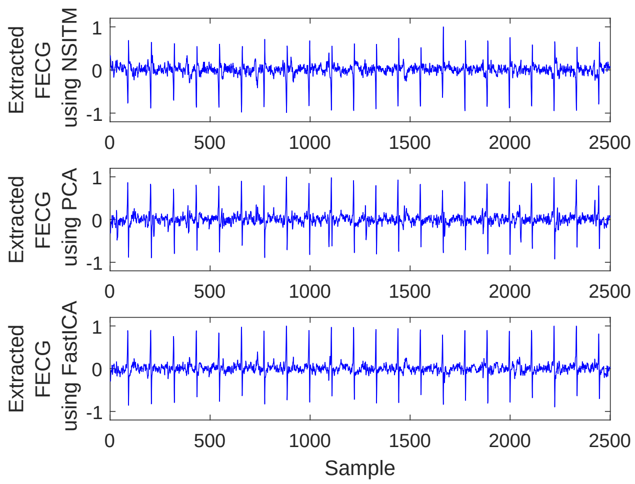

FIGURE 5.5: Extracted FECG signals from ECG signals in Fig. 5.2, using NSITM, PCA, and FastICA, assuming $M = 7$ (five abdominal signals $x_1(n)$-$x_5(n)$ and two thorax signals $x_6(n)$-$x_7(n)$)

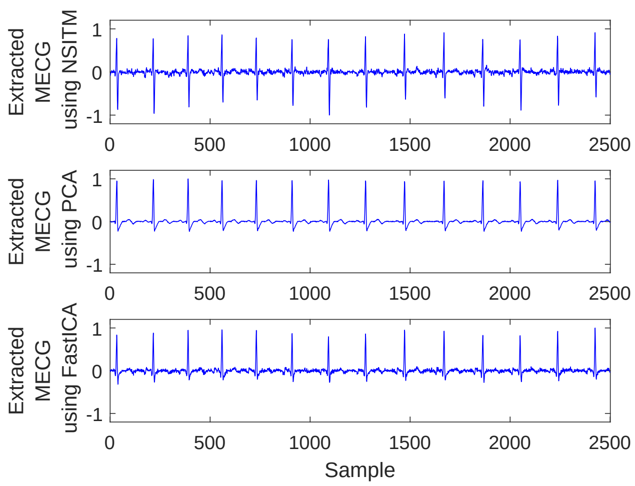

FIGURE 5.6: Extracted MECG signals from ECG signals in Fig. 5.2, using NSITM, PCA, and FastICA, assuming $M = 7$ (five abdominal signals $x_1(n)$-$x_5(n)$ and two thorax signals $x_6(n)$-$x_7(n)$)

variety of instrumentation with differing frequency response, resolution, and configuration. The sampling frequency for all data is 1 kHz. We selected the data files (a04, a08, a14, a15, a25) from the database, and used them in this experiment. Then, we followed the same simulation procedure as in Section 5.5.1. For illustration purposes, we visualize only the results of file a15 due to the excessive number of figures. However, their results for FHR estimation were recorded in Table 5.2.

Figure 5.7 illustrates the recorded abdominal ECG signals, file a15, with $M = 4$. We selected a block of 5000 data samples, from 0-4999. Figures 5.8-5.9 illustrate the extracted FECG and MECG signals, respectively, using the selected algorithms. Figure 5.8 shows unsatisfactory extraction of FECG signals using all algorithms (the proposed NSITM algorithm, as well as the PCA and FastICA algorithms). This is due to the absence of thorax signals from the input ECG mixture. However, all used algorithms were successfully extracting the MECG signals from the ECG mixture, as shown in Fig. 5.9. Figure 5.8 shows that both FECG and MECG R peaks exist, and marked by red dashed lines and green dashed lines, respectively [1] [35]. The ACF has periodic hanning windows. Each window is centered at the locations of one of the MECG R peaks shown in Fig. 5.9. As these MECG R peaks exist also at the same locations in Fig. 5.8, we apply the ACF to all signals in this figure, thus removing the MECG R peaks. The locations of the ACF are illustrated in Fig. 5.8 by block arrows. The length of the ACF window is a variable quantity and depends upon the duration of the QRS complex of the selected MECG signal. In this simulation, a length of 20 samples were found appropriate in removing the MECG R peaks, for the used file a15. For other used files, the length of ACF must be selected between 20 and 45 samples, to avoid the removal of portions of the required FECG signal when the two signals are very close in their locations. Our method may fail in MECG removal if the the locations of FECG and MECG R peaks overlap.

Figure 5.10 illustrates the clean extracted FECG signals of Fig. 5.8 after the removal of MECG signals by ACF. The first signal from the top is the abdominal ECG signal $x_1(n)$, which is considered at the top of the figure for illustration purposes, since it contains a reference annotation taken from LightWAVE annotation viewer [30]. It is clear from Fig. 5.10 that the proposed NSITM algorithm,

[1] The red dashed lines and the green dashed lines are at the left and the right side of Fig. 5.8, respectively. These MECG R peaks can be removed by adaptive comb filter (ACF)

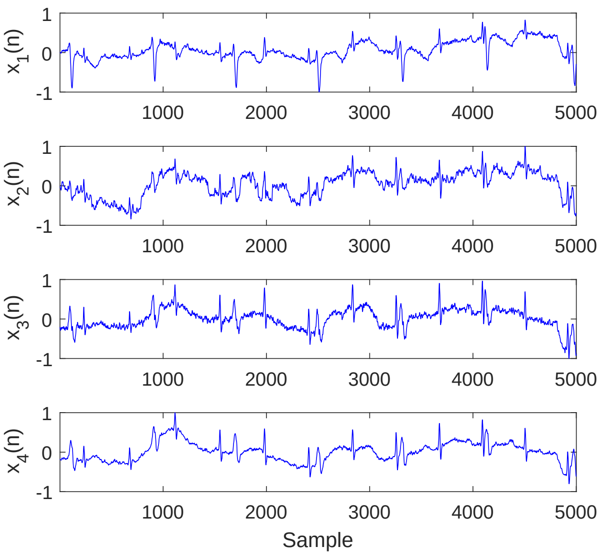

FIGURE 5.7: Recorded abdominal ECG signals from Physionet Challenge 2013 data set a, file a15, $M = 4$, $N = 5000$, data samples from $0 - 4999$.

the PCA algorithm, and the FastICA algorithm were successfully extracting the FECG and MECG signals from the ECG mixture. The extraction performances will be considered later in Section 5.5.4.

From Fig. 5.10 and applying (5.18)–(5.19), the mean values of the FHR are estimated and shown in Table 5.2. Next, the simulation is repeated for other files (a4, a8, a14, a25) and their results for FHR estimation were recorded also in Table 5.2. Comparing the average value of the annotated FHR (141.24) [30] with the results in Table 5.2, it is clear that NSITM algorithm has the best estimation of the FHR (140.8). The FastICA is coming next with FHR equals to 143.3. The PCA has the lowest score (137). In general, the proposed NSITM algorithm is successfully extracting FECG signals with the highest closest values of FHR to the reference FHR.

To ensure the stability of extraction performance over time, the simulation is repeated by taking blocks of data samples from 5000-9999, and from 55000-59999 which is the last available data samples. Results from the first block is shown in Figs. 5.11-5.14 while Figs. 5.15-5.18 illustrate the results from the second block.

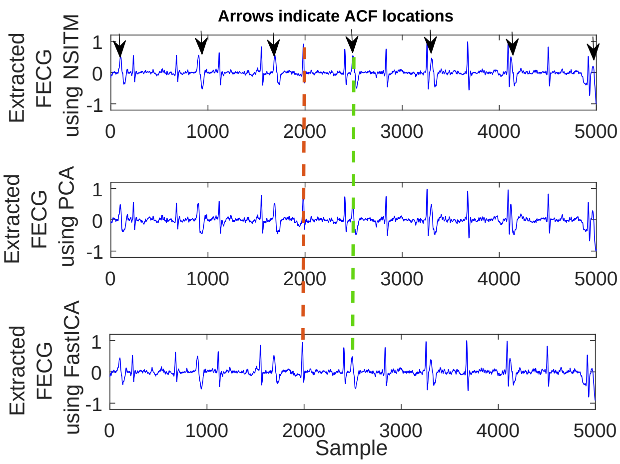

FIGURE 5.8: Unsatisfactory Extracted FECG signals from ECG signals in Fig. 5.7, using NSITM, PCA, and FastICA, assuming $M = 4$. Both FECG and MECG R peaks exist. For illustration, only one marked FECG peak and one marked MECG peak are shown by red dashed lines (left located) and green dashed lines (right located), respectively. The block arrows indicate the position of the ACF used to remove the MECG R peaks.

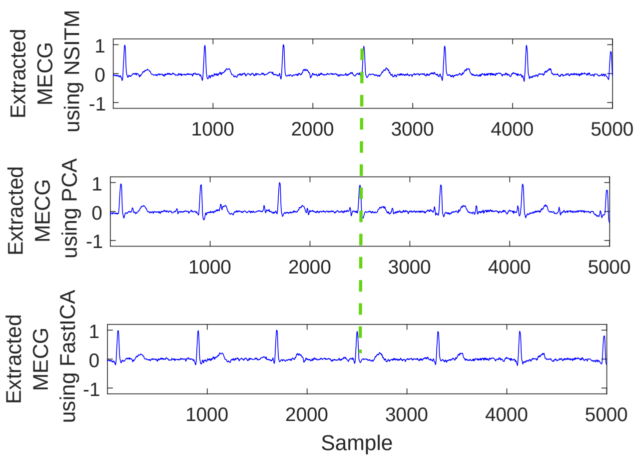

FIGURE 5.9: Extracted MECG signals from ECG signals in Fig. 5.7, using NSITM, PCA, and FastICA, assuming $M = 4$. Only MECG R peaks exist. For illustration, only one marked MECG peak is shown by green dashed lines.

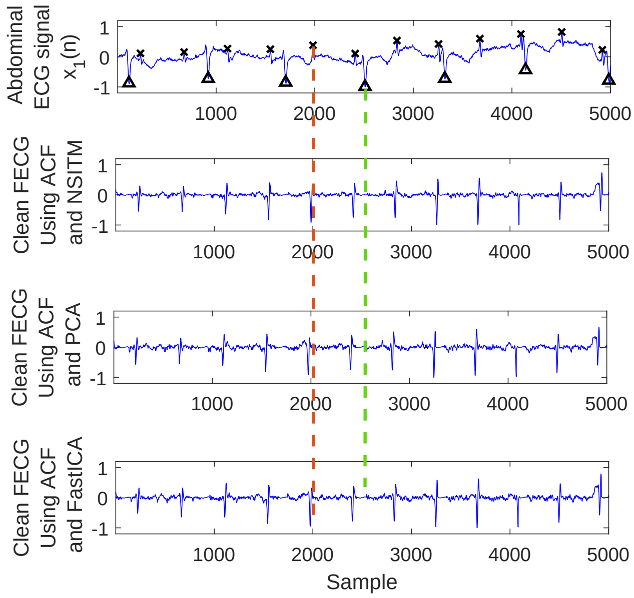

FIGURE 5.10: Clean extracted FECG signals of Fig. 5.8 after the removal of MECG signals by ACF, and based on R peaks locations in Fig. 5.9. The 'x' and 'Δ' markers refer to the reference positions of the R peaks in FECG and MECG signals, respectively. The red dashed lines refers to one position of the extracted FECG R peaks. The green dashed lines refers to one position of the removed MECG R peaks.

The results obtained are very similar to the results using data samples from 0-4999, except that PCA fails in extracting the FECG signal for data samples from 55000-59999, as shown in Fig. 5.8. In general, the proposed NSITM algorithm as well as the other algorithms are successfully extracting both FECG and MECG signals from the abdominal ECG mixture if ACF is used to remove the MECG R peaks from the unsatisfactory extracted FECG signals shown in Fig. 5.8, Fig. 5.12, and Fig. 5.16, respectively.

TABLE 5.1: Evaluation of detected FECG R peaks using SE, ACC, and PPV. The mean values of FHR is also shown

Algorithm	**Abdomen**	**Thorax**	**Detected peaks**	**TP**	**FP**	**FN**	**SE (%)**	**ACC (%)**	**PPV (%)**	**Mean of FHR (bpm)**
PCA	1	3	24	22	2	2	91.6	84.6	91.6	133.4
	2	2	22	19	3	2	90.4	82.6	90.4	125.3
	3	2	27	22	5	3	88	73.3	81.4	133.8
	3	3	28	22	6	3	88	70.9	78.5	133.8
	3	4	29	18	11	1	94.7	60	62	120.7
				Mean	**values**	**⟶**	**90.54**	**74.28**	**80.78**	**129.4**
FastICA	1	3	23	22	1	2	91.6	88	95.6	133.7
	2	2	22	15	7	2	88.2	82.5	68.1	110.8
	3	2	24	22	2	1	95.6	88	91.6	133.7
	3	3	25	22	3	1	95.6	84.6	88	133.7
	3	4	24	22	2	1	91.6	88	91.7	134.5
				Mean	**values**	**⟶**	**92.52**	**86.22**	**87**	**129.28**
NSITM	1	3	23	22	1	1	95.6	91.6	91.6	133.4
	2	2	23	22	1	0	100	95.6	95.6	123.4
	3	2	22	22	0	1	95.6	95.6	100	133.7
	3	3	23	22	1	1	95.6	91.6	95.6	133.8
	3	4	23	22	1	0	100	95.6	95.6	134.5
				Mean	**values**	**⟶**	**97.36**	**94**	**95.68**	**133.76**

TABLE 5.2: Evaluation of detected FECG R peaks using SE, ACC, and PPV. The mean values of FHR is also shown

Algorithm	**File number**	**Abdominal**	**Detected peaks**	**TP**	**FP**	**FN**	**SE (%)**	**ACC (%)**	**PPV (%)**	**Mean of FHR (bpm)**
PCA	a04	4	131	126	5	3	97.7	94.1	96.2	137.1
	a08	4	130	122	7	6	95.3	90.4	94.6	134.3
	a14	4	133	126	7	6	95.5	90.6	94.7	133.3
	a15	4	131	125	6	5	96.1	91.9	95.5	134.8
	a25	4	131	126	5	4	96.9	93.3	96.2	125.7
				Mean	**values**	$\longrightarrow$	**96.3**	**92.1**	**95.4**	**137**
FastICA	a04	4	130	126	4	3	97.7	94.6	96.9	143.1
	a08	4	130	123	7	4	96.8	91.8	94.6	144.4
	a14	4	130	124	6	3	95.6	88	91.6	145.7
	a15	4	130	124	6	4	96.8	92.5	95.4	146.1
	a25	4	131	124	7	3	97.6	92.5	94.6	136.9
				Mean	**values**	$\longrightarrow$	**96.9**	**91.8**	**94.6**	**143.3**
NSITM	a04	4	130	127	3	2	98.4	96.2	97.6	142.4
	a08	4	131	126	5	3	97.7	94.1	96.2	140.7
	a14	4	130	129	1	0	100	99.2	99.2	139.8
	a15	4	130	127	3	1	99.2	96.9	97.7	137.1
	a25	4	131	127	4	1	99.2	96.2	96.9	144.3
				Mean	**values**	$\longrightarrow$	**98.9**	**96.5**	**97.5**	**140.8**

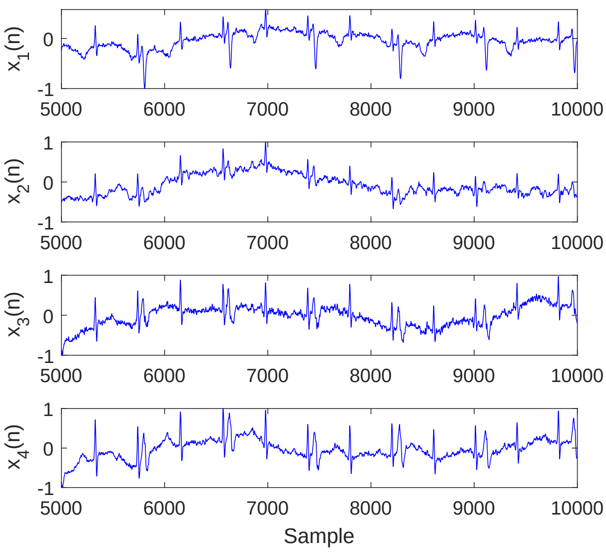

FIGURE 5.11: Recorded abdominal ECG signals from Physionet Challenge 2013 data set a, file a15, $M = 4$, $N = 5000$, data samples from $5000 - 9999$.

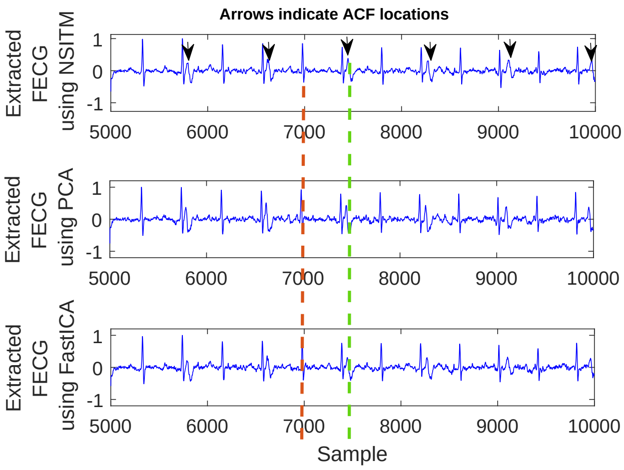

FIGURE 5.12: Unsatisfactory Extracted FECG signals from ECG signals in Fig. 5.11, using NSITM, PCA, and FastICA, assuming $M = 4$. Both FECG and MECG R peaks exist. For illustration, only one marked FECG peak and one marked MECG peak are shown by red dashed lines (left located) and green dashed lines (right located), respectively. The block arrows indicate the position of the ACF used to remove the MECG R peaks.

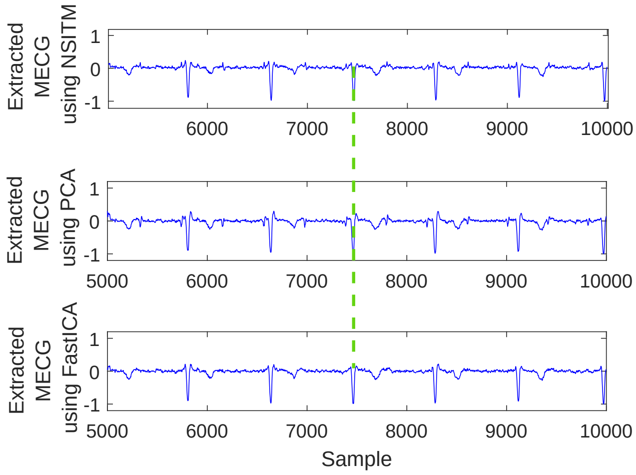

FIGURE 5.13: Extracted MECG signals from ECG signals in Fig. 5.11, using NSITM, PCA, and FastICA, assuming $M = 4$. Only MECG R peaks exist. For illustration, only one marked MECG peak is shown by green dashed lines.

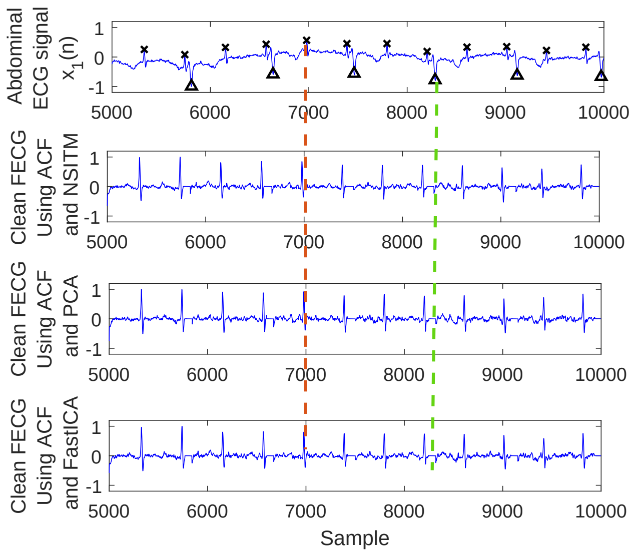

FIGURE 5.14: Clean extracted FECG signals of Fig. 5.12 after the removal of MECG signals by ACF, and based on R peaks locations in Fig. 5.13. The 'x' and 'Δ' markers refer to the reference positions of the R peaks in FECG and MECG signals, respectively. The red dashed lines refers to one position of the extracted FECG R peaks. The green dashed lines refers to one position of the removed MECG R peaks.

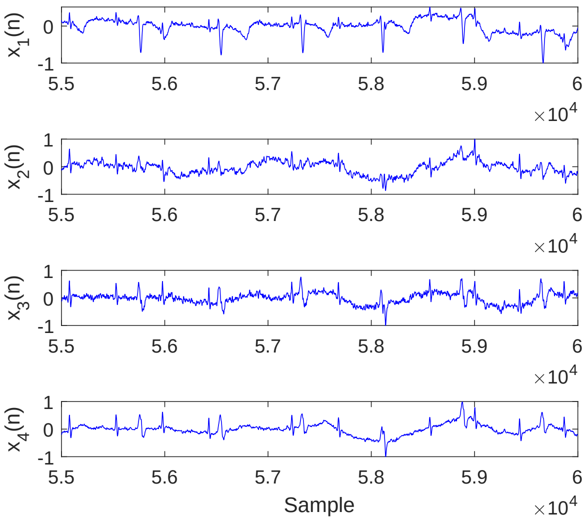

FIGURE 5.15: Recorded abdominal ECG signals from Physionet Challenge 2013 data set a, file a15, $M = 4$, $N = 5000$, data samples from $55000 - 59999$.

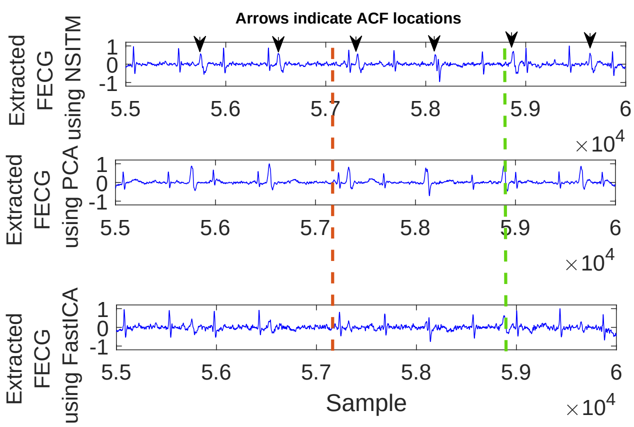

FIGURE 5.16: Unsatisfactory Extracted FECG signals from ECG signals in Fig. 5.15,using NSITM, PCA, and FastICA, assuming $M = 4$. Both FECG and MECG R peaks exist. For illustration, only one marked FECG peak and one marked MECG peak are shown by red dashed lines (left located) and green dashed lines (right located), respectively. The block arrows indicate the position of the ACF used to remove the MECG R peaks.

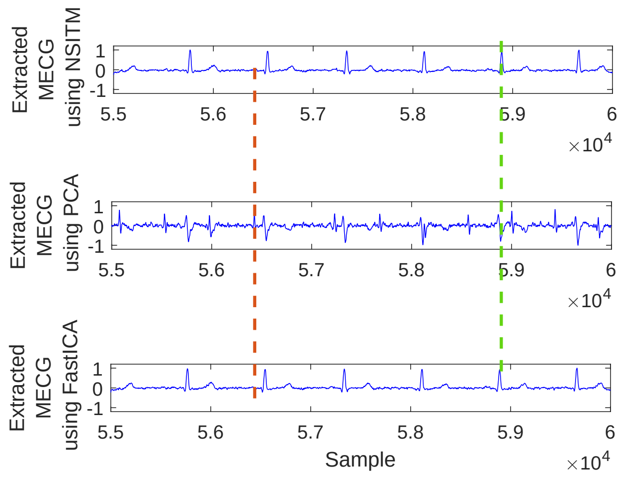

FIGURE 5.17: Extracted MECG signals from ECG signals in Fig. 5.15, using NSITM, PCA, and FastICA, assuming $M = 4$. Only MECG R peaks exist using NSITM, and FastICA. However, both FECG and MECG R peaks exist using PCA. For illustration, one marked FECG peak and one marked MECG peak are shown by red dashed lines and green dashed lines, respectively.

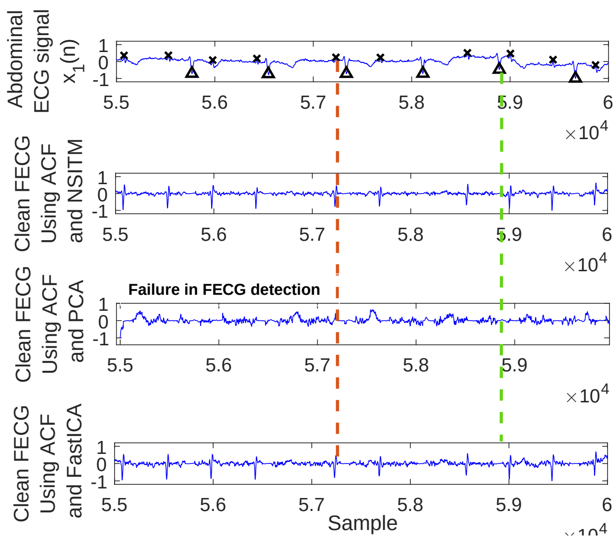

FIGURE 5.18: Clean extracted FECG signals of Fig. 5.16 after the removal of MECG signals by ACF, and based on R peaks locations in Fig. 5.17. The 'x' and 'Δ' markers refer to the reference positions of the R peaks in FECG and MECG signals, respectively. The red dashed lines refers to one position of the extracted FECG R peaks. The green dashed lines refers to one position of the removed MECG R peaks.

5.5.3 Evaluation metrics of FECG R peaks detection

In this simulation, we used the sensitivity (SE), the accuracy (ACC), and the positive predictive value (PPV) to evaluate the performance of the FECG R peaks detection [4, 7, 17]. we used the same real ECG Data in Sections 5.5.1 and 5.5.2. The SE, ACC, and PPV are computed as follows:

$$\mathrm{SE}\ \% = \frac{\mathrm{TP}}{\mathrm{TP}+\mathrm{FN}} \times 100\% \tag{5.20}$$

$$\mathrm{ACC}\ \% = \frac{\mathrm{TP}}{\mathrm{TP}+\mathrm{FN}+\mathrm{FP}} \times 100\% \tag{5.21}$$

$$\mathrm{PPV}\ \% = \frac{\mathrm{TP}}{\mathrm{TP}+\mathrm{FP}} \times 100\% \tag{5.22}$$

where TP, FN, and FP are true positive, false negative, and false positive, respectively. We followed the same simulation procedure explained in Sections 5.5.1 and 5.5.2 then measured SE, ACC, and PPV using (5.20), (5.21), and (5.22), respectively. Results were recorded in Tables 5.1-5.2.

From the results in Table 5.1, it is clear that the the proposed NSITM algorithm scores the highest mean values in SE, ACC, and PPV, as compared with other algorithms. The mean value of FHR computed using NSITM algorithm is close to the expected value (134 bpm), whereas the values diverge using PCA and FastICA (129.4 bpm and 129.28 bpm, respectively). Thus, NSITM algorithm has resulted in significant improvement in FECG signal detection as compared with other algorithms used in this paper.

From the results in Table 5.2, it is clear that the the proposed NSOTM algorithm scores the highest mean values in SE, ACC, and PPV, as compared with other algorithms. The mean value of FHR computed using NSITM algorithm is close to the expected value (141.24 bpm), whereas the values diverge using PCA and

FastICA (137 bpm and 143.3 bpm, respectively). Thus, NSITM algorithm has resulted in significant improvement in FECG signal detection as compared with other algorithms used in this paper.

5.5.4 FECG extraction using synthesized ECG data

To study the extraction performance of the proposed algorithms, the ECG signals (FECG and MECG) must be first modelled then mixed according to (5.1). The modelling of ECG signals involves the generation of P, QRS, and T waves shown in Fig. 5.1. This can be accomplished using the synthesized data taken from Physionet/Fetal ECG Synthetic Database (FECGSYNDB) [31, 32]. This database and its collection methods are described in [33]. Each signal had a duration of 5 minutes, and was sampled at 250 Hz with a 16-bit resolution. The FECG and MECG signals are generated by treating each abdominal signal component (e.g. foetal/maternal ECG or noise signals) as an individual source, whose signal is propagated onto the observational points, also called the electrodes. Thus, the database provides separate waveform files for each signal source [31, 32]. the simulator generates 34 ECG channels (32 abdominal and 2 maternal ECG reference channels). Adding the three individual signals (FECG, MECG, and noise) per channel is then needed to generate the ECG mixture [34]. In our experiment, we selected four abdominal channels (10, 11, 18, 19) and the two reference channels (33 and 34) with different signal to noise ratio (SNR), equals to 0 dB, 6 dB, and 12 dB, respectively. We selected eight pregnant women with simulated pregnancy numbers (01, 02, 03, 06, 07, 08, 09, 10). The selected event is maternal heart rate (MHR) /FHR acceleration / deceleration plus noise. As there are many entries needed to download a file, the file name format is long. To simplify the file format and use it in the paper, we propose a short file format. Table 5.3 illustrates examples of how to rename the downloaded files for different simulated pregnancy numbers, SNR, and signal type. Other file names can also be obtained based on this table.

Figure 5.19 illustrates the synthesized abdominal FECG, MECG, and noise signals, from channel (10), assuming simulated pregnancy number = 01, SNR =12 dB, and event of MHR/FHR acceleration / deceleration plus noise. The signal number (4) from the top is the mixture signal after adding the FECG, MECG, and noise signals. Other signals from channels (11, 18, 19) and their corresponding mixtures were not shown in the paper due to excessive number of figures. Fig. 5.20 illustrates the synthesized maternal reference ECG (MECG) signals, from channels (33-34). The proposed NSITM algorithm was then applied to these six signals (the four abdominal mixture signals plus the two reference signals) to extract the FECG and MECG signals. The simulation is repeated to extract the FECG and MECG based on PCA and FastICA algorithms, for comparison purposes. The extracted FECG and MECG signals from all algorithms are illustrated in Fig. 5.21 and Fig. 5.22, respectively. Comparing the synthesized FECG and MECG signals shown in Fig. 5.19 with the extracted FECG and MECG signals shown in Fig. 5.21–5.22, it is clear that the all algorithms were successfully extracting FECG and MECG signals from their mixture, since all extracted signals (MECG and FECG) match the original signals (MECG (10) and FECG (10)), respectively.

To evaluate the FECG extraction performance of the previous simulation, we used the similarity performance index (SPI) [7, 21], the source-to-interference ratio (SIR), the source-to-artifacts ratio (SAR), and the source-to-distortion ratio (SDR) [36]. We Define $\boldsymbol{y}_i(n), i = 1, 2, \ldots, L$ as the i^{th} row vector of the extracted matrix $\boldsymbol{Y}$. The extracted signal $\boldsymbol{y}_i(n)$ is estimated using PCA, FastICA, an NSITM algorithms. We also define $\boldsymbol{s}_i(n)$ as the corresponding i^{th} row vector of the source matrix $\boldsymbol{S}$, having the same form of $\boldsymbol{Y}$, as in (5.9). Then the SPI is computed as

$$\mathrm{SPI} = \frac{1}{L}\sum_{i=1}^{L} 10\log_{10}\left|\frac{\langle \boldsymbol{y}_i(n), \boldsymbol{s}_i(n)\rangle}{\sqrt{\langle \boldsymbol{y}_i(n), \boldsymbol{y}_i(n)\rangle\,\langle \boldsymbol{s}_i(n), \boldsymbol{s}_i(n)\rangle}} - 1\right|, \tag{5.23}$$

where $L = 2$ (the FECG and MECG sources), and $\langle . \rangle$ denotes the inner product. To compute SIR, SAR, and SDR, it is required first to decompose the extracted

TABLE 5.3: Examples of how to rename the files downloaded from FECGSYNDB large database [32], assuming SNR = 0 dB, 3 dB, and 12 dB. The paper file name is used in this paper to shorten the long file name from [32]. Its format is XYYZZ, where X is an abbreviation for the synthesized signal, and is equal to F (for FECG), or M (for MECG), or N (for Noise), YY is the simulated pregnancy number (00-10), ZZ is the SNR (00 dB, or 06 dB, or 12 dB). The 'l1' code in the downloaded file name refers to the repetition number (1 to 5). It was selected as 1 in this paper.

Simulated pregnancy number	**SNR**	**Type of synthesised signal**	**File name used in the paper**	**File name downloaded from [32]**
		FECG	F0100	`sub01/snr00dB/sub01_snr00dB_l1_fecg1`
01	0 dB	MECG	M0100	`sub01/snr00dB/sub01_snr00dB_l1_MECG`
		Noise	N0100	`sub01/snr00dB/sub01_snr00dB_l1_noise1`
		FECG	F0506	`sub05/snr06dB/sub05_snr06dB_l1_fecg1`
05	6 dB	MECG	M0506	`sub05/snr06dB/sub05_snr06dB_l1_MECG`
		Noise	N0506	`sub05/snr06dB/sub05_snr06dB_l1_noise1`
		FECG	F1012	`sub10/snr12dB/sub105_snr12dB_l1_fecg1`
10	12 dB	MECG	M1012	`sub10/snr12dB/sub10_snr12dB_l1_MECG`
		Noise	N1012	`sub10/snr12dB/sub10_snr12dB_l1_noise1`

signals $\boldsymbol{y}_i(n)$, as follows

$$\boldsymbol{y}_i(n) = \boldsymbol{s}_{target} + \boldsymbol{e}_{interf} + \boldsymbol{e}_{noise} + \boldsymbol{e}_{artif}, \tag{5.24}$$

where $\boldsymbol{s}_{target}$ is the component of $\boldsymbol{s}_i(n)$ in $\boldsymbol{y}_i(n)$, $\boldsymbol{e}_{interf}$, $\boldsymbol{e}_{noise}$, and $\boldsymbol{e}_{artif}$ are the interference, noise and artifact error terms, respectively. Second, the terms are

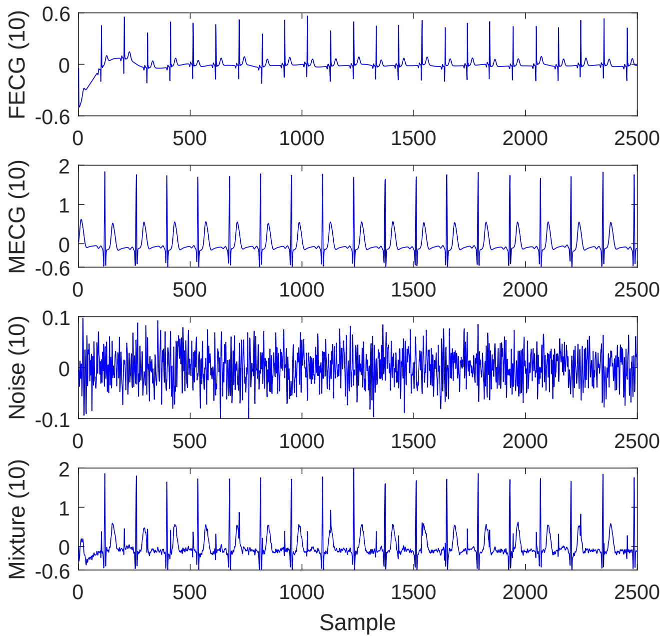

FIGURE 5.19: Synthesized abdominal FECG, MECG, and Noise signals, from channel (10), using [32]. Assuming simulated pregnancy number = 01, SNR = 12 dB, and event of MHR /FHR acceleration / deceleration plus noise. The corresponding paper file names are F0112, M0112, and N0112. The signal number (4) from the top is the mixture signal after adding the FECG, MECG, and noise signals.

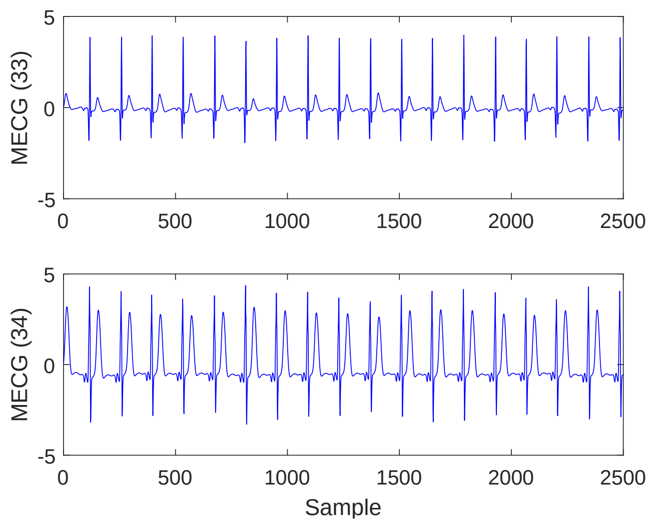

FIGURE 5.20: Synthesized maternal reference ECG (MECG) signals, from channels (33−34), using [32]. Assuming the same simulation settings used in Fig. 5.19. The corresponding paper file name is M0112.

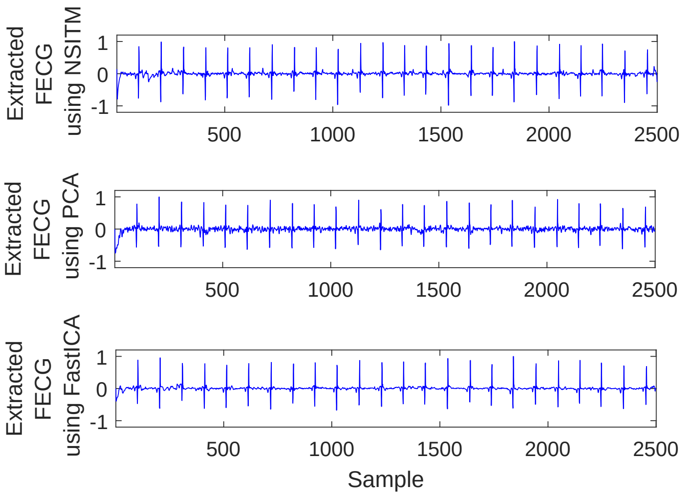

FIGURE 5.21: Extracted FECG signals using NSTM, PCA, and FastICA algorithms.

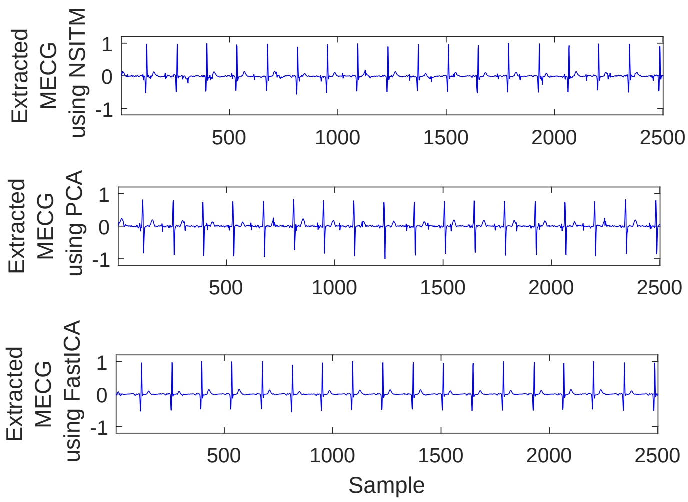

FIGURE 5.22: Extracted MECG signals using NSTM, PCA, and FastICA algorithms.

TABLE 5.4: Comparison between the FECG extraction performances (SPI, SIR, SAR, and SDR), using the proposed NSITM, PCA, and FastICA algorithms. Assuming SNR = 0 dB. Data are collected from Physionet/Fetal ECG Synthetic Database (FECGSYNDB).

		Paper file names								
Extraction metric	Algorithm	F0100 M0100 N0100	F0200 M0200 N0200	F0300 M0300 N0300	F0600 M0600 N0600	F0700 M0700 N0700	F0800 M0800 N0800	F0900 M0900 N0900	F1000 F1000 N1000	Average
SIR (dB)	PCA	14.6	25.4	39.8	27.6	28.2	34.4	28.4	17.7	27.01
	FastICA	22.7	26.4	29.3	31.7	27.2	39.4	24.3	23.3	28.09
	NSITM	**24.5**	**28.1**	**29.1**	**32.7**	**21.6**	**35.7**	**33.04**	**16.1**	**27.6**
SAR (dB)	PCA	−11.9	−0.33	8.86	12.6	3.98	2.8	−12.4	0.36	0.49
	FastICA	−2.42	6.44	5.9	2.6	4.41	2.47	−0.56	3.1	2.74
	NSITM	**−2.2**	**6.5**	**6.43**	**6.47**	**−3.9**	**2.21**	**1.6**	**.5**	**2.57**
SDR (dB)	PCA	−12.7	−0.38	8.8	12.4	3.8	2.8	−13.01	0.2	0.24
	FastICA	−2.43	6.4	5.8	2.55	4.1	2.41	−0.52	3.03	2.66
	NSITM	**−2.4**	**6.4**	**6.09**	**6.2**	**−4.1**	**2.2**	**1.57**	**3.1**	**2.38**
SPI (dB)	PCA	−1.3	−6.6	−12.6	−10.2	−8.6	−8.01	−6.9	−5.5	−7.4
	FastICA	−5.1	−10.37	−9.7	−7.2	−8.6	−7.6	−5.8	−7.3	−7.7
	NSITM	**−5.2**	**−11.03**	**−10.6**	**−10.7**	**−4.12**	**−6.5**	**−11.3**	**−7.6**	**−8.38**

computed using BSS EVAL toolbox, as follows [37]

$$\mathrm{SIR} = 10\log_{10}\frac{\|\boldsymbol{s}_{target}\|_2^2}{\|\boldsymbol{e}_{interf}\|_2^2}, \tag{5.25}$$

$$\mathrm{SAR} = 10\log_{10}\frac{\|\boldsymbol{s}_{target}+\boldsymbol{e}_{interf}+\boldsymbol{e}_{noise}\|_2^2}{\|\boldsymbol{e}_{artif}\|_2^2}, \tag{5.26}$$

$$\mathrm{SDR} = 10\log_{10}\frac{\|\boldsymbol{s}_{target}\|_2^2}{\|\boldsymbol{e}_{interf}+\boldsymbol{e}_{noise}+\boldsymbol{e}_{artif}\|_2^2}. \tag{5.27}$$

The simulation was repeated by first fixing SNR at 0 dB then varying simulated pregnancy numbers from 01 to 10. For each step the SPI, SIR, SAR, and SDR were computed then the average values were computed. The simulation is repeated by varying SNR to 6 dB then to 12 dB. Results of simulation are recorded in Tables 5.4-5.6. Results from the proposed NSITM algorithm are provided in bold letters in these tables. The average values of the extraction performances were plotted as shown in Fig. 5.23. Results from Fig. 5.23 indicates that for SNR equals to 0 dB, the proposed NSITM algorithm shows considerable improve over others in terms of SPI. However, is shows a slightly less values in terms of SIR, SAR, and

TABLE 5.5: Comparison between the FECG extraction performances (SPI, SIR, SAR, and SDR), using the proposed NSITM, PCA, and FastICA algorithms. Assuming SNR = 6 dB. Data are collected from Physionet/Fetal ECG Synthetic Database (FECGSYNDB).

Paper file names

Extraction metric	Algorithm	F0103 M0103 N0103	F0203 M0203 N0203	F0303 M0303 N0303	F0603 M0603 N0603	F0703 M0703 N0703	F0803 M0803 N0803	F0903 M0903 N0903	F1000 F1030 N1030	Average
	PCA	17.6	19.8	15.6	12.4	25.3	16.4	19.2	20.1	18.3
SIR	FastICA	8.1	27.2	19.3	26.1	26.4	20.9	22.1	21.8	22.7
(dB)	**NSITM**	**14.6**	**36.7**	**18.9**	**33.1**	**32.5**	**22.2**	**41.74**	**24.8**	**28.0**
	PCA	−13.8	−0.96	3.1	7.2	5.82	−3.3	−1.9	−0.83	−0.58
SAR	FastICA	1.9	4.56	5.1	2.4	5.88	3.6	5.5	−0.91	3.5
(dB)	**NSITM**	**−2.17**	**4.23**	**4.2**	**6.3**	**6.77**	**5.06**	**6.92**	**1.47**	**4.1**
	PCA	−13.8	−1.62	3.05	7.1	5.77	−3.5	−2.1	−0.84	−0.742
SDR	FastICA	1.1	4.55	5.1	2.35	5.81	3.3	5.2	−0.9	3.31
(dB)	**NSITM**	**−3.17**	**4.23**	**3.7**	**6.2**	**6.75**	**4.8**	**6.82**	**1.41**	**3.84**
	PCA	−1.67	−6.4	−7.9	−9.3	−10.1	−3.4	−4.07	−2.1	−5.62
SPI	FastICA	−6.2	−9.2	−9.6	−7.01	−9.6	−8.36	−9.47	−3.1	−7.82
(dB)	**NSITM**	**−4.6**	**−9.5**	**−9.3**	**−11.5**	**−10.7**	**−10.8**	**−13.7**	**−3.6**	**−9.21**

TABLE 5.6: Comparison between the FECG extraction performances (SPI, SIR, SAR, and SDR), using the proposed NSITM, PCA, and FastICA algorithms. Assuming SNR = 12 dB. Data are collected from Physionet/Fetal ECG Synthetic Database (FECGSYNDB).

Paper file names

Extraction metric	Algorithm	F0112 M0112 N0112	F0212 M0212 N0212	F0312 M0312 N0312	F0612 M0612 N0612	F0712 M0712 N0712	F0812 M0812 N0812	F0912 M0912 N0912	F1012 F1012 N1012	Average
	PCA	16.1	22.8	33.4	19.8	27.3	41.6	22.5	26.3	26.2
SIR	FastICA	25.7	39.8	33.4	49.5	36.3	28.7	15.5	33.1	32.7
(dB)	**NSITM**	**36.6**	**30.9**	**29.8**	**28.9**	**26.9**	**18.7**	**24.9**	**21.3**	**27.2**
	PCA	−10.2	−0.6	3.01	10.8	7.0	7.0	−11.8	2.78	1.05
SAR	FastICA	0.24	6.5	7.93	4.97	5.7	0.23	−6.5	1.11	2.52
(dB)	**NSITM**	**0.099**	**5.97**	**8.33**	**9.66**	**5.6**	**0.58**	**−0.39**	**4.35**	**4.27**
	PCA	−10.3	−0.66	2.99	9.9	7.1	7.01	−12.1	2.73	0.829
SDR	FastICA	0.21	6.5	7.91	4.97	5.68	0.15	−7.07	1.1	2.43
(dB)	**NSITM**	**0.089**	**5.91**	**8.23**	**9.51**	**5.4**	**0.38**	**−0.6**	**4.18**	**4.14**
	PCA	-1.6	-6.35	-11.4	-13.8	-11.0	-10.8	-9.7	-7.18	-8.98
SPI	FastICA	-2.16	-10.6	-11.4	-8.9	-9.5	-7.07	-4.3	-5.93	-7.48
(dB)	**NSITM**	-5.9	-10.6	-12.6	-14.2	-9.6	-5.7	-7.07	-9.1	-9.35

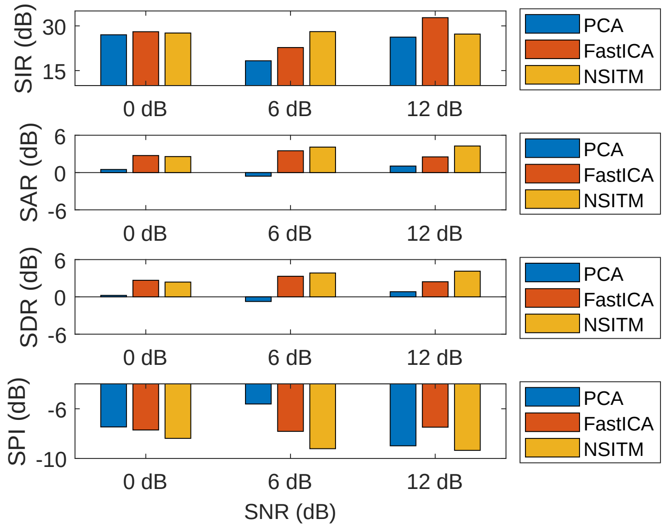

FIGURE 5.23: Comparing between Extraction metrics using NSTM, PCA, and FastICA algorithms.

SDR, as compared with the FastICA, that scores the highest performance measure. For SNR equals to 6 dB, the proposed NSITM method has the highest score. For SNR equals to 12 dB, the proposed NSITM method showed the highest scores in SAR, SDR, and SPI, and its SIR is the next highest score after the FastICA. As a general conclusion, the extraction performances of NSITM algorithm are improved with the increase in SNR.

5.6 Conclusion

A noninvasive FECG detection and extraction algorithm, referred to as NSITM, has been presented. The design problem has been formulated and an analysis has also been provided. The proposed algorithm was simulated using real ECG data and synthesised ECG data. Results using (DAISY) real data have shown successful extraction of FECG and MECG signals, using the proposed NSITM algorithm, when selecting number of abdominal signals to be 3 and 5, with 2 reference signals taken from thorax. Using the same data, the R peaks detection were evaluated by varying the number of abdominal and thorax signals. The average values of SE, ACC, and PPV using NSITM have shown the highest scores as compared with other algorithms used in the paper. The estimated average FHR using NSITM has shown minimum deviation from the reference FHR, as compared with PCA and FastICA. Results using real data from (Physionet/set a) have shown uncleaned extracted FECG signals due to the existence of MECG R peaks in the FECG signals. The MECG peaks have been removed using filtering process, thus extracting clean FECG signals. The robustness of the proposed algorithm over time was checked and results have shown success in extracting the required FECG signals. The R peaks detection were evaluated by considering five different real data. The average values of SE, ACC, and PPV using NSITM have shown the highest scores as compared with other algorithms. The estimated average FHR using NSITM has shown minimum deviation from the reference FHR, as compared with PCA and FastICA.

Results of applying NSITM algorithm to (Physionet/synthesized data) have shown successful extracting of both FECG and MECG signals from all eight data signals used in simulation, and for all selected SNR values, with MHR/FHR acceleration/deceleration plus noise being selected as the event type. The average values of the extraction performance metrics (SIR, SAR, SDR, and SPI) for the NSITM algorithm have mostly shown significant improvement compared to other algorithms, when SNR was increased.

Bibliography

[1] Karvounis, E.C., Tsipouras, M.G. and Fotiadis, D.I., 2009. Detection of fetal heart rate through 3-D phase space analysis from multivariate abdominal recordings. IEEE Transactions on Biomedical Engineering, 56(5), pp.1394-1406.

[2] Sameni, R. and Clifford, G.D., 2010. A review of fetal ECG signal processing; issues and promising directions. The open pacing, electrophysiology and therapy journal, 3, p.4.

[3] Zhongliang, L.U.O., 2012. Fetal electrocardiogram extraction using blind source separation and empirical mode decomposition. Journal of Computational Information Systems, 8(12), pp.4825-4833.

[4] Sutha, P. and Jayanthi, V.E., 2018. Fetal electrocardiogram extraction and analysis using adaptive noise cancellation and wavelet transformation techniques. Journal of medical systems, 42(1), p.21.

[5] Debals, O., Van Barel, M. and De Lathauwer, L., 2016. Löwner-based blind signal separation of rational functions with applications. IEEE Transactions on Signal Processing, 64(8), pp.1909-1918.

[6] Shi, Z. and Zhang, C., 2007. Blind source extraction using generalized autocorrelations. IEEE Transactions on Neural Networks, 18(5), pp.1516-1524.

[7] Ma, Y., Xiao, Y., Wei, G. and Sun, J., 2017. Foetal ECG extraction using non-linear adaptive noise canceller with multiple primary channels. IET Signal Processing, 12(2), pp.219-227.

[8] Zarzoso, V., Nandi, A.K. and Bacharakis, E., 1997. Maternal and foetal ECG separation using blind source separation methods. Mathematical Medicine and Biology: A Journal of the IMA, 14(3), pp.207-225.

[9] Hwang, W.L., Lu, K.S. and Ho, J., 2018. Constrained null space component analysis for semiblind source separation problem. IEEE transactions on neural networks and learning systems, 29(2), pp.377-391.

[10] Da Poian, G., Bernardini, R. and Rinaldo, R., 2016. Separation and analysis of fetal-ECG signals from compressed sensed abdominal ECG recordings. IEEE Transactions on Biomedical Engineering, 63(6), pp.1269-1279.

[11] Taha, L.Y. and Abdel-Raheem, E., 2018. Efficient blind source extraction of noisy mixture utilising a class of parallel linear predictor filters. IET Signal Processing, 12(8), pp.1009-1016.

[12] Taha, L.Y. and Abdel-Raheem E., 2018. "Extraction of Fetal Electrocardiogram signals using Blind Source Extraction Based Parallel Linear Predictor Filter," accepted paper, IEEE International Symposium on Signal Processing

[13] Ye, Y., Zhang, Z.L., Zeng, J. and Peng, L., 2008. A fast and adaptive ICA algorithm with its application to fetal electrocardiogram extraction. Applied Mathematics and Computation, 205(2), pp.799-806.

[14] Shadaydeh, M., Xiao, Y. and Ward, R.K., 2008, August. Extraction of fetal ECG using adaptive Volterra filters. In 2008 16th European Signal Processing Conference (pp. 1-5). IEEE.

[15] Swarnalatha, R. and Prasad, D.V., 2010. Maternal ECG cancellation in abdominal signal using ANFIS and wavelets. Applied Science, 10, pp.868-77.

[16] Niknazar, M., Rivet, B. and Jutten, C., 2013. Fetal ECG extraction by extended state Kalman filtering based on single-channel recordings. IEEE Transactions on Biomedical Engineering, 60(5), pp.1345-1352.

[17] Behar, J., Andreotti, F., Zaunseder, S., Oster, J. and Clifford, G.D., 2016. A practical guide to non-invasive foetal electrocardiogram extraction and analysis. Physiological measurement, 37(5), p.R1.

[18] Chen, R.B. and Wu, Y.N., 2007. A null space method for over-complete blind source separation. Computational Statistics and Data Analysis, 51(12), pp.5519-5536.

[19] Hwang, W.L. and Ho, J., 2015. Null space component analysis for noisy blind source separation. Signal Processing, 109, pp.301-316.

[20] Taha, L.Y. and Abdel-Raheem, E., 2017, April. A null space approach for complete and over-complete blind source separation of autoregressive source signals. In 2017 IEEE 30th Canadian Conference on Electrical and Computer Engineering (CCECE) (pp. 1-4).

[21] Taha, L.Y. and Abdel-Raheem, E., 2018. A Computationally Efficient Blind Source Extraction Using Idempotent Transformation Matrix. Circuits, Systems, and Signal Processing, pp.1-21.

[22] Javidi, S., Mandic, D.P. and Cichocki, A., 2010. Complex blind source extraction from noisy mixtures using second-order statistics. IEEE Transactions on Circuits and Systems I: Regular Papers, 57(7), pp.1404-1416.

[23] Hyvarinen, A., Karhunen, J. and Oja, E., 2001. Independent component analysis and blind source separation.

[24] Martinek, R., Kahankova, R., Jezewski, J., Jaros, R., Mohylova, J., Fajkus, M., Nedoma, J., Janku, P. and Nazeran, H., 2018. Comparative effectiveness

of ICA and PCA in extraction of fetal ECG from abdominal signals: Toward non-invasive fetal monitoring. Frontiers in physiology, 9.

[25] Kanjilal, P.P., Palit, S. and Saha, G., 1997. Fetal ECG extraction from single-channel maternal ECG using singular value decomposition. IEEE Transactions on Biomedical Engineering, 44(1), pp.51-59.

[26] Haghpanahi, M. and Borkholder, D.A., 2013, September. Fetal ECG extraction from abdominal recordings using array signal processing. In Computing in Cardiology 2013 (pp. 173-176). IEEE.

[27] Kim, C.M., Park, H.M., Kim, T., Choi, Y.K. and Lee, S.Y., 2003. FPGA implementation of ICA algorithm for blind signal separation and adaptive noise canceling. IEEE Transactions on Neural Networks, 14(5), pp.1038-1046.

[28] Vuksanovic, B. and Alhamdi, M., 2013. AR-based method for ECG classification and patient recognition. International Journal of Biometrics and Bioinformatics (IJBB), 7(2), p.74.

[29] http://homes.esat.kuleuven.be/â ijsmc/daisy/daisydata.html

[30] https://physionet.org/challenge/2013/

[31] Goldberger, A.L., Amaral, L.A., Glass, L., Hausdorff, J.M., Ivanov, P.C., Mark, R.G., Mietus, J.E., Moody, G.B., Peng, C.K. and Stanley, H.E., 2000. PhysioBank, PhysioToolkit, and PhysioNet: components of a new research resource for complex physiologic signals. Circulation, 101(23), pp.e215-e220.

[32] https://physionet.org/physiobank/database/fecgsyndb/

[33] Andreotti, F., Behar, J., Zaunseder, S., Oster, J. and Clifford, G.D., 2016. An open-source framework for stress-testing non-invasive foetal ECG extraction algorithms. Physiological measurement, 37(5), p.627.

[34] Behar, J., Andreotti, F., Zaunseder, S., Li, Q., Oster, J. and Clifford, G.D., 2014. An ECG simulator for generating maternal-foetal activity mixtures on abdominal ECG recordings. Physiological measurement, 35(8), p.1537.

[35] Wei, Z., Xueyun, W. and Hongxing, L., 2013. Noninvasive fetal ECG estimation using adaptive comb filter. Computer methods and programs in biomedicine, 112(1), pp.125-134.

[36] Vincent, E., Gribonval, R. and Févotte, C., 2006. Performance measurement in blind audio source separation. IEEE transactions on audio, speech, and language processing, 14(4), pp.1462-1469.

[37] Févotte, C., Gribonval, R. and Vincent, E., 2005. BSS-EVAL toolbox user guide–Revision 2.0.

Chapter 6

Conclusions and future work

6.1 Conclusions

In this work, two blind source extraction and one blind source separation algorithms have been proposed to solve for the unknown parameters (input sources and the mixing matrix) in the BSS mixture equation. The algorithms are based on computing new transformation matrices that have shown to be successfully estimating the the unknown sources. The sources used in this dissertation are speech, Gaussian, and ECG signals.

The first algorithm is named as the blind source extraction using parallel linear predictor filter (BSE-PLP). This algorithm is based on computing a transformation matrix from the the covariance matrix of the whitened data. Then, use the matrix as an input to linear predictor filters whose coefficients being the unknown sources. As the transformation matrix has unity norm and unity eigenvalues, the filter becomes independent on the mixture signal norm and eigenvalues variations, thus solving drastically the ambiguity due to the dependency of the filter on the mixture power levels if the mixture is considered as the filter input. Furthermore,

the unity eigenvalues of the matrix result in a very fast convergence in two iterations. Simulation results, using speech and Gaussian signals, show that the model is capable of extracting the unknown source signals and removing noise when the input signal to noise ratio is varied from –20 dB to 80 dB. The algorithm has been applied to extract both the maternal and fetal ECG signals. Simulation results show that the model is successfully extracting all the unknown FECG and MECG signals, for both synthesized and real ECG data. The algorithm is also tested using the sensitivity and accuracy R-peak extraction metrics. The recorded values for the two metrics are 95.45% and 91.3%, respectively, and show considerable improvements as compared to PCA, FastICA, and SOBI algorithms.
The second algorithm is named as the blind source extraction using idempotent transformation matrix (ITM). This algorithm computes the ITM with less computational complexity as compared with the standard singular value decomposition (SVD) method. New optimization problem was defined according to the proposed matrix equation, and solved by an iterative algorithm with low computational complexity. The proposed method is tested using speech, Gaussian, and ECG signals. The performance measures used in this work are the signal-to-interference ratio, signal-to-distortion ratio, and signal-to-artifact ratio. Simulation results show that the proposed algorithm significantly separate the source signals with better performance measures as compared with the state of the art approaches such as the BSE-PLP, second order blind identification (SOBI), principal component analysis (PCA), and fast independent component analysis (FastICA).
The third algorithm is named as the blind source separation using null space approach. This algorithm has been designed for autoregressive (AR) signals and for complete and over-complete cases. Analysis of a mixture equation is carried out to estimate the separating matrix using the null space of the input mixture. Simulation results show that the method is successfully separating speech and Gaussian signals from their mixture with MSE less than 0.14. The approach has been extended to extract the Fetal ECG and the maternal ECG form the ECG

abdominal and maternal signals. Two transformation matrices has been designed for this purpose, named as Null space idempotent transformation matrix (NSITM) and the dual null space matrix (DNSM). First, the ECG mixture signals are used to compute the transformation matrices based on the mixture covariance matrix and on the null space of the mixture. Then, the fetal ECG signal is extracted from the null space of the transformation matrices. The algorithms are tested to extract the FECG and MECG signals, as well as to detect the R peaks. Real ECG Data considered in this paper are collected from DAISY and Physionet databases. The synthesized ECG data are collected from Physionet/Fetal ECG Synthetic database. Results from real database indicate improvement in average FECG heart rate estimation and in R peaks evaluation metrics, as compared with values from principal component analysis (PCA) and fast independent component analysis (FastICA) algorithms. Results from synthesized ECG data show successful extracting of both FECG and MECG signals from all data. The extraction performances of the synthesized ECG data show considerable improvement over other algorithms used in this work, when signal-to-noise ratio (SNR) increases from 0 dB to 12 dB.

6.2 Future directions

The hardware structure of the linear predictor filter in BSE-PLP algorithm can be implemented in parallel. Thus, the overall system becomes a BSS rather than BSE, since all unknown signal can be extracted, simultaneously. Furthermore, the convergence time of the PLP filter is very fast (2 iterations). Thus, a real time BSS system based on PLP algorithm is a viable solutions to fast extraction of the unknown signals. Also, the estimation of extraction time of BSE-PLP algorithm, and comparing it with extraction times of other algorithms, needs further investigation. Furthermore, The algorithm needs more investigations to apply it for real ECG data and address the merits and pitfalls of the algorithm for different subjects, events, and signal-to-noise ratio.

The Null space algorithms based on idempotent transformation matrix needs more investigation and modifications to include the noise in the original mixture equation. Type of noise could be stationary or non stationary.

All designed algorithms have been seen to be successfully working with instantaneous mixture. The work can be extended to consider the convolutive mixture, especially in speech and ECG signal extraction. Time-frequency BSS is a viable approach to solve this problem.

Appendix A: Proof of Theorem 1

Let the whitened matrix $\widetilde{\mathbf{X}}(n)$ be expressed by

$$\widetilde{\mathbf{X}}(n) = \begin{pmatrix} \widetilde{x}_1(n) & \widetilde{x}_1(n-1) & \cdots & \widetilde{x}_1(n-N+1) \\ \widetilde{x}_2(n) & \widetilde{x}_2(n-1) & \cdots & \widetilde{x}_2(n-N+1) \\ \vdots & \vdots & \vdots & \vdots \\ \widetilde{x}_M(n) & \widetilde{x}_M(n-1) & \cdots & \widetilde{x}_M(n-N+1) \end{pmatrix}$$
$$= \begin{pmatrix} \widetilde{\mathbf{x}}_1(n) \\ \widetilde{\mathbf{x}}_2(n) \\ \cdots \\ \widetilde{\mathbf{x}}_M(n) \end{pmatrix} \tag{A.1}$$

where $\widetilde{\mathbf{x}}_i(n) = [\widetilde{x}_i(n)\widetilde{x}_i(n-1)\ldots\widetilde{x}_i(n-N+1)], i = 1, 2, \ldots, M,$ is the i^{th} zero mean whitened row vector whose variance, $var(.)$, is equal to unity [1]. Then

$$var(\widetilde{\mathbf{x}}_i(n)) = \frac{1}{N}\sum_{j=0}^{N-1}\widetilde{x}_i^2(n-j)$$
$$= \frac{1}{N}\|\widetilde{\mathbf{x}}_i(n)\|_2^2 = 1, \tag{A.2}$$

where $\|.\|_2$ is the Euclidean norm (spectral norm) [2]. From (A.2) and [3], the norm of $\widetilde{\mathbf{x}}_i(n)$ and the maximum eigenvalue of $\widetilde{\mathbf{x}}_i^T(n)\widetilde{\mathbf{x}}_i(n)$, denoted by $\lambda_{max}(\widetilde{\mathbf{x}}_i^T(n)\widetilde{\mathbf{x}}_i(n))$

will be

$$\|\widetilde{\mathbf{x}}_i(n)\|_2^2 = \lambda_{max}(\widetilde{\mathbf{x}}_i^T(n)\widetilde{\mathbf{x}}_i(n)) = N. \tag{A.3}$$

From (A.3), we have

$$\lambda_{max}(\widetilde{\mathbf{X}}(n)^T\widetilde{\mathbf{X}}(n)) = \lambda_{max}(\widetilde{\mathbf{x}}_i^T(n)\widetilde{\mathbf{x}}_i(n)) = N, \tag{A.4}$$

$$\lambda_{max}(\widetilde{\mathbf{X}}(n)^T\widetilde{\mathbf{X}}(n)) = \|\widetilde{\mathbf{X}}(n)\|_2^2 = N, \tag{A.5}$$

then from (2.14) and (A.5), we have

$$\lambda_{max}(\mathbf{R}(n)) = \|\mathbf{R}(n)\|_2 = 1, \tag{A.6}$$

$$\|\mathbf{R}_k(n)\|_2 < 1, k = 1, 2, \ldots, N. \tag{A.7}$$

Defining $\mathbf{tr}(.)$ as the trace operator, then from (2.14) and (A.1), $\mathbf{tr}(\mathbf{R}(n))$ is given by

$$\begin{aligned}\mathbf{tr}(\mathbf{R}(n)) &= \frac{1}{N}\mathbf{tr}\left[\widetilde{\mathbf{X}^T}(n))\widetilde{\mathbf{X}}(n))\right] \\ &= \frac{1}{N}\sum_{j=0}^{N-1}\sum_{i=1}^{M}\widetilde{x}_i^2(n-j) = \frac{1}{N}\sum_{i=0}^{M}\| \widetilde{\mathbf{x}}_i(n)\|_2^2.\end{aligned} \tag{A.8}$$

From (A.4) and (A.8)

$$\mathbf{tr}(\mathbf{R}(n)) = M. \tag{A.9}$$

The value of $\mathbf{tr}(\mathbf{R}(n))$ can also be calculated from the eigenvalues of $\mathbf{R}(n)$, denoted by $\lambda_k(\mathbf{R}(n))$, [4]

$$\mathbf{tr}(\mathbf{R}(n)) = \sum_{k=1}^{N}\lambda_k(\mathbf{R}(n)), \tag{A.10}$$

then for M mixture input signals and $N > M$, there will be M non zero eigenvalues and $N - M$ zero eigenvalues. Thus, from (A.9) and (A.10), we have

$$\sum_{k=1}^{N} \lambda_k(\mathbf{R}) = \sum_{k=1}^{M} \lambda_k(\mathbf{R}) = M. \tag{A.11}$$

Solving (A.6) and (A.11) for $\lambda(\mathbf{R}(n))$ we obtain

$$\begin{aligned} \lambda_k(\mathbf{R}(n)) &= \lambda_{max}(\mathbf{R}(n)) = 1, k = 1, 2, \ldots, M, \\ &= \lambda_{min}(\mathbf{R}(n)) = 0, k = M+1, \ldots, N. \end{aligned} \tag{A.12}$$

As matrix $\mathbf{Q}(n) = \mathbf{R}(n) - \mathbf{I}_N$, then

$$\begin{aligned} \lambda_k(\mathbf{Q}(n)) &= \lambda_k(\mathbf{R}(n)) - 1, \\ &= 0, k = 1, 2, \ldots, M, \qquad \text{(A.13)} \\ &= -1, k = M+1, M+2, \ldots, N, \\ \|\mathbf{Q}(n)\|_2 &= 1. \qquad \text{(A.14)} \end{aligned}$$

Bibliography

[1] Romano, J.M.T., Attux, R., Cavalcante, C.C. and Suyama, R., 2016. Unsupervised signal processing: channel equalization and source separation. CRC Press.

[2] Puntanen, S., 2007. Matrix Algebra: Theory, Computations, and Applications in Statistics by James E. Gentle. International Statistical Review, 75(3), pp.435-435.

[3] Johnson, R.A. and Wichern, D.W., 2002. Applied multivariate statistical analysis (Vol. 5, No. 8). Upper Saddle River, NJ: Prentice hall.

[4] Bose, T. and Meyer, F., 2003. Digital signal and image processing. John Wiley and Sons, Inc..

Appendix B: Proof of Theorem 2

Next, the derivation of the transformation property of $\mathbf{R}(n)$ is provided. From (2.1) and (2.15), we have

$$\begin{aligned}\mathbf{X}(n) &= \mathbf{A}\left[\mathbf{S}(n)\mathbf{R}(n) + \mathbf{W}(n)\mathbf{T}_s(n)\right] + \mathbf{G}(n) \\ &= \mathbf{X}(n)\mathbf{R}(n) + \mathbf{V}_1(n),\end{aligned} \tag{B.1}$$

where $\mathbf{V}_1(n) = \mathbf{T}_s(n) + \mathbf{G}(n)\mathbf{Q}(n)$ is a white noise matrix correlated with $\mathbf{V}(n)$ according to the central limit theorem [1]. From (2.15) and multiplying (B.1) by $\mathbf{S}(n)$, and using the transpose rule $(\mathbf{X}(n)\mathbf{R}(n))^T = \mathbf{R}^T(n)\mathbf{X}^T(n)$, we have

$$\begin{aligned}\mathbf{S}(n)\mathbf{X}^T(n) &= \left[\mathbf{S}(n)\mathbf{R}(n) + \mathbf{W}(n)\mathbf{T}_s(n)\right]\mathbf{R}^T(n)\mathbf{X}^T(n) + \mathbf{S}(n)\mathbf{V}_1^T(n) \\ \mathbf{S}(n)\mathbf{X}^T(n) &= \mathbf{S}(n)\mathbf{R}(n)\mathbf{R}^T(n)\mathbf{X}^T(n) + \mathbf{V}_2(n)\mathbf{X}^T(n) + \mathbf{S}(n)\mathbf{V}_1^T(n),\end{aligned} \tag{B.2}$$

where $\mathbf{V}_2(n) = \mathbf{W}(n)\mathbf{T}_s(n)\mathbf{R}^T(n)$ is a white noise term. For noise free condition, (B.2) is reduced to $\mathbf{S}(n) = \mathbf{S}(n)\mathbf{R}(n)\mathbf{R}^T(n)$, which, if compared with the noise free condition in (2.15), i.e, ($\mathbf{S}(n) = \mathbf{S}(n)\mathbf{R}(n)$), will result in

$$\mathbf{R}(n) = \mathbf{R}(n)\mathbf{R}^T(n) = \mathbf{R}^2(n), \tag{B.3}$$

and in general, we can write

$$\mathbf{R}(n) = \mathbf{R}^k(n), k = 2, 3, \ldots. \tag{B.4}$$

For noisy case, an assumption is required for (B.2). Without loss of generality, we shall assume that $\mathbf{S}\mathbf{V}_1^T(n) = \mathbf{V}_3(n)\mathbf{X}^T(n)$, where $\mathbf{V}_3(n)$ is another white noise term correlated with $\mathbf{V}_2(n)$ and $\mathbf{V}_3(n)$. Under this assumption, (B.2) can be reduced to $\mathbf{S}(n) = \mathbf{S}(n)\mathbf{R}(n)\mathbf{R}^T(n) + \mathbf{V}_2(n) + \mathbf{V}_3(n)$. Comparing the result with (2.15), we get

$$\mathbf{R}(n) = \mathbf{R}(n)\mathbf{R}^T(n) + \Psi(n), \tag{B.5}$$

where $\Psi(n) \subset \mathbb{R}^{N\times N}$ is the noise error term between $\mathbf{V}_2(n)+\mathbf{V}_3(n)$ and $\mathbf{W}(n)\mathbf{T}_s(n)$ in (2.15). As the correlation between the two noise terms is high, their difference $\Psi(n)$ is small. Thus, (B.3) is being used in this chapter, as an approximation to (B.5). Simulation results in Fig. 2.4 confirm that.

Bibliography

[1] Ahmadian, P., Sanei, S., Ascari, L., González-Villanueva, L. and Umiltà, M.A., 2013. Constrained blind source extraction of readiness potentials from EEG. IEEE Transactions on Neural Systems and Rehabilitation Engineering, 21(4), pp.567-575.

Vita Auctoris

NAME:	Luay Yassin Taha
PLACE OF BIRTH:	Basra, Iraq
YEAR OF BIRTH:	1959
EDUCATION:	University of Windsor, Windsor, Ontario 2014-2019 Ph.D. Electrical Engineering
	UKM University, Bangi, Malaysia 2005-2009 Ph.D. Micro-Engineering and Nano-Electronic
	University of Technology, Baghdad, Iraq 1982-1985 M.Sc. Control and Instrumentation
	University of Basra, Basra, Iraq 1976-1980 B.Sc. Electrical Engineering

Published Work

- Taha, L.Y. and Abdel-Raheem, E., 2018. Efficient blind source extraction of noisy mixture utilising a class of parallel linear predictor filters. IET Signal Processing, 12(8), pp.1009-1016, 2018.

- Taha, L.Y. and Abdel-Raheem, E., 2018. A Computationally Efficient Blind Source Extraction Using Idempotent Transformation Matrix. Circuits, Systems, and Signal Processing, pp.1-21, 2018, Springer publisher.

- Taha, L.Y. and Abdel-Raheem, E., 2018. Extraction of Fetal Electrocardiogram signals using Blind Source Extraction Based Parallel Linear Predictor Filter. In the proceedings of the IEEE International Symposium on Signal Processing and Information Technology (ISSPIT), Louisville, Kentucky, USA, Dec. 6–8, 2018, pp. 208–211.

- Taha, L.Y. and Abdel-Raheem, E., 2017, April. A null space approach for complete and over-complete blind source separation of autoregressive source signals. In the proceedings of the 30th Canadian conference on Electrical and Computer Engineering (CCECE), Windsor On, Canada, 30 April–3 May, 2017.

- Rita T. Abdulmunam, Luay Y. Taha, Paul Ivey, "Wind Energy Harvesting Systems: A Better Understanding of their Sustainability". Journal of Clean Energy Technologies, vol. 5, No. 5, September 2017.

- Al-Laith Taha, Luay Taha and Esam Abdel Raheem, "FastICA Architecture Utilizing FPGA and Iterative Symmetric Orthogonalization for Multivariate Signals" in the 2015 IEEE International Symposium on Signal Processing and Information Technology (ISSPIT), Abu Dhabi, pp. 279-284.

- Rita T. Abdulmunam, Luay Y. Taha, Paul Ivey, "Simulation and Experimental Study of a Multi-Poles Variable Capacitor for Electrostatic Wind Energy

Harvester", Turkish Journal of Electrical Engineering & Computer Sciences, 2015, pp. 1-12. Available online: http://journals.tubitak.gov.tr/havuz/elk-1212-87.pdf

- Rita T. Abdulmunam, Luay Y. Taha, Paul Ivey. "Electrostatic Harvester for Wind Energy Harvesting and Wind Speed Remote Sensing", the 28th annual IEEE Canadian Conference on Electrical and Computer Engineering (CCECE'2015), Halifax, Nova Scotia, pp. 412-417.

- Rita T. Abdulmunam, Luay Y. Taha, Paul Ivey, "Wind Energy Harvesting using Electrostatic Converter for Wireless Sensor Networks ", 14th International Conference on Optimization of Electrical and Electronic Equipment OPTIM 2014, May 22-24, 2014, Brasov, Romania.

- Rita T. Abdulmunam, Luay Y. Taha, Paul Ivey, "Modeling of low power electrostatic wind energy harvester for macro scale applications", International Journal of Information and Electronics Engineering, Vol. 2, No. 6 (2012) pp 912-917.

- Rita T. Abdulmunam, Luay Y. Taha, Paul Ivey, "Design consideration for electrostatic energy harvester", Applied Mechanics and Materials vol. 110-116 (2012) pp 5173-5178.

- Luay Y. Taha , B. Y. Majlis and Ahmad AL- Ali, "Analysis of a MEMS piezoelectric microgenerator using network placement method",IEEE International Conference on Semiconductor Electronics, ICSE2012, Kuala - Lumpur, Malaysia, Sep 2012.

- Abdulmunam, R. T., Taha, L. Y., Ivey, P. C, "Simulink model of an integrated rotary electrostatic energy harvester" , Optimization of Electrical and Electronic Equipment (OPTIM), 2012 13th International Conference , Romania, pp. 1006–1011, May, 2012.

- Luay Y. Taha , B. Y. Majlis and Ahmad AL- Ali, "Design of MEMS Piezoelectric microgenerator using Voltage and Power Optimization; Proc. of the ICSE2010 conference, Kuala - Lumpur, Malaysia, 28 June – 30 June 2010, pp 313 – 316.

- Luay Y. Taha , B. Y. Majlis and Ahmad AL- Ali, "Modelling and Analysis of a transformer based MEMS piezoelectric vibration type microgenerator ", Published paper in the IEEE International Conference on Semiconductor Electronics, ICSE2006, Kuala - Lumpur, Malaysia, 29 Nov – 1 Dec 2006.

- L. Y. Taha , B. Y. Majlis and A. A. Ahmad, "Directional study on MEMS microgenerator"; International Conference on MEMS and Nanotechnology, ICMN'06 14-15 March 2006, Kuala Lumpur, Malaysia, pp. 182-189.

- Luay Y. Taha , Elena. I. Gaura , Robert. M. Newman, Alison Todman , "Universal smart micro-sensor Interface: Comparative and design issues", 2nd IEEE GCC conference & Exhibition , Manama, kingdom of Bahrain, Nov. 23-25, 2004.

- Luay Y. Taha, "Design of IEEE 488 software/Hardware bus interface for NEC PC", 1st Electrical and Electronic Institute conference, Mousail, Iraq, 1994.

- Luay Y. Taha and G.T. Ibrahim, "New method for echo detection using simplified complex cepstrum". First scientific conference on radar and signal processing, Baghdad 1987.

- Luay Y. Taha and W.H. Abdulla," Data acquisition system using the IEEE 488 interface bus", Microprocessor and Microsystems. vol.11 No.9, Nov. 1987, pp. 493-498.

- Faris A. and W.H. Abdulla and Luay Y. Taha, "A two pass speech recognition system", Conference of higher education, Iraq 1988.